

ELECTRICAL CONDUCTIVITY STRUCTURE OF THE LOWER
CRUST AND UPPER MANTLE IN WESTERN CANADA

by

BERNARD CANER

B.Sc., University of Alberta, 1960

M.Sc., University of British Columbia, 1964

A THESIS SUBMITTED IN PARTIAL FULFILMENT OF
THE REQUIREMENTS FOR THE DEGREE OF
DOCTOR OF PHILOSOPHY

in the Department

of

GEOPHYSICS

We accept this thesis as conforming to the
required standard

THE UNIVERSITY OF BRITISH COLUMBIA

July, 1969

In presenting this thesis in partial fulfilment of the requirements for an advanced degree at the University of British Columbia, I agree that the Library shall make it freely available for reference and Study.

I further agree that permission for extensive copying of this thesis for scholarly purposes may be granted by the Head of my Department or by his representatives. It is understood that copying or publication of this thesis for financial gain shall not be allowed without my written permission.

Bernard Caner

Department of Geophysics

The University of British Columbia
Vancouver 8, Canada

Date July 25, 1969

ABSTRACT

Geomagnetic induction techniques have been used to study the structure of the crust and upper mantle in western Canada. Geomagnetic depth-sounding (GDS) has been used primarily for mapping, and magnetotellurics (MT) for quantitative interpretation. Self-consistent models of electrical conductivity structure have been derived from the combined MT/GDS data.

The conductivity structure models have been considered in conjunction with other relevant geophysical information: heat-flow, seismology and aeromagnetic surveys. No definite petrological models can be derived because of the order-of-magnitude uncertainties in the relations between electrical conductivity, temperature and composition. However, if we exclude geochemically improbable solutions, the following two distinct results can be extracted:

- a) In southwestern Canada (boundaries not clearly defined, but at least as far east as Lethbridge), the uppermost mantle is moderately conducting (resistivity 30-50 ohm-meters). This indicates a temperature of at least 750°C at depth 35 km., and provides independent confirmation (without assumptions of crustal structure) of the heat-flow derived estimates of Roy et al (1968b).
- b) In a sharply delineated region starting from about 0-30 km west of the Rocky Mountain Trench, the lower crust (from a depth of about 10-15 km) is conductive. The most likely interpretation is a hydrated lower crust, as proposed by Hyndman and Hyndman, 1968. Hydration alone is sufficient to explain the observed conductivities, i.e. higher temperatures are not necessarily required for this model. However, given the information from (a) above, some partial melting of hydrated granitic materials should occur in this zone; this is in good agreement with the geological evidence of granitic intrusives in this region.

TABLE OF CONTENTS

	PAGE
ABSTRACT	(i)
TABLE OF CONTENTS	(ii)
LIST OF FIGURES	(iv)
I. INTRODUCTION	
A) Preface and acknowledgements	1
B) Historical background	2
C) Thesis outline	8
D) Theory	11
II. MAGNETO-TELLURICS	
A) Introduction	18
B) Instrumentation	23
C) Data	25
D) Interpretation - eastern stations	33
E) Interpretation - western stations	42
F) Summary - conductivity structure	47
III. GEOMAGNETIC DEPTH-SOUNDING	
A) Introduction	50
B) Instrumentation	50
C) Mapping	52
D) Quantitative interpretation	61
IV. OTHER GEOPHYSICAL INFORMATION	
A) Introduction	78
B) Heat flow	78
C) Seismology	81
D) Aeromagnetic surveys	84

V. PETROLOGICAL INTERPRETATION

A) Summary of data	98
B) Electrical conductivity of the lower crust and upper mantle	98
C) Petrological models	105
D) Conclusions	109

REFERENCES

113

LIST OF FIGURES

	PAGE
I-1. Location of GDS stations in North America up to 1966	5
I-2. Location of GDS and MT stations in western Canada	10
II-1. Location of MT stations used in this report	21
II-2. Schematic lay-out and frequency response of MT instrumentation used at Pincher and Penticton	22
II-3a. Section of MT recording in the long-period band, eastern stations	26
II-3b. Section of MT recording in the long-period band, western stations	27
II-4. Sections of MT recording, short-period band	28
II-5. Apparent resistivity plotted against period for all six stations	29
II-6. Polarization plot at Fernie	32
II-7. Conductivity structure models, eastern stations	35
II-8. Conductivity structure models, western stations	43
II-9. Combined conductivity structure for both regions	48
III-1. Magnetogram copies from pairs of stations at latitudes 51°N, 49.5°N, and 33°-35°N.	53
III-2. Location of GDS stations in western Canada	54
III-3. GDS recordings from Cache Creek - Prince George profile and Victoria	57
III-4. M-ratios as a function of geomagnetic latitude for Cache Creek - Prince George profile	58
III-5. Sections of GDS recordings, Pincher, Salmo, and Penticton	62
III-6. M-ratios as a function of period, Penticton normalized with respect to Pincher	63
III-7. 14-day recordings of Z, Pincher and Penticton	64
III-8. Fourier amplitudes for the diurnal variations at Pincher and Penticton	65

III-9.	GDS conductivity structure models, Penticton/Pincher, spatial wavelengths ≥ 3000 km	68
III-10.	GDS conductivity structure models, Penticton/Pincher, spatial wavelengths ≤ 1000 km	69
III-11.	GDS conductivity structure models, Pincher vs. hypothetical "eastern" structure	73
III-12.	GDS conductivity structure models, Penticton/Pincher, with surface layer	74
IV-1.	Location of aeromagnetic profiles	87
IV-2.	Magnetic data and topography, profile A	88
IV-3.	Magnetic data and topography, profile B	89
IV-4.	Superimposed filtered magnetic data from profiles A and B	91
IV-5.	Filtered magnetic data, profile C	92
IV-6.	Filtered magnetic data, profile D	93
V-1.	Outline of discontinuity defined by GDS and aeromagnetic data	99
V-2.	Final conductivity structure models	100
V-3.	Electrical conductivity of some rocks and minerals	101
V-4.	Electrical conductivity as a function of temperature	104
V-5.	Effects of hydration and melting on electrical conductivity of rocks	108
V-6.	Geotherms and melting zones	110
V-7.	Combined petrological model, lat. 49.3°N	111

I-A) Preface and Acknowledgements

The major part of this thesis has been written at the "publishable paper" level, i.e. relatively lean and concentrated. In the course of preparation, some of the chapters have already been published or submitted for publication, as outlined below. In each case the primary work (planning, organization, almost all data processing, and all interpretation) was carried out by the candidate; the contribution of the co-authors was limited to operation of field-stations and some routine data processing. However, significant contributions were received from these co-authors in reviewing the completed results, as well as from internal reviewers, journal editors, and referees. This feed-back has been incorporated in the thesis. In particular, Dr. R.M. Ellis and Dr. W.F. Slawson at the University of British Columbia, and Dr. E.R. Niblett, Dr. P.H. Serson, and Dr. K. Whitham at the Dominion Observatory have greatly contributed towards the reliability of this work. I should also like to acknowledge the organizational support and personal encouragement provided by Dr. J.A. Jacobs, former head of the Department of Geophysics; by Dr. R.D. Russell, his successor, and by Dr. P.H. Serson, Chief of the Division of Geomagnetism at the Dominion Observatory. Financial support from the Department of Energy, Mines and Resources is also gratefully acknowledged.

Reference to published sections of this thesis:

Chapter II: Caner, B., P.A. Camfield, F. Andersen, and E.R. Niblett.

"A large-scale magneto-telluric survey in western Canada", submitted to Can. J. Earth Sciences, 1969.

Chapter III: Caner, B., D.R. Auld, and P.A. Camfield. "Geomagnetic depth-sounding in western Canada". In preparation, to be submitted to the Journal of Geophysical Research.

Chapter IV (Section D): Caner, B. "Long aeromagnetic profiles and crustal structure in western Canada", to be published in Earth and Planetary Science Letters, 1969.

Chapter V: Caner, B., "Electrical conductivity structure in western Canada and petrological interpretation". To be published in the Journal of Geomagnetism and Geoelectricity. (Symposium on multidisciplinary studies of unusual regions of the upper mantle, Madrid, Sept. 1969).

I-B) Historical Background

The electrical conductivity structure of the earth's crust and upper mantle can be determined by observations of fluctuations in the natural geomagnetic and geoelectric (telluric) fields. The periodicities of interest for this type of work range from about 1 second to about 10^5 seconds. Two basic methods are in use: a) magnetotellurics (MT), where the two horizontal magnetic (H_x , H_y) and two horizontal telluric (E_x , E_y) components are recorded; b) geomagnetic depth-sounding (GDS) where the three components (two horizontal, one vertical) of the magnetic field are recorded (H_x , H_y , H_z , or more usually H , D , Z in magnetic coordinates). Theoretically, the two methods are equivalent, but in practice their execution (and sometimes the results obtained) are different. Rikitake (1966) has outlined the relative advantages of the two methods and their limitations for particular situations. A very superficial outline of the comparative merits and ranges of usefulness is shown in the following table. A summary and bibliography of the literature has been published by Fournier (1966).

MAGNETO-TELLURICS (MT)Advantages

1. Single-station interpretation possible.
2. Source dependent only for periods > 1000 sec.
3. Interpretation subject to only moderate bias in selection of conductivity structure models.

Disadvantages

1. Results (entire spectrum) strongly dependent on surface conditions.
2. Experimental difficulties at long periods.
3. Logistics complicated (long lines, ground contacts).

Primary usefulness (open to argument!)

1. Periods < 1000 sec. (surface layers and crust).
2. Quantitative confirmation (at a few selected sites) of results previously obtained by GDS.

GEOMAGNETIC DEPTH-SOUNDINGDisadvantages

- Network or profile required.
- Interpretation strongly source dependent.
- Interpretation strongly dependent on personal bias, since two station models are involved for each data set.

Advantages

- Results relatively independent of surface conditions.
- Experimentally simple, entire spectrum.
- Logistics simple, cheap.

Periods > 1000 sec.

(lower crust and mantle).

Mapping and preliminary surveys of large areas for delineation of anomalous regions.

In North America, MT data obtained at a few scattered locations indicated the existence of a highly conducting zone at depths variously

reported as between 35 km and 140 km (for example, Cantwell and Madden, 1960; Niblett and Sayn-Wittgenstein, 1960; Srivastava and Jacobs, 1964; Vozoff and Ellis, 1966; Plouff, 1966). The stations were too scattered to provide any large-scale models for the structure under the continent, and the main impetus for systematic work in this field came from GDS.

Although low Z/H ratios had been noted earlier at Tucson (Bartels et al, 1939), the density of permanent observatories in North America was too low to permit the type of pioneering GDS work which was possible in Japan (Rikitake, 1959) and Europe (Wiese, 1956). The introduction of portable variographs during the IGY opened up this field in North America. Matsushita (1960) noted that the Z amplitudes of sudden commencements recorded at several stations at latitude 39.5°N were different, and suggested differences in subsurface conductivity structure as a possible explanation; however, the stations were too widely spaced (about 400 km) for any consistent pattern to be derived. The main break came with Schmucker's work during 1959-1962 in the southwest U.S.A. (Schmucker, 1964). He delineated a sharp discontinuity in the character of recorded geomagnetic data (specifically in the amplitude of fluctuations in Z with periods of 15-60 minutes) along an E-W profile crossing the Cordillera at latitude 32°N (profile A on Fig. I-1). The discontinuity occurred between Las Cruces (LAC) and Cornudas (COR) in New Mexico; to the east of this transition, the ratio of vertical to horizontal amplitudes for bay-type features was roughly three times higher than at the western stations. Schmucker (1964) interpreted this attenuation to be caused by a step in a highly conducting sub-stratum from a depth of 320 km under the eastern region to a depth of 160 km under the western region. Two of the permanent Canadian observatories (Alert and Mould Bay) were also found to be "anomalous" in their Z/H ratios (Whitham, 1965); it became

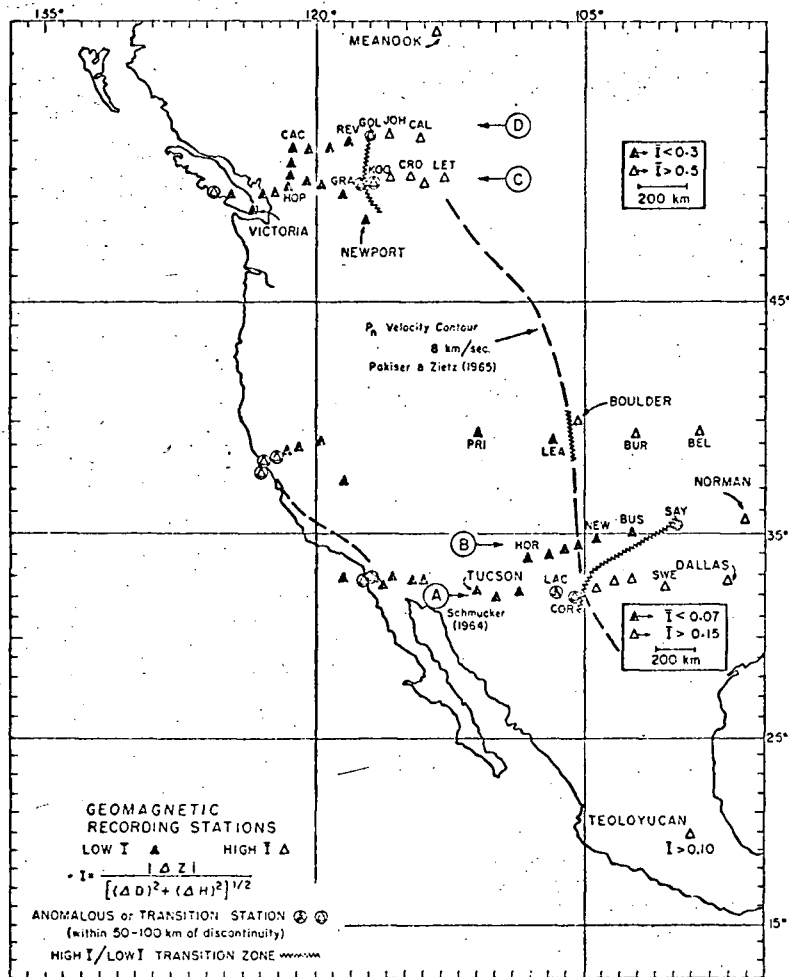


Fig. I-1. Location of GDS stations in North America, up to 1966 (after Caner et al, 1967).

clear that these GDS "anomalies" are not nearly as rare as previously supposed.

In 1963, a long-term GDS project was initiated by the Institute of Earth Sciences at the University of British Columbia, in cooperation with the Dominion Observatory's Division of Geomagnetism at Victoria, and co-ordinated by the author. Hyndman (1963) operated an east-west GDS profile at latitude 49.5°N , from Westham Island (near Vancouver) to Lethbridge in Alberta - profile C on Figure I-1. His results provided the basic ground work for all subsequent surveys in this area. Hyndman observed the same pattern as Schmucker in the southwest U.S.A.: stations to the east of a discontinuity (located in the Kootenay Lake region) showed Z/H ratios about 2-3 times higher than stations to the west. Whitham (1965) estimated that the observed attenuation could be explained by a rise of conducting material to within about 200 km of the surface under the western region, a structure compatible with Schmucker's interpretation in the southwest U.S.A.

In 1964, Hyndman's profile was extended towards the west in order to study the "coast effect" on geomagnetic recordings. The results (Lambert and Caner, 1965) are not directly relevant to the present study of the main inland discontinuity. During 1965 and 1966, attention was again focussed on the inland discontinuity and two further profiles were operated by W.H. Cannon and C.E. Livingstone: one at latitude 35°N in the southwest U.S.A. (profile B on Figure I-1) and one at latitude 51°N (profile D) between Cache Creek, B.C., and Calgary. The aim of these two profiles, which were about 200 km to the north of the two earlier profiles of Schmucker and Hyndman, was to verify that these discontinuities were in fact the borders of large-scale continental features rather than just isolated anomalies. The results (Caner et al, 1967) confirmed this fact, although

on profile B the discontinuity was found about 200 km to the east of its expected position. Caner et al (1967) attempted quantitative interpretation of the combined data from all profiles; using different structural models, they concluded that a rise of conducting material to within 25-35 km of the surface under the western region could explain the observed attenuation in Z - considerably shallower than the previous estimates.

In October 1966, Gough and Reitzel operated a GDS profile at latitude 38.5°N , and confirmed the preliminary results previously inferred from the more widely spaced IGY stations of Matsushita (1960); the discontinuity was clearly located at longitude 106° . Subsequent work (Gough and Anderson, 1968) at intermediate latitudes has since confirmed the existence of this feature across the entire U.S.A. The discontinuity follows roughly the line of the Rocky Mountains, but detailed profiling shows significant departures (100-200 km) to either side of this line. It is clear that the term "anomaly" can hardly be applied to a feature covering perhaps as much as a quarter of the continental area. In the following work, the term "anomalous" has been applied only to stations where the ratio Z/H is a function of azimuth, i.e. indicative of deep-seated lateral inhomogeneities - for example, Alert (Whitham and Andersen, 1962) and the Kootenay Lake Station (Hyndman, 1963; Caner et al, 1967). All other GDS data, whatever the actual value of the Z/H ratio, is considered "normal", representative of a particular conductivity structure. Although several second-order differences have been observed, the feature of main interest remains the large region of low Z/H ratio defined by the above results for western North America. The interest in this feature is heightened by the fact that the same region (although not so sharply delineated) is also characterised by high heat-flow (Lee and Uyeda, 1965;

Roy et al, 1968), low seismic Pn velocities, and absence of long-wavelength "static" magnetic features (Pakiser and Zietz, 1965). If successfully tied in with this other geophysical evidence, the geomagnetic induction results could therefore be of considerable interest to: a) delineate the exact boundaries of this "western-type" or "Cordilleran" geophysical region, and b) help interpret its causes and origin. In particular, it has been suggested (Caner and Cannon, 1965) that the observed effects could be the surface expressions of an inland continuation of the East Pacific Rise.

With the major conductivity structure regions being delineated by GDS, it becomes possible to interpret the data from the widely scattered MT stations in a more systematic manner as representative of certain regions. Swift (1967) operated several MT stations in the southwest U.S.A., following Schmucker's GDS profile; his results confirmed the existence of a zone of high conductivity at shallow depth under the western region.

I-C) Thesis outline

The main objectives of this work are:

- 1) Determination of the electrical conductivity structure of the lower crust and upper mantle in western Canada, using geomagnetic induction methods. Integrated GDS/MT methodology has been used; such an approach has not previously been applied to large-scale investigations of this nature.
- 2) Derivation of a petrological model for these depths (10-60 km) in this region. This model is based primarily on the electrical conductivity structure, but compatibility with other relevant geophysical information is maintained.

To achieve the above objectives, the earlier work described in the preceding section has been extended, and several new lines of approach were started (Figure I-2). In GDS, mapping has been continued with a north-south profile from Prince George to Cache Creek, and with several fill-in stations in the vicinity of discontinuities; also a higher-quality data set was obtained for one pair of stations to permit detailed quantitative analysis.

The main emphasis of the work has shifted to MT, to provide more reliable information on the subsurface conductivity structures responsible for the observed GDS effects. The MT work involved a large-scale field survey involving simultaneous operation at 5 stations.

Although chronologically the GDS work preceded the MT work, they have been presented in the reverse order for a more logical pattern (since the MT structure models are required for testing of the GDS results). The experimental requirements for the two methods vary widely and most work in these two fields is carried out in separate surveys. The GDS and MT projects described in this report were also carried out in separate operations, but operational conditions were set up in such a way as to permit combined interpretation, or at least mutual control. Specifically, GDS has been used mainly for large-scale mapping and MT for detailed quantitative interpretation at selected "representative" locations. The relative functions performed by the MT and GDS data in this work can perhaps be loosely described by analogy with drill-hole logging and seismic exploration: drilling (MT) provides detailed information at high cost at a few selected locations; the structures (horizons) can then be mapped economically over much wider areas by seismic surveys (GDS).

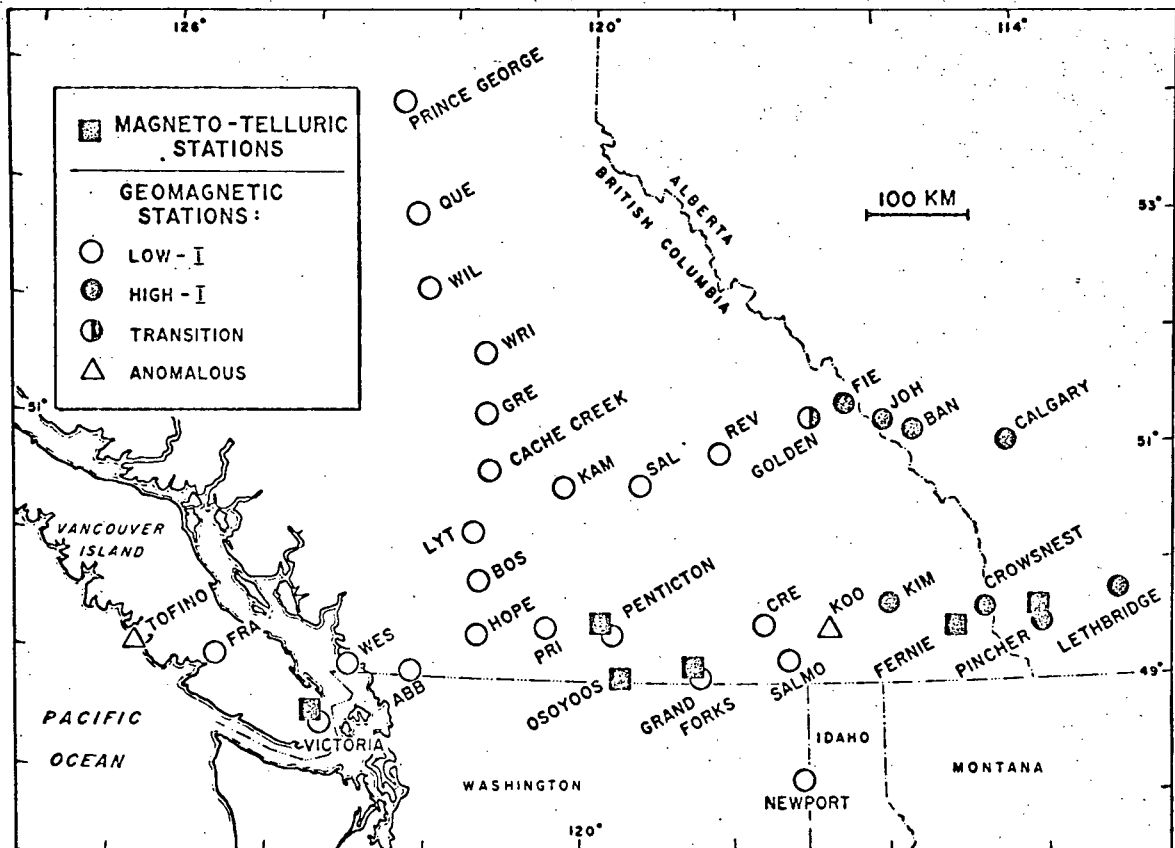


Fig. I-2. Location of GDS and MT stations in western Canada

The results from all the GDS and MT data have been combined to provide a reliable and self-consistent conductivity structure model for southwest Canada. Other relevant geophysical evidence has also been examined. Detailed analysis has been carried out on several long aeromagnetic profiles; the observed smoothing of long-wavelength features in the western region has been tied in with the geomagnetic induction results.

A self-consistent petrological model for the lower crustal and upper mantle structure has been derived to satisfy all the above data. It is shown that this is not a unique solution, since the order-of-magnitude uncertainties in the relations between conductivity, temperature, and composition preclude any such confidence in the petrological models.

I-D) Theory

A brief outline of the theory applicable in geomagnetic induction work is given below. The outline is based on the theoretical work of Price (1962) and Wait (1962), and is essentially an adaptation of subsequent developments by others (particularly Srivastava, 1965 and Whitham, 1963).

From the field equations for a general linear isotropic medium we can obtain expressions for the electric and magnetic fields within a conductor, for external inducing fields. Assuming $E_z = 0$, and neglecting displacement currents, these are:

$$\underline{E} = e^{i\omega t} Z(z) \left[\left(\frac{\partial P}{\partial y} \right) \underline{j}_x - \left(\frac{\partial P}{\partial x} \right) \underline{j}_y \right] \quad (1)$$

$$\underline{H} = -\frac{1}{i\omega} e^{i\omega t} \left[\frac{\partial P}{\partial x} \frac{\partial Z}{\partial z} \underline{j}_x + \frac{\partial P}{\partial y} \frac{\partial Z}{\partial z} \underline{j}_y + V^2 Z P \underline{j}_z \right] \quad (2)$$

V is a constant which defines the horizontal scale of the source field ($\lambda = 2\pi/V$), and the functions P and Z are defined by the following

relations:

$$\frac{\partial^2 P}{\partial x^2} + \frac{\partial^2 P}{\partial y^2} + V^2 P = 0 \quad (3)$$

$$\frac{\partial^2 Z}{\partial z^2} = [V^2 + 4\pi i \omega S(z)] Z \quad (4)$$

Consider a horizontally layered earth; within each layer of thickness h , the conductivity S is constant; the solution for (4) is:

$$Z = A e^{Uz} + B e^{-Uz} \quad (5)$$

where $U^2 = V^2 + 4\pi i \omega S$

Substituting (5) into (1) and (2) and taking the ratio, we obtain an expression for the "impedance" within the layer:

$$\frac{E_x}{H_y} = - \frac{i\omega}{U} \frac{A e^{Uz} + B e^{-Uz}}{A e^{Uz} - B e^{-Uz}} \quad (6)$$

$$\text{or } \frac{E_x}{H_y} = - \frac{i\omega}{U} \coth [Uz - \ln(A/B)^{1/2}] \quad (7)$$

Taking into account the continuity at the interfaces, the "impedance" in each layer can be expressed as a function of the impedance in the adjacent layer above it, and the "surface impedance" by a complex function of all "n" layers:

$$\left(\frac{E_x}{H_y} \right)_{z=0} = \frac{i\omega}{U_1} \coth \left\{ U_1 h_1 + \coth^{-1} \left[\frac{U_1}{U_2} \coth [U_2 h_2 + \dots \right. \right. \\ \left. \left. \dots + \coth^{-1} \left(\frac{U_2}{U_3} \coth (U_3 h_3 + \dots \coth^{-1} \frac{U_{n-1}}{U_n}) \right) \right] \right\} \quad (8)$$

with an identical expression (opposite sign) for the orthogonal set E_y/H_x .

The above equation (8) is the basic generalized formula for MT work, defining the impedance of an n-layer conductivity structure as a function of frequency. The curves of the observational parameter observed at the surface (E_x/H_y or E_y/H_x as a function of frequency) are compared to model curves for various assumed conductivity structures. More usually the "apparent resistivity", $\rho_a = 0.2(E/H)^2 T$, is plotted against period T .

The preceding theoretical development assumes diffusion of the electromagnetic field through the conductors. If plane polarized electromagnetic waves normally incident on the surface are assumed, the relations can be derived in a different way by using the transmission and reflection coefficients at the boundaries. The "Cagniard-type" curves thus derived are numerically equivalent to the special case of $V = 0$, i.e. infinite spatial wavelength, in the generalized equation.

In practice, it is found that the effect of finite sources ($V \neq 0$) becomes significant only for fairly extreme values ($V > 0.005 \text{ km}^{-1}$, i.e. $\lambda < 1000 \text{ km}$), and even then only for the longer-period range of most practical MT data sets. Below these periods, the two formulae ("diffusion" and "Cagniard") are numerically identical for all realistic values of V . It is therefore possible to use the much simpler Cagniard formulae for preliminary model fitting and for many-layer cases where the generalized equation becomes prohibitively complicated for computation. Nomographs for graphical solutions to "Cagniard" models are available (Fournier, 1965) and can be used for rough "first-guess" approximations, to be refined by comparison with published master curves (Srivastava, 1967), and finally by comparison with computer-generated model curves based on the generalized formula.

For interpretation of GDS data, the ratio H_z/H_y or H_z/H_x is the observational parameter. Substituting (5) into (2) and taking the ratio, we obtain:

$$\frac{H_z}{H_x} = \frac{V^2}{U} \frac{P}{\partial P / \partial x} \frac{A e^{Uz} + B e^{-Uz}}{A e^{Uz} - B e^{-Uz}} \quad (9)$$

Following the same procedure as before, the ratio H_y/H_x at the surface can be obtained for an n-layer conductivity structure:

$$\left(\frac{H_z}{H_x} \right)_{z=0} = \frac{P}{\partial P / \partial x} \frac{V^2}{U} \coth \left\{ U, h, \dots \quad \begin{array}{l} \text{same as} \\ \text{eq'n No. 8} \end{array} \right\} \quad (10)$$

This is the basic equation used for interpreting the GDS data in this report. The main difference between this expression and the one used for MT is the presence of the factor $V^2 P / \partial P / \partial x$. The MT expression (equation 8) is a fully explicit function of frequency (or period T), spatial wavelength, and conductivity structure parameters (h, S) at the site: $E/H = f(T, V, h, S)$. The GDS expression (equation 10) is of the form $Z/H = V^2 \cdot F(P) \cdot f^1(T, V, h, S)$, where $F(P)$ is not an explicit function of the station parameters. This difference emphasizes the main weakness of the GDS method when used for quantitative interpretation. The V^2 term indicates that the Z/H ratio is heavily affected along the entire frequency band by the value of the inducing field wavelength (whereas it affected only the long periods in MT). More serious is the fact that the term $F(P) = P / \partial P / \partial x$ is entirely indeterminate. The potential function P and its horizontal gradients can be determined only by data from a large-scale network of stations covering an area much larger than the conductivity structure being studied. Such analytic determinations from surveys using large numbers (20-40) of simultaneous stations are being planned (Gough and Reitzel, 1967). However, for the profile-type surveys

described in this work (4-8 stations), the factor $F(P)$ remains indeterminate. In practice, the method of analysis is therefore based on simultaneously recorded data from at least two stations, one representing the unknown conductivity structure, and one a "standardizing" station with (hopefully!) known conductivity structure (Whitham, 1963; Caner et al, 1967).

For such two-station work, the unknown term $V^2 \cdot F(P)$ drops out in the ratio:

$$\frac{(Z/H) \text{ Station 1}}{(Z/H) \text{ Station 2}} = \frac{f^1(T,V,h,S) \text{ Station 1}}{f^1(T,V,h,S) \text{ Station 2}} = \frac{Q_1}{Q_2} ;$$

this ratio can be evaluated as a function of T for various combinations of conductivity structure parameters at the two stations. In practice, interpretation is usually carried out on the squares of the above Q -factors, i.e. on the ratio $M = Q_1^2/Q_2^2$, partly by analogy with the traditional MT parameter $\rho_a = 0.2(E/H)^2 T$, partly for computational convenience when using power spectral components rather than Fourier amplitudes. It is clear that such "two-station" model fitting leaves far too much latitude for personal bias and other uncertainties, unless one of the structures is reliably known. It will also be shown that although the main V^2 term has been cancelled out, for many practical models the M -ratio in GDS is still more dependent on V than the apparent resistivity in MT.

The two formulae derived for the MT and GDS cases (equations 8 and 10) are very similar in structure, and their relation is in fact deceptively simple:

$$\frac{E}{H} = \frac{i\omega}{V^2} \cdot \frac{1}{P} \cdot \frac{\partial P}{\partial x} \cdot \frac{Z}{H} \quad (11)$$

The use of combined MT/GDS methods (i.e. recording of all 5 components simultaneously) would therefore seem to be the obvious way to overcome some of the ambiguities; since each set can provide independent interpretation, the redundancy of information in the combined data should provide a more reliable solution. For example, the above relation between E/H and Z/H could be used to evaluate the source field parameters. In particular, if the factor $P/\delta P/\delta x$ is independent of frequency (as has been assumed in most cases), the value of V can be derived directly.

Watanabe (1964) and Srivastava (1965) have suggested methods for deriving self-consistent models from such combined data. In practice, such "5-component" work runs into difficulties. For example, broadband MT information is usually obtained from different sets of data (short-period band, long-period band), not necessarily simultaneous, and therefore not necessarily possessing the same source-field parameters. Even if obtained during the same disturbance, there is no reason to presuppose that the shorter-period (say 10-100 sec) fluctuations are necessarily caused by the same generating mechanism as the longer-period (100-10000 sec) ones; there is in fact good reason to believe that this is not the case, as the spatial coherence of shorter-period fluctuations is far lower than that of long-period ones, indicating generating currents of smaller scale.

For the work described in this report, such self-consistent GDS/MT conductivity structure models were derived in a more pedestrian manner dictated by practical considerations (mainly the non-simultaneity of most of the GDS and MT surveys). The MT models for certain areas were derived separately, with the maximum amount of internal control (clustering of stations, etc.); the GDS model curves for these structures were then computed and compared to the observed GDS data for these areas. If

necessary, the MT models were then readjusted until satisfactory agreement could be reached.

All the above theoretical developments assume homogeneous horizontally stratified structures, and of small enough scale so that the sphericity of the earth can be ignored. The assumption of homogeneity can be checked experimentally for each set of data: in MT, apparent resistivities must be equal in the two orthogonal directions, i.e. $E_x/H_y = E_y/H_x$ for all frequencies; in GDS, the ratio $Z/(H_x^2 + H_y^2)^{1/2}$ must be independent of the azimuth of the inducing field vector, i.e. of the ratio H_x/H_y . Reliable analytic methods for handling non-isotropic data are as yet not available. In MT some special cases of faults and dikes have been worked out with some simplifying assumptions; in GDS, such attempts have been disappointingly unsuccessful in providing reasonable interpretation (see for example Rikitake and Whitham, 1964). Although the direction of the anisotropy axes can usually be derived from both MT (Bostick and Smith, 1962) and GDS (Parkinson, 1962) anisotropic data, the determination of conductivity structures remains unreliable, in spite of the increasingly complex and elegant computational methods which are being used to process the anisotropic data. Even more embarrassing is the fact that MT anisotropies at various "apparent depths" are found in areas where no such anisotropies are shown by GDS.

In view of the above limitations, the quantitative work described in this report has been restricted as far as possible to isotropic data. Since the primary purpose of the work is practical determination of conductivity structure, such an approach is justified. It simply means choosing ones experimental conditions intelligently in order to minimize analytical difficulties and the resulting uncertainties in interpretation.

In practice, this means avoiding a) analysis on data from stations with known anisotropies (such as Kootenay Lake), and b) siting of new MT stations in the vicinity of known boundaries between conductivity structure regions. Since the particular structure being studied covers an area of continental proportions, there is no difficulty in satisfying these simple restrictions on station choice.

The term "anisotropic" as used in this thesis refers only to data, i.e. to an azimuth-dependence of the observational parameter. The term "inhomogeneity" is used for actual conductivity structures in the earth. These are somewhat arbitrary semantic definitions, since "inhomogeneity" as used here would result from both anisotropic conductivity media and structural inhomogeneities such as faults or dykes.

II. MAGNETO-TELLURICS

II-A) Introduction

GDS mapping has defined a clear distinction between two regions in Canada, with the discontinuity following roughly the line of the Rocky Mountain Trench. The GDS data have been shown to be compatible with the existence of a conducting layer about 15 km. thick at depth about 25 km., i.e. in the lower crust or upper mantle (Caner et al, 1967). However, profile-type GDS surveys do not lend themselves readily to quantitative interpretation - although they are ideally suited for large-scale mapping. The observational parameter (Z/H , the ratio of vertical to horizontal amplitude) is not an explicit function of the subsurface conductivity structure parameters. Unless a wide station network is available to permit separation of internal and external fields, interpretation has to be carried out on the data obtained simultaneously at two stations, in order to eliminate the unknown terms. The use of two assumed

conductivity structures for model fitting leaves an unacceptably large amount of latitude for personal bias; for all practical purposes the solution is indeterminate unless the conductivity structure is known for at least one of the stations.

By contrast the MT method provides results which can be interpreted for a single station with only the usual amount of personal bias, i.e. in the choice of the particular models to be checked against the observational data. Although the method has many disadvantages compared to GDS, such MT observations at a number of selected sites can therefore be used to "calibrate" the GDS results for a particular region. The MT survey described in this paper was deliberately designed to provide such calibration for the GDS results in western Canada. A similar MT survey was carried out in the southwest U.S.A. by Swift (1967). Most of the MT data previously obtained in western Canada covered only the shorter periods (< 1000 secs.) and are therefore inadequate to provide information at the lower crustal and upper mantle depths required for calibration of the GDS data. Longer-period data sets were obtained at Meanook in northern Alberta (Niblett and Sayn-Wittgenstein, 1960; Srivastava and Jacobs, 1964) and at Victoria (Caner and Auld, 1968). However, both these sites are too far from the areas of direct interest and not representative of the main regions in other ways (proximity to source currents at Meanook, and possibly coastal effects at Victoria).

The stations used in this survey (Figure II-1) were not laid out in profiles to cover maximum area, since the region had already been thoroughly mapped by GDS. Instead, they were clustered in two groups: one cluster of three stations in the western region (Penticton, Grand Forks, Osoyoos) and one cluster (Pincher, Fernie) in the eastern region. In

addition, data from the Vulcan station of Vozoff and Ellis (1966) has been used in support of the eastern cluster. The stations were located in areas known (from GDS mapping) to be "normal", i.e. not in the immediate vicinity of deep-seated anisotropies or of the main discontinuity between the two zones.

The purpose of this clustering is to improve the reliability of the derived conductivity structure models. The interpretation of MT data usually suffers from a number of ambiguities: surface layer effects, anisotropies, and to a lesser extent source field wavelengths. By recording simultaneously in a closely spaced cluster, some of these ambiguities can be eliminated. Clearly the models for the stations within each cluster must agree within reason for depths greater than their separating distance, and for simultaneously recorded disturbances must use the same source field parameters. By combining the results from several stations, restraints are imposed on the solution which minimize the influence of personal bias. In addition it can be expected that some stations would show anisotropic characteristics, i.e. the observed apparent resistivities are a function of azimuth. The treatment of anisotropic data presents one of the main difficulties in the interpretation of MT data. Theoretical treatments for such data have been worked out (for example Bostick and Smith, 1962; Wiese, 1965; O'Brien and Morrison, 1967), but their practical value has not been verified experimentally. By recording in clusters within a region known to be homogeneous below upper crustal depths, the treatment of any anisotropic data from one station can be verified experimentally by comparison with data from the other stations (hopefully isotropic) within the cluster.

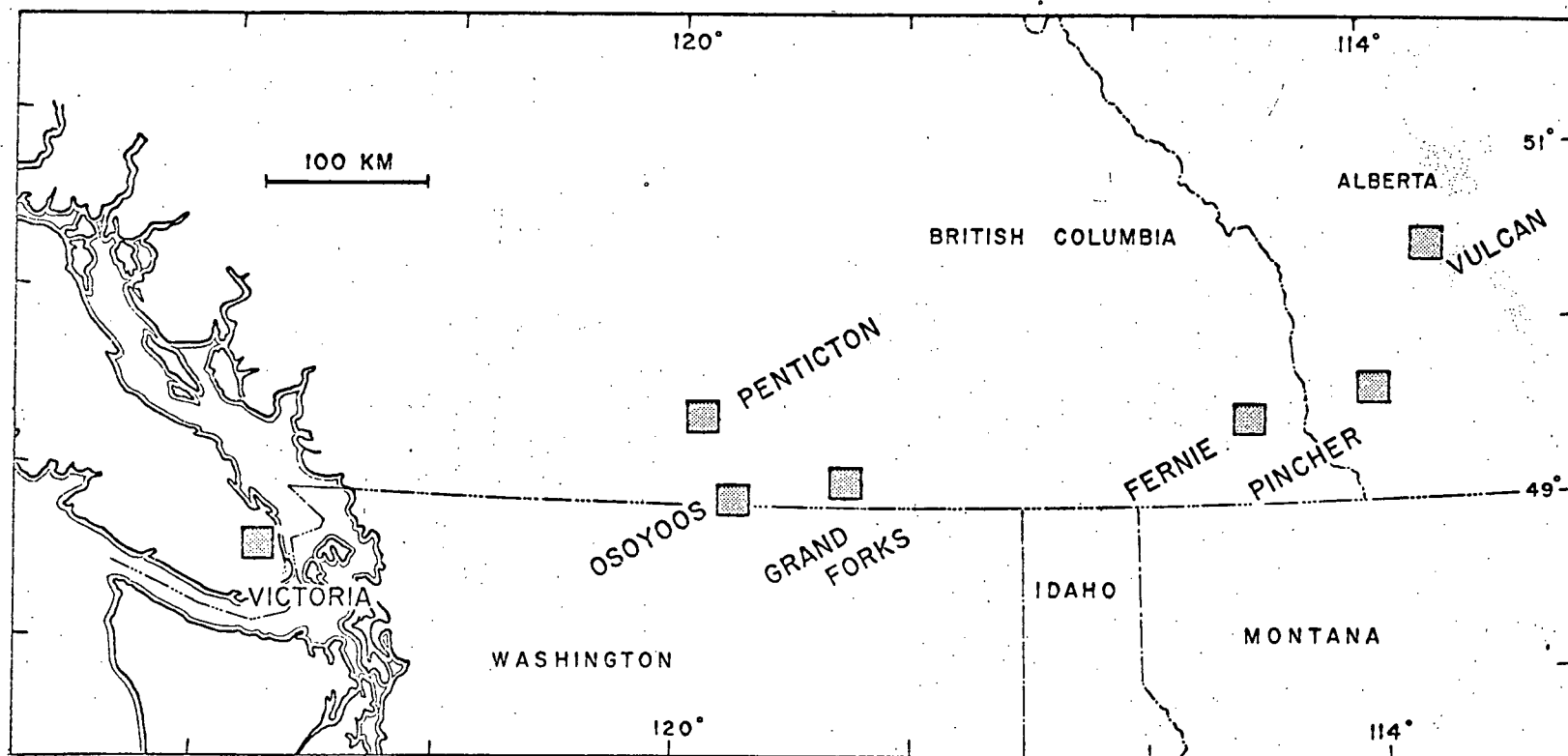


Fig. II-1. Location of MT stations covered in Chapter II, as well as the Vulcan station of Vozoff and Ellis (1966) and the Victoria station of Caner and Auld (1968).

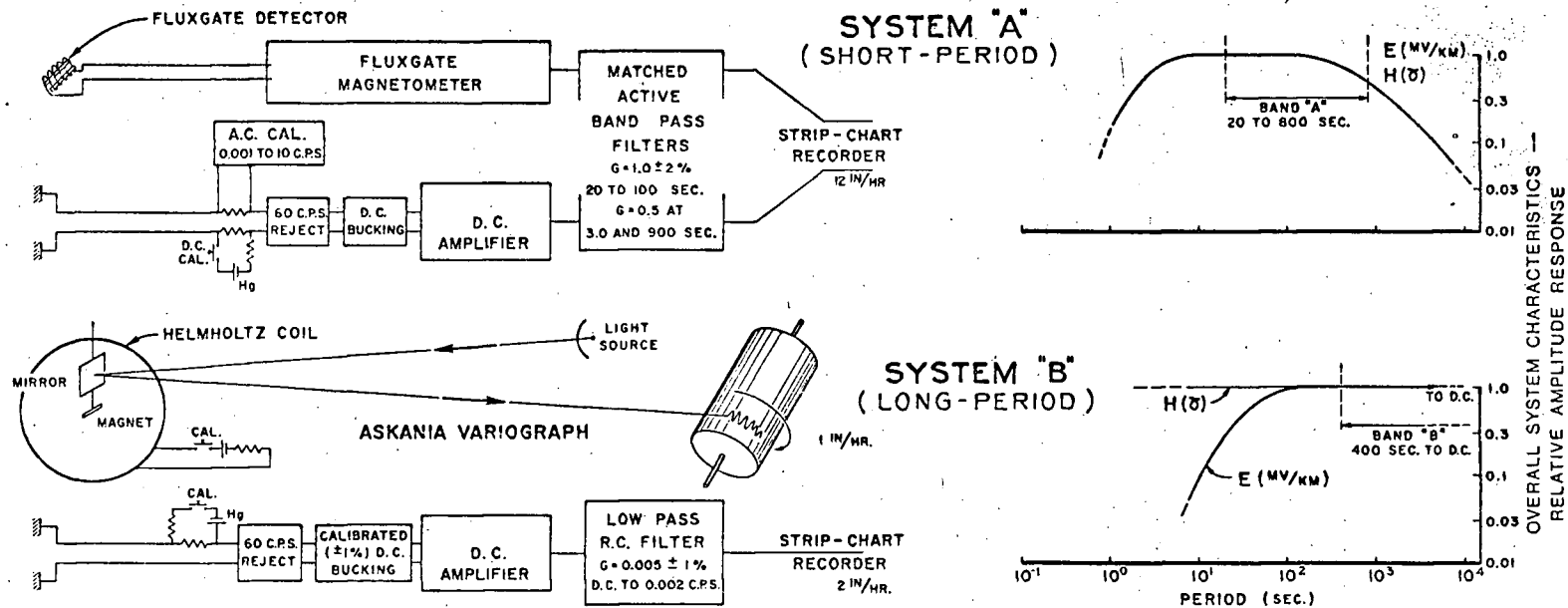


Figure II-2. Schematic lay-out and frequency response of MT instrumentation used at Pincher and Pentiction.

II-B) Instrumentation

Within each cluster one station was considered as "primary" (Pincher in the east, Penticton in the west), and took priority in the allocation of equipment, servicing, and installation quality (length of telluric lines in particular). The equipment used at these two stations is shown schematically in Figure II-2. Two separate systems were used for the magnetic components: portable three component Askania GV-3 variographs for the long-period band (DC to 400 sec. period), and three-component fluxgate magnetometers for the short-period band (800 to 20 sec. period). The latter is a portable transistorized version of Serson's (1957) station magnetometer. The same telluric system was used for both frequency bands. The electrodes were formed by lead plates (2' x 2') buried at depths of about 5'; contact resistances were negligible in comparison to the input impedance of the amplifiers. The telluric systems were aligned in magnetic coordinates, E_{NS} or E_X and E_{EW} or E_Y , i.e. rotated 21-22° clockwise of geographic coordinates. This provides orthogonality with the recorded magnetic components D (magnetic east west) and H (magnetic north south). Line lengths varied between 400 and 700 meters at the secondary stations and between 860 and 1000 meters at Pincher and Penticton. The telluric signals were amplified by Medistor type A-61RB DC microvoltmeter amplifiers, modified for MT work by inclusion of calibration circuits and 60 Hz rejection filters (see Figure II-2). Filters were used to shape the amplifier output for the two frequency bands.

The same basic equipment was used at the secondary stations (Ferne and Grand Forks), with the following exceptions: a) Medistor amplifiers were not available for the tellurics, and comparable circuits constructed in the laboratory were used; b) no Askania variographs were operated, and

apparent resistivities in the long-period band were computed using the magnetic data from the nearest primary station. As will be shown later, the horizontal magnetic components at these long periods are homogeneous over long distances and can be considered constant in amplitude over the short distances between the primary and secondary stations (< 100 km) within each cluster.

At the fifth station (Osoyoos) no magnetic detectors were available, and all apparent resistivity data (long and short period bands) were computed using the magnetic data from Penticton or Grand Forks. Since the short-period fluctuations cannot be reliably assumed constant even over these short distances, the accuracy of the short-period data at Osoyoos is therefore not very high. In addition, some difficulty was encountered in aligning the telluric lines in the magnetic coordinate system. The station was located on a plateau on top of Mount Kobau, at altitude 6000 ft., and because of topographical limitations, the telluric lines had to be misaligned by 15° with respect to magnetic coordinates. All telluric data were therefore derived by computational axis rotation, adding to the inaccuracies at this station.

The long-period equipment was operated continuously at all stations for the entire seven-week duration of the survey (May 17 to July 7, 1967). Only two sets of short-period equipment were available, and these were shifted halfway through the survey to provide about 3 weeks operation at each station. An attempt was made to extend the data to the diurnal fluctuations (24, 12 and 8 hour periods), hence the relatively long telluric lines and deeply buried electrodes at the two primary stations. The attempt was unsuccessful, as no uninterrupted recording of sufficient duration (say > 10 days) could be obtained. Apart from accidental interruptions (line breakages or equipment failures), the dynamic range

of the telluric recording systems was insufficient to accommodate both the high sensitivities required for the measurement of the diurnal fluctuations (of the order of 0.5 mv/km), and the requirements for continuous "on-scale" range during major disturbances with excursions exceeding hundreds of mv/km.

II-C) Data

An example of a section of long-period recording is shown in Figures II-3a and II-3b, for a disturbance recorded simultaneously at all stations. Scale bars are 50 gamma or 25 mv/km, and all components are plotted to the same scale except Fernie E_Y . The coherency between the electric and orthogonal magnetic components is generally very good, although in visual comparisons the rapid fluctuations are over-accentuated in the telluric traces and tend to obscure the longer-period features which are more prominent in the magnetic traces. A comparison of the horizontal magnetic components (D and H) between Penticton and Pincher (400 km apart) indicates the spatial uniformity of the horizontal field for long-period variations, and justifies the use of the amplitudes from primary stations for computations of apparent resistivity at secondary stations less than 100 km distant. A third Askania variograph was also operated simultaneously at Salmo, about half-way between the two clusters, and confirmed the uniformity of the horizontal field over the region.

An example of sections of short-period recording is shown in Figure II-4; these are not simultaneous at any of the stations. At the two primary stations, PIN (Pincher) and PEN (Penticton), visual coherence between the telluric and magnetic traces is still good, although not as clear as for the longer-period data. At the secondary stations, the recordings are of poorer quality; some of their limitations will be

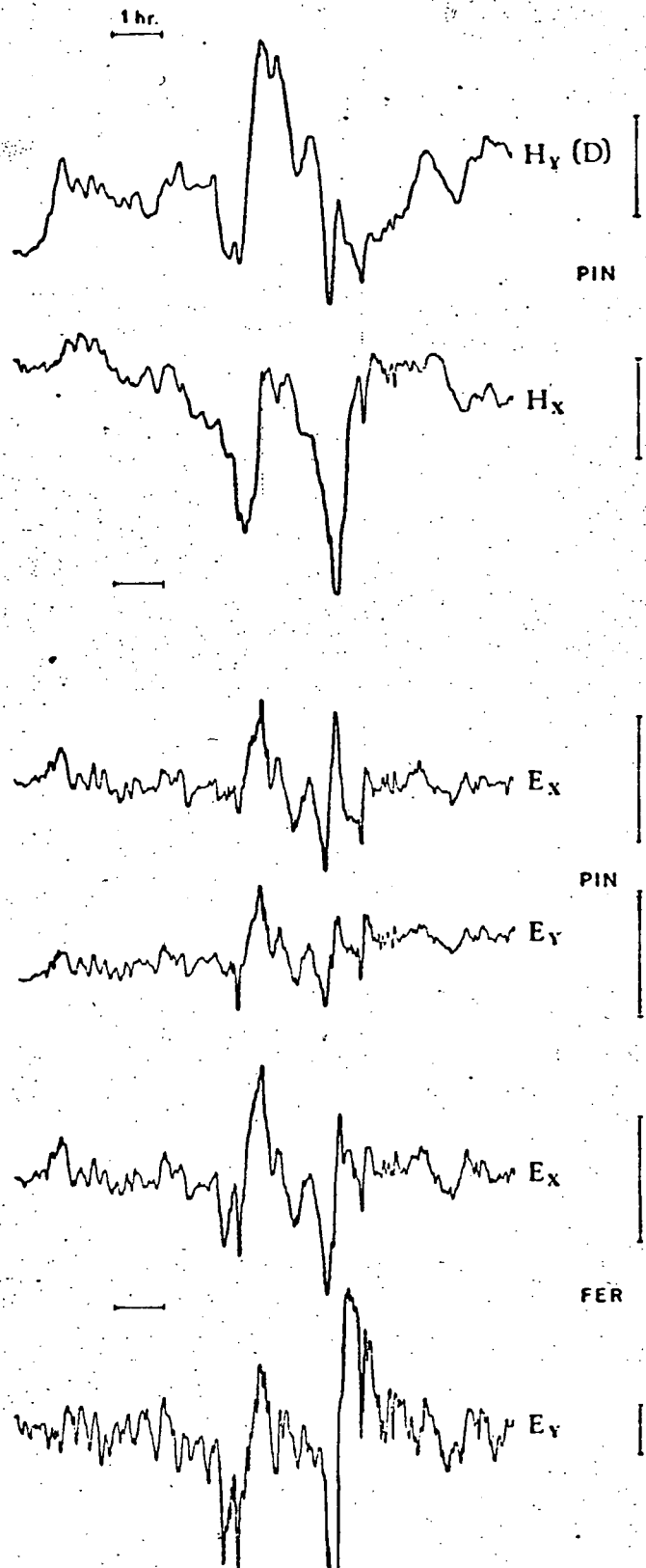


Fig. II-3a. Section of simultaneous MT recording in the long-period band, eastern stations. Scale bars are 50 gamma or 25 mv/km, and all traces are plotted to same scale except Fernie E_y.

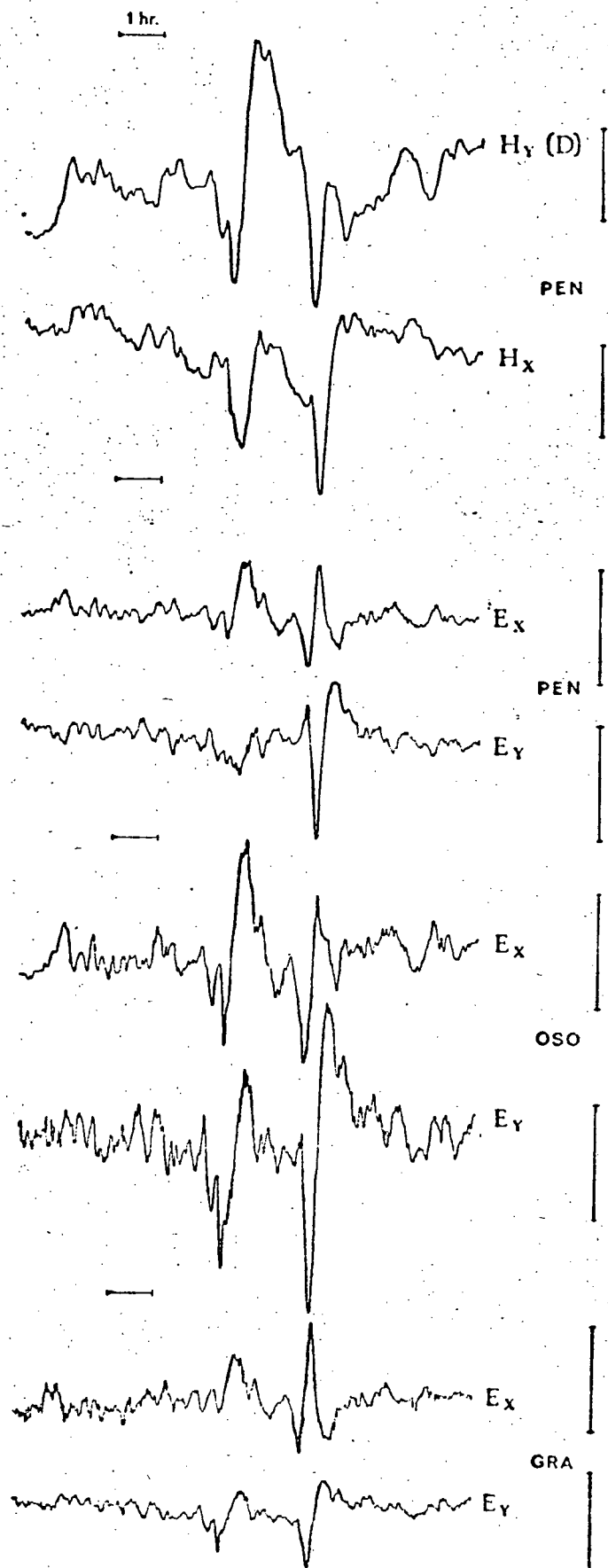


Fig. II-3b. Section of simultaneous MT recording in the long-period band, western stations. Scale bars are 50 gamma or 25 mv/km, and all traces are plotted to same scale.

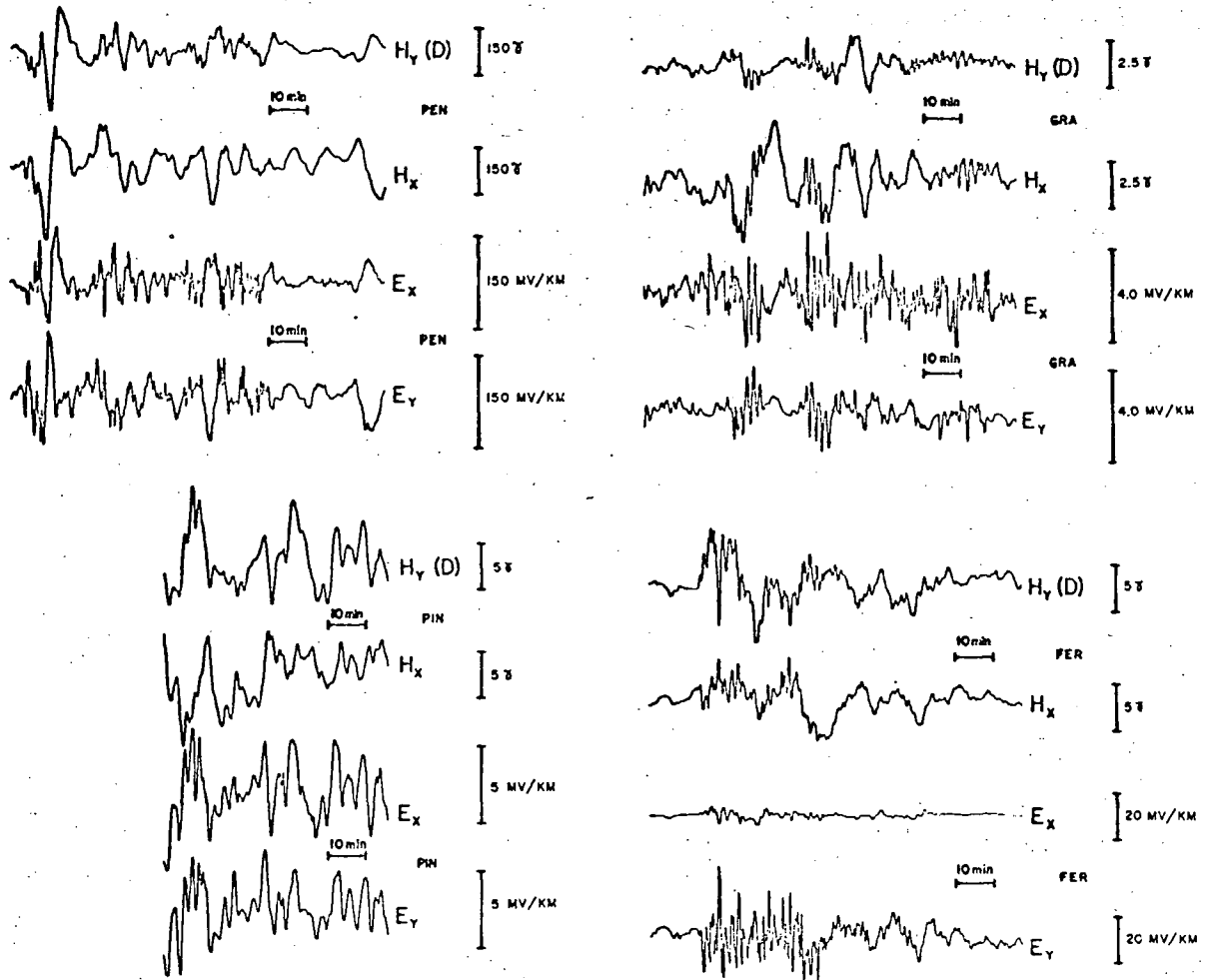


Fig. II-4. Sections of MT recordings in the short-period band.

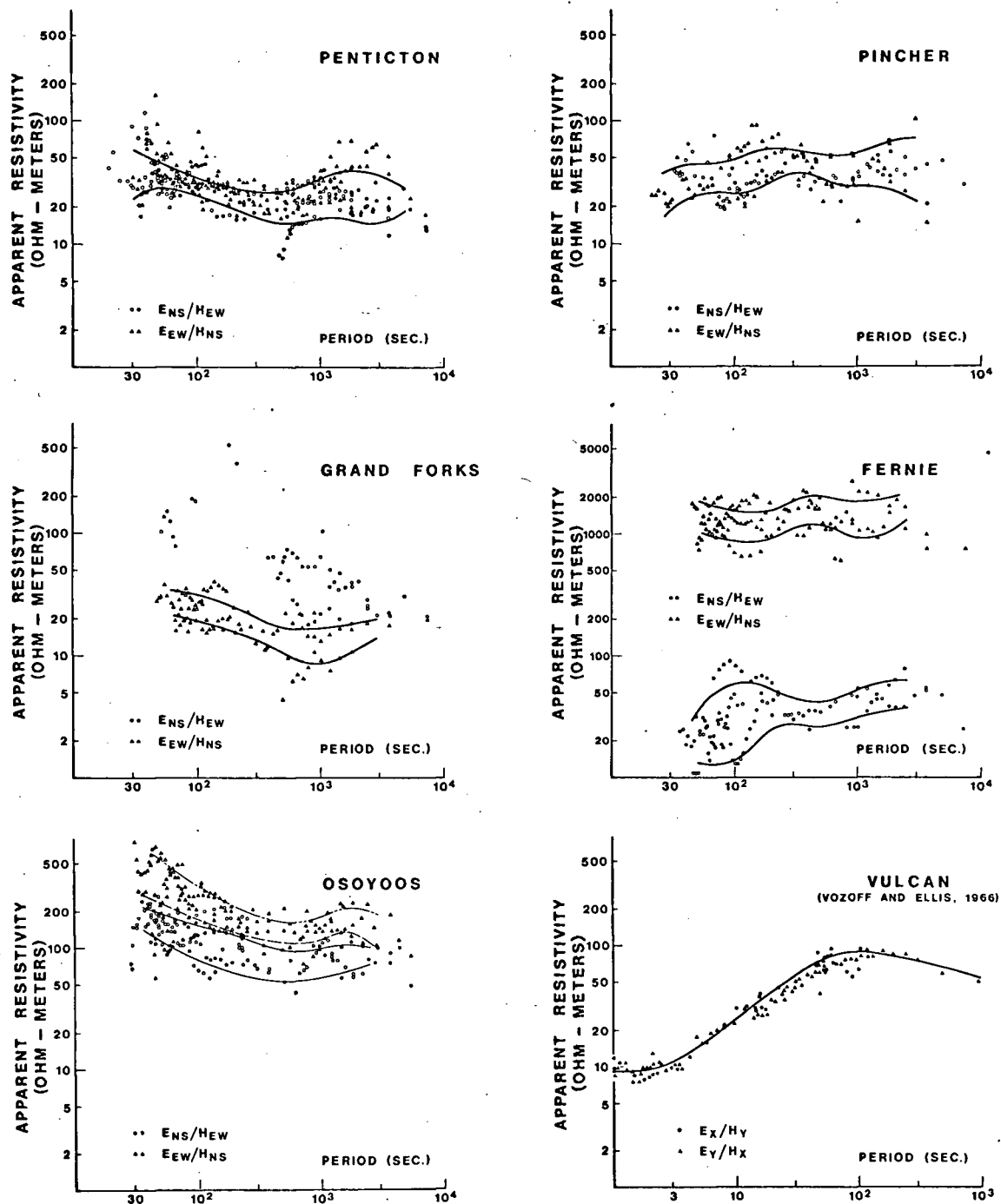


Fig. II-5. Apparent resistivity plotted as a function of period for all stations. Note different resistivity scale for Fernie, and different period scale for Vulcan.

discussed further on.

Selected sections of record from all stations were digitized for processing, using either commercial services or a Dobbie-McInnes Pencil Follower. The digitizing interval for the long-period band (originally recorded at 1 or 2 in/hr) is 72 seconds. For the short-period band (recorded at 12 in/hr), the digitizing interval is 6 or 15 seconds, although some sections were digitized at closer intervals in an unsuccessful attempt to extract information for periods below 10 seconds. The resulting time series varied in length between $N = 500$ and $N = 1500$ data points. At least three series for each band were used at each station for each of the four components. A total of 122 time series were used in the analyses. The time series were processed using routine power spectral techniques (Blackman & Tuckey, 1958), and apparent resistivities computed as a function of period: $\rho_a = 0.2 (E/H)^2 T$.

The plots of apparent resistivity as a function of period are shown in Figures II-5, a to f. Only data points for which the coherency between orthogonal E and H exceeded 0.75 have been included; points for which it exceeded 0.95 are identified by solid symbols. For the Vulcan data of Vozoff and Ellis (1966) all points shown are for coherency $R > 0.90$. On each plot are also drawn smoothed bands of mean \pm standard deviation; these have been computed using triple weighting for the high-coherence ($R > 0.95$) points. These plots are discussed separately for each station:

Pincher. An adequate amount of data were collected between 20 and 7000 sec. periods. The data are isotropic, i.e. apparent resistivities computed from E_{NS}/H_{EW} fall within the same range as those computed from E_{EW}/H_{NS} ; this permits interpretation using simple, horizontally layered, conductivity structure models.

Vulcan. The data points shown have been replotted from Vozoff and Ellis (1966); the data are also isotropic. The solid curve represents their interpretation of these data: a sedimentary surface layer of thickness 3.6 km, a resistive upper crust (1000 ohm-meters), and a conducting zone (30 ohm-meters) starting at depth 35 km.

Fernie. The data are highly anisotropic, with apparent resistivity ratios of about 1:50 between the two axes (i.e. telluric amplitudes in the EW direction about 6-8 times higher than those in the NS direction).

Fortuitously the observational axes coincide with the principal axes of the anisotropy; polarization plots in both frequency bands show a highly eccentric telluric ellipse, the major axis coinciding with the observational EW axis (Fig. II-6). Interpretation can therefore be carried out directly in the principal directions of the anisotropy, without computational axis rotation.

Penticton. A large amount of coherent data were collected in all components, including some good data at very long periods (to 7500 secs). The data are isotropic and can be interpreted with horizontally-stratified conductivity structures.

Grand Forks. The location was found to be very noisy, mainly atmospheric electric discharges, but possibly including industrial interference and amplifier noise as well. The E_{NS} component in particular was almost never free of noise. A reasonable amount of data were collected for the E_{EW}/H_{NS} set, but only a few widely scattered points were obtained from E_{NS}/H_{EW} . Superficial consideration of the data points in Figure 5 might indicate some anisotropy. However, the gradual convergence of the E_{NS}/H_{EW} points towards the E_{EW}/H_{NS} band at long periods is more consistent with the assumption that the E_{NS} data are dominated by short-period noise. If

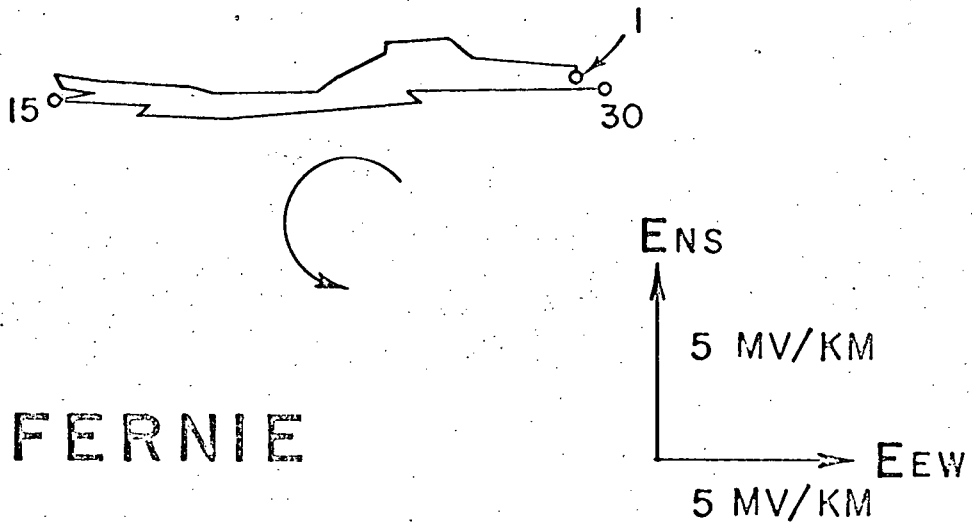
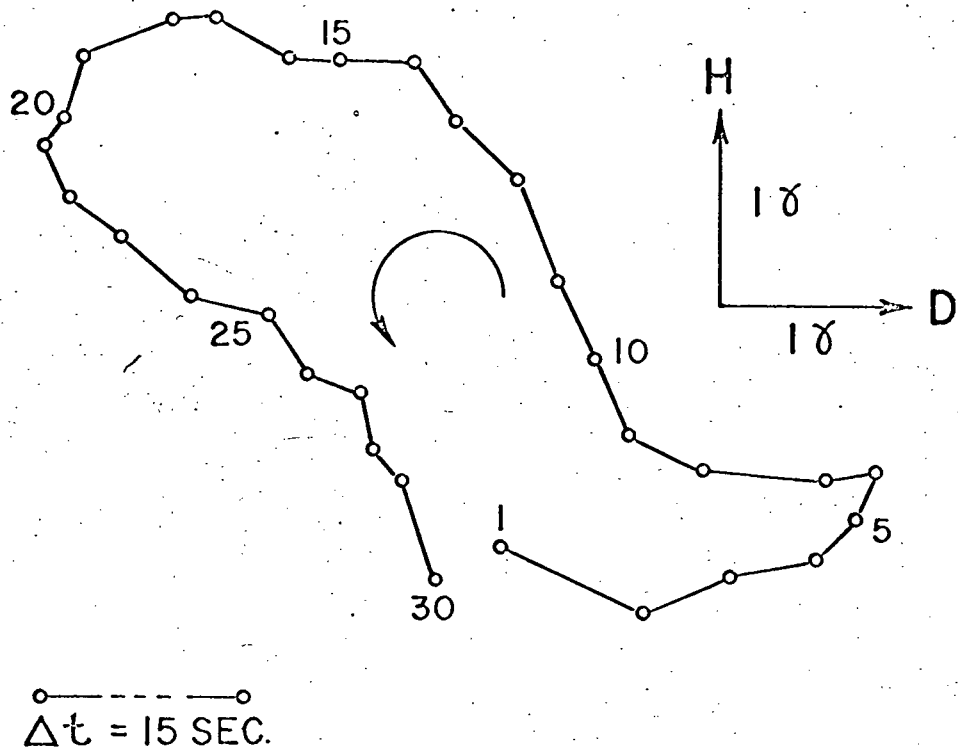


Fig. II-6. Polarization plot at Fernie.

appropriate filtering is applied to prevent spectral leakage from shorter-period noise, the long-period (> 1000 sec) E_{NS} data are in fact shifted slightly downwards into the E_{EW} band. No filtering was found practicable for the shorter-period data. Interpretation was carried out on the E_{EW}/H_{NS} data alone, on the assumption that it is representative of both components of an isotropic set.

Osoyoos. The Osoyoos data is apparently anisotropic, with apparent resistivities in the EW direction higher by a factor of about two than those in the NS direction (a factor of about 1.2 - 1.4 difference in the amplitudes of telluric components). Since no magnetic components were recorded at this site, computational tensor analysis could not be attempted. In any case it is doubtful if the difference is significant in view of the low quality of the site, with the somewhat greater uncertainties in line-length measurements, significant electrode altitude differences (i.e. possible contributions from vertical telluric components), and edge effects caused by the proximity of the electrodes to the sharp altitude drop-offs from the mountain-top plateau. The observed difference (factor of about 1.2 - 1.4) is frequency independent, and is well within the possible range of combined inaccuracies in the two components caused by the above effects.

II-D) Interpretation - Eastern Stations

Model curves for different conductivity structures have been fitted to the experimental data, using the formulas of Srivastava (1965, 1967). These are based on Wait's (1962) and Price's (1962) theory, involving finite horizontal wavelengths for the inducing magnetic fields (see Section I-D). In practice, for almost all the cases reported in this paper, the results were indistinguishable from those which could have been obtained from the simpler Cagniard (1953) plane-wave theory, i.e. using infinite spatial wavelengths; this confirms Madden and Nelson's

(1964) analysis of the difference between the two methods.

The Pincher data can best be considered in conjunction with the Vulcan data of Vozoff and Ellis (1966) - see Figure II-7a. The frequency ranges of the two data sets are complementary, and since the two stations are only 110 km apart, the major deep structural features should be the same at the two sites. The heavy line (Model 72) on the Vulcan data of Figure II-7a represents the original interpretation of Vozoff and Ellis (1966): a sedimentary surface layer of thickness 3.6 km, a resistive upper crust of thickness 35 km, and a "base" resistivity of 30 ohm-meters. The surface layer was composed of three distinct layers, using information from oil-well conductivity logs; for purposes of fitting long-period models it can be replaced by a single layer of same overall thickness (3.6 km) with an equivalent integrated resistivity of 16 ohm-meters.

Oil-well logs in the Pincher area were examined, and the two deepest wells (one 4.8 km deep 15 km to the SW, and one 4.1 km deep 15 km to the SE) did not penetrate the basement rocks. We have assumed a thickness of 4.8 km for the sedimentary surface layer; for this thickness an integrated resistivity of 11 ohm-meters is required to fit the data. From the point of view of fitting models to long-period data this assumption is arbitrary, since completely equivalent models can be constructed using different combinations of thickness and resistivity for the surface layer.

Model 82 on Figure II-7a represents a good fit to the Pincher data, in reasonable agreement with the Vulcan model. The slight discrepancy in the depth to the conducting layer (35 km at Vulcan, 30 km at Pincher) can readily be resolved: a) it could be real; a dip of 5 km over a distance of 110 km is quite reasonable, particularly since MT data from stations

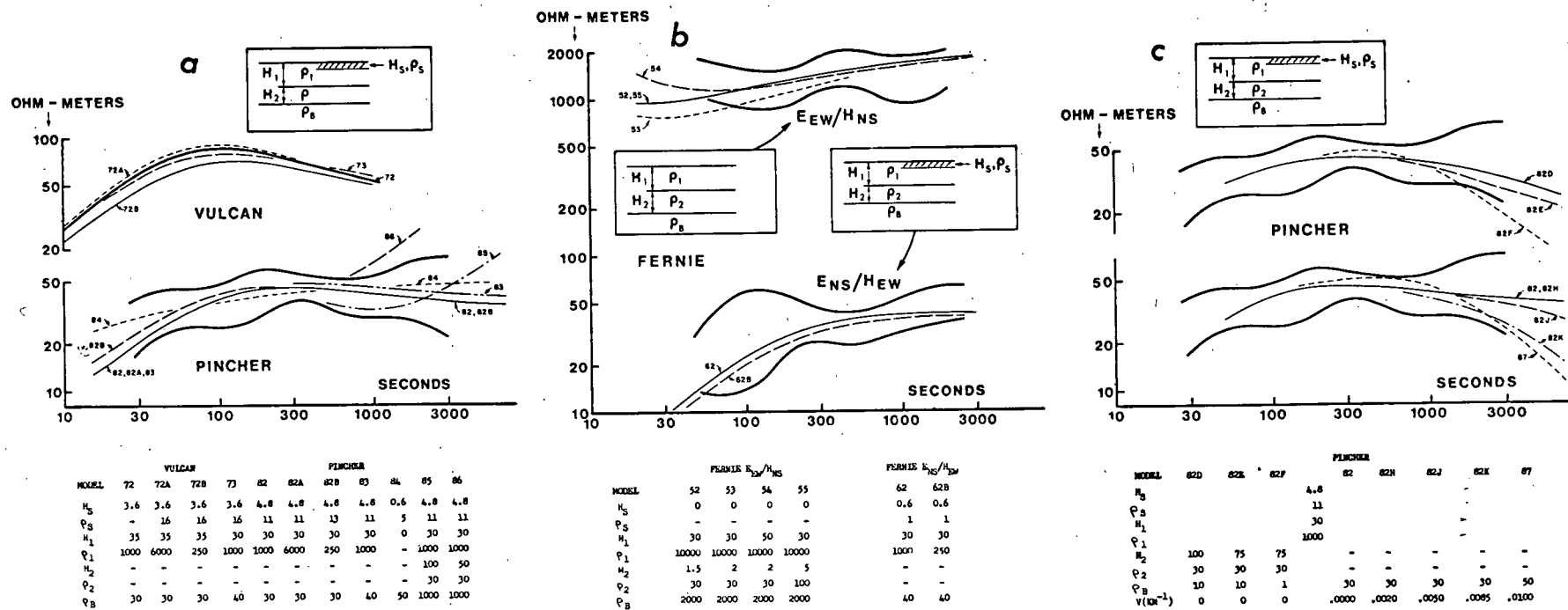


Figure II-7. Conductivity structure models, eastern stations.

further north and east indicate even greater depths (Vozoff and Ellis, 1966; Niblett and Sayn-Wittgenstein, 1960); b) the short-period data at Vulcan does not provide high resolution for depths and can easily be reinterpreted; for example, Model 73 provides as good fit to the Vulcan data as Model 72, and is in exact agreement with Model 83 at Pincher (conducting layer of resistivity 40 ohm-meters starting at depth 30 km).

A resistivity of 1000 ohm-meters has been assigned to the upper crustal layer for all the above models. This chosen value is flexible within fairly wide limits. For example, Model 82A (resistivity 6000 ohm-meters) is indistinguishable from Model 82 (1000 ohm-meters); Model 82B (resistivity 250 ohm-meters) can also be accommodated with only slight changes in surface layer parameters. In fact the Pincher data by itself can be fitted without any resistive upper crust at all: Model 84 for example, with material of resistivity 50 ohm-meters starting right below a thin surface layer. It is only inclusion of the shorter-period data from Vulcan which clearly indicates the existence of a resistive upper crust, but even these short-period data cannot resolve the actual resistivity value in this layer. For example, Model 72A (6000 ohm-meters) is barely distinguishable from Model 72 (1000 ohm-meters); even Model 72B (250 ohm-meters) can be accommodated, although barely so, by some adjustments in surface layer parameters. Consequently, the combined Vulcan/Pincher data can be satisfied by any upper crustal resistivity value above about 250 ohm-meters, without any upper limit. Although most MT models have been constructed with values of 1,000 or 10,000 ohm-meters for the upper crustal layer, it should be clearly understood that this is simply a convenient choice representing a wide range of possible values. This lack of resolving power for high-resistivity layers is inherent in almost all MT data, even though not always explicitly

recognized. Even short-period data cannot provide adequate resolution if obtained over conductive surface layers, as is the case for Vulcan and for the vast majority of published MT data. Only short-period data (1 - 2 second periods) obtained directly over the resistive medium (for example, Cantwell and Madden, 1960; Caner and Auld, 1968) can define its resistivity value. If the shortest periods are attenuated by a conductive surface layer, this resolution is lost; for periods over 10 sec these relatively thin resistive layers are virtually transparent (for example, for periods of 10 and 100 seconds, the electromagnetic skin depth in material of 1000 ohm-meters is 50 and 160 km respectively).

Moving to the Fernie data (Figure II-7b) we are faced with the difficulty of interpreting the strongly anisotropic data. As previously explained, the two sets of curves represent the apparent resistivities in the two "principal" directions, i.e. parallel and perpendicular to the axes of a presumed inhomogeneity in subsurface conductivity structure. The mathematical methods developed for handling anisotropic data have been applied mostly to relatively short-period data (<10 - 100 sec periods), and could be explained by anisotropies or structural inhomogeneities in the surface or upper crustal layers, presumably on the assumption that the two apparent resistivity curves converge at much longer periods. Although such an approach may be valid for converging curves, it is difficult to justify for curves which remain separated at very long periods. Inhomogeneities can reasonably be expected in the sedimentary surface layers and upper crustal rocks, but become progressively more difficult to conceive as the depth increases. Structures required to interpret highly anisotropic long-period data such as that of Figure II-7b

strain the credibility, particularly since no deep-seated anisotropies are indicated by GDS. It is therefore the author's view that such drastic broad-band anisotropies with parallel curves and no GDS confirmation have a more trivial origin: an anomalous surface distortion of the telluric currents, in effect a "measurement error" caused by poor sampling (electrodes too shallow, lines too short, unsuitable surface medium, etc.). This view is strengthened by the fact that in these cases (see for example the Victoria data, Caner and Auld, 1968) the two curves are practically parallel along a very wide frequency range; a fixed multiplying factor applied to the amplitudes of either one of the measured E components brings the two curves into agreement along the entire frequency range.

The Fernie data provides an excellent opportunity to test this particular type of anisotropic data. The area has previously been mapped by GDS, and we know that there are no major conductivity inhomogeneities at lower crustal depths. The Fernie location was bracketed by two normal (i.e. isotropic) GDS stations: Kimberley 55 km to the west and Crowsnest 40 km to the east. Simultaneous recordings of the same type (eastern, high Z) were obtained at Pincher Creek and Lethbridge (Hyndman, 1963). Both Pincher and Fernie therefore lie within the horizontally-stratified eastern region; constraints should therefore be applied to the choice of models so that reasonable structural similarity is maintained between the two sites.

The data for the major principal direction of the anisotropy (EW, upper curves on Figure II-7b) can readily be interpreted by a uniform medium of resistivity 1200-1500 ohm-meters, with or without a thin conducting surface layer, and extending to at least 400 km in depth.

Clearly such an EW structure is unacceptable in view of the models derived for Pincher, 70 km to the east and within the same conductivity structure zone. If we look for a layer of conductivity 30 ohm-meters at depth 30 km as indicated at Pincher and Vulcan, we find that for Fernie EW it cannot exceed 1.5 km in thickness (Model 52); Model 53, with thickness 2 km, is already outside the acceptable range. If we assume a difference in depth, i.e. that the conducting layer has dipped from 30 km at Pincher to 50 km at Fernie, a layer as thick as 2 km of 30 ohm-meters can be fitted to the data (Model 54). If we accept a moderate change in resistivity for the conducting layer, say 100 ohm-meters instead of 30, a layer thickness of 5 km at depth 30 km becomes acceptable. (Model 55, indistinguishable from Model 52). If we accept both changes in depth and resistivity, a thickness of up to 7 km could be acceptable for a layer of resistivity 100 ohm-meters at depth 50 km. It is clear that not even remotely acceptable agreement can be found between the Pincher/Vulcan Models and the Fernie EW data. Models 85 and 86 on Figure II-7a show that the thickness of the conducting layer (30 - 40 ohm-meters) at Pincher must be at least 75 km if it is underlain by resistive material. Although moderate changes in the parameters of a conducting layer can be accepted over the 70 km distance between Pincher and Fernie, it is inconceivable that its thickness could have pinched out from over 75 km to less than 5 km over such a short distance - particularly since the GDS mapping shows no discontinuity in this region.

No such difficulty is encountered in finding agreement between the Pincher/Vulcan models and the Fernie NS data (lower set of curves on Figure II-7b). Models 62 and 62B both fit the data, in exact agreement with

Models 73 at Vulcan and 83 at Pincher. The postulated surface layer (0.6 km of 1 ohm-meters) is of course entirely arbitrary, since no nearby well-logs or stations with very short-period MT data are available; the results would be unchanged by the assumption of entirely different surface conditions with roughly the same ratio H_s/ρ_s . The resistivity of the upper crust is also indefinite, as for the Pincher models, and any value above about 250 ohm-meters could fit the data.

An inordinate amount of effort appears to have been spent on detailed discussion of the Fernie data. From the primary point of view of this survey, i.e. determination of conductivity structure in a particular region, it adds only moderate support to the Pincher/Vulcan models. However it is of more general interest as an experimental check on the treatment of highly anisotropic data of a particular type (broadband parallel curves). It confirms that only one of the curves has real physical meaning (apparently the minor principal direction). The other curve (major principal direction) represents an artificial enhancement of the measured telluric signal, probably by anomalous concentrations of currents by surface features. It is very difficult to express this analytically, but it indicates that unless anisotropies are also demonstrated by GDS data, long-period anisotropic MT data do not necessarily prove the existence of a real inhomogeneity at depth.

To summarize, the data at the eastern cluster (Pincher, Vulcan, Fernie NS) can be fitted by the following conductivity structure model: an arbitrary conducting surface layer, a resistive layer (> 250 ohm-meters) of thickness 30-35 km, underlain by material of resistivity 30-40 ohm-meters (possibly as high as 50 ohm-meters). The thickness of this conducting zone is uncertain, but lower limits can be derived

from the Pincher data (Figures II-7a and 7c). No drastic changes in resistivity (increase to 1000 ohm-meters, Models 85 and 86 on Figure II-7a, or decrease to 1 ohm-meter, Model 82F on Figure II-7c) can be accepted for thicknesses of less than about 90 - 100 km (i.e. overall depth of 120-130 km). Moderate changes (to 10 ohm-meters) are acceptable for thicknesses as low as 75 km, i.e. overall depth about 100 km (Model 82E).

One further relevant point is the question of spatial source field parameters. All the above models were derived using very large horizontal wavelengths (>10000 km), and are indistinguishable from models derived using the simpler method of Cagniard (1953) which is equivalent to the infinite wavelength case. Madden and Nelson (1964), Srivastava (1965), and others have shown that the effect of finite wavelengths is not serious for most MT data; the effect becomes significant only at the long-period end of the data. In GDS however, the finite wavelengths affect the data over the entire frequency range. Quantitative work in GDS (Whitham, 1963; Caner et al, 1967) has provided acceptable models only for values of V , the wave-number parameter in Price's (1962) expressions, of the order of 0.01 km^{-1} . This corresponds to wavelengths of the order of 600-800 km ($\lambda = 2\pi/V$). Figure II-7c (lower set of curves) shows the effect of varying the value of V . Model 82H ($V = 0.002 \text{ km}^{-1}$) is indistinguishable from $V = 0$, the infinite wavelength case. Model 82J ($V = 0.0050 \text{ km}^{-1}$) is readily acceptable, and even $V = 0.0085 \text{ km}^{-1}$ (Model 82K) is possible without drastically altering the conductivity structure interpretation. In fact, the observational data point scatter at the long periods can readily be explained by variable V values in the range 0 to

0.0080 km^{-1} , i.e. horizontal wavelengths between infinity and 800 km. If we increase the base-layer conductivity to 50 ohm-meters, V as low as 0.01 km^{-1} is acceptable - though barely so (Model 87). This confirms that for this type of MT data, the Cagniard (1953) method is sufficiently accurate, yet compatibility with the lower wavelengths derived in GDS is not excluded.

II-E) Interpretation - Western Stations

The data for Penticton (PEN) and Grand Forks (GRA) are of the same type and can be considered together (Figure II-8a). The conductivity structure models require a thin conducting surface layer at both stations in order to fit these data. We have used 0.45 km at Penticton and 0.60 km at Grand Forks, with resistivity 2 ohm-meters, but this is a flexible choice; identical results at the longer periods can be obtained with various other combinations of surface layer thickness and resistivity.

The resistive upper crust is much thinner than at the eastern stations - about 15 km. Here again the same uncertainty applies for the exact value of resistivity in this layer. For example models 31 and 31A (1000 and 6000 ohm-meters respectively) at Grand Forks are indistinguishable, and even Model 31B (250 ohm-meters) can barely be resolved (Figure II-8a). In fact, since no short-period station is available in the western cluster, the resistive layer could be omitted entirely from the models; for example in Model 24 at Penticton, a slightly thicker (19 km) upper crustal layer of resistivity 35 ohm-meters can replace the previous combination of a highly conducting surface layer and a resistive upper crust. The existence of a resistive upper crustal layer can be inferred from other evidence: the eastern region models, the Victoria data (Caner and Auld, 1968) and DC

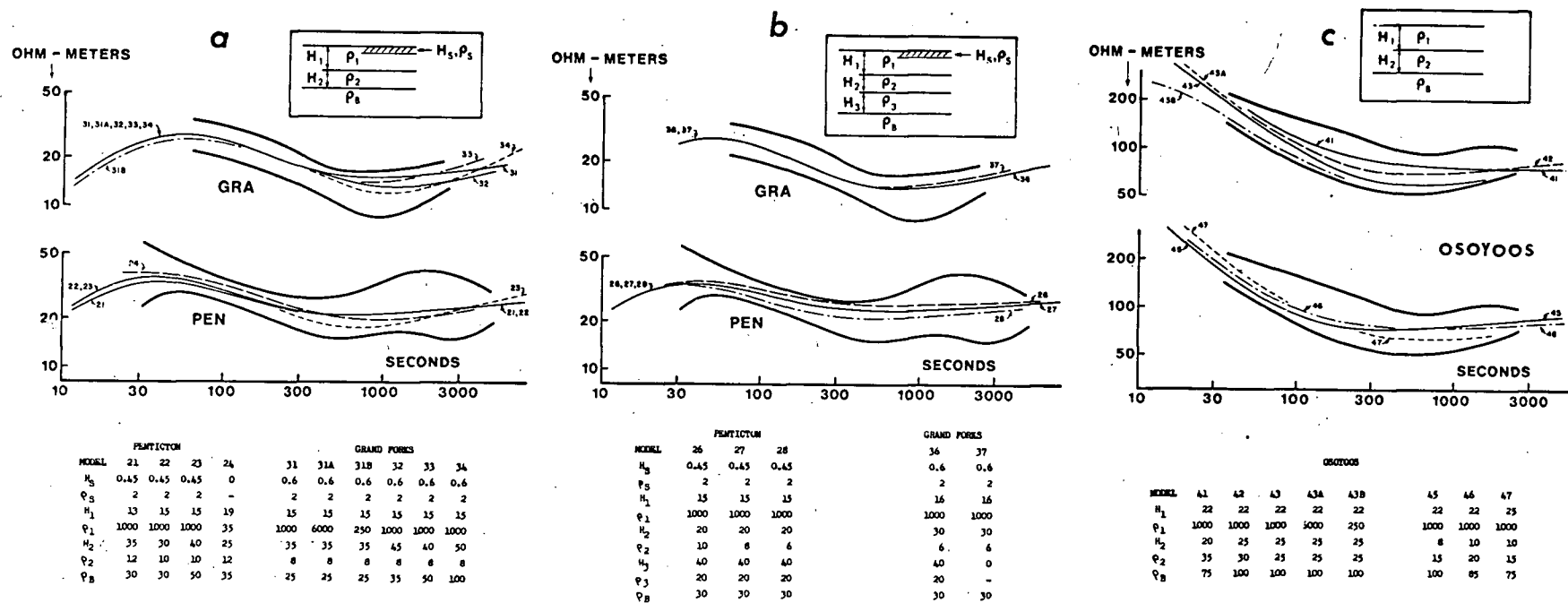


Figure II-8. Conductivity structure models, western stations.

resistivity surveys in western North America (Cantwell et al, 1965; Cantwell and Orange, 1965; Keller et al, 1966; Jackson, 1966). Such a layer has therefore been included in the subsequent models, with an arbitrarily assigned resistivity of 1000 ohm-meters. Fortunately the conductivity structure models are not critically affected by any assumptions about this layer, as can be seen from comparison of the models shown in Figure II-8a.

Below the resistive upper crust, the data indicate very clearly a conducting layer of resistivity 8-10 ohm-meters; this is in turn underlain by higher resistivity material. The "best fit" for the parameters of this layer is slightly different for the two stations. At Penticton it indicates a resistivity of 10-12 ohm-meters starting at depth 13-15 km (Models 21-23 on Figure II-8a), whereas at Grand Forks, it indicates a resistivity of 6-8 ohm-meters starting at depth 15-16 km (Models 31-34). However, the data bands are wide enough to provide latitude for full agreement on a value of 8-10 ohm-meters at depth 15 ± 2 km. We have avoided showing a "perfect agreement" pair of models for the two stations with resistivity 9 ohm-meters; quoting an odd value such as "9 ohm-meters" would imply a degree of accuracy which is certainly not justified by the data used to derive these models.

Below this conducting layer the resolution becomes poor. Although the resistivity does clearly increase again below this layer, it is hard to define at what depth and towards what value this occurs. A layer thickness of 30 km underlain by 30 ohm-meters (Model 22 on Figure II-8a) or a thickness of 40 km underlain by 50 ohm-meters (Model 23) give equally good fit to the Penticton data. Similar combinations of these parameters fit at Grand Forks (Models 31-33); even a layer thickness of 50 km underlain by 100 ohm-meter material (Model 34) can be

acceptable. It is clear that conditions at depths below about 30-40 km can be defined only within a fairly broad range of values at the western stations.

The above models were derived on the assumption that there is a distinct boundary between the conducting layer (8-10 ohm-meters) and the base material (30-50 ohm-meters). This need not be the case; additional "transition" layers can be postulated with equally good fit to the data, such as for example the models shown in Figure II-8b. The top of the conducting layer is still at the same value (about 10 ohm-meters) and at the same depth (15 ± 2 km); however, its thickness can be reduced from 30-40 km to 20 km, if we introduce a transition layer (20 ohm-meters) between it and the base medium. In effect, below the conducting layer we cannot distinguish between the case of sharply layered structures and the case of a gradual transition from 10 ohm-meters at depth 35 km to 30-50 ohm-meters at some undefined depth of the order of 75 km.

Moving to the Osoyoos data, it proved difficult to find good agreement with the Penticton/Grand Forks models. As previously explained, the Osoyoos data is of very poor quality; nonetheless an attempt has been made to derive some models which would agree with the other stations. Models were fitted to the NS data; this arbitrary choice is based on: a) the evidence of Fernie, where the lower set of curves was proven to be the "correct" one, and b) internal consistency - i.e. somewhat better agreement with the data from Penticton. Figure II-8c shows several model curves fitted to these data. The depth to the conducting layer has been taken as 22 km for the upper set on this Figure; this is somewhat extreme in comparison to the depth of 15-16 km derived for Penticton, but not

impossible. With this depth we find that the minimum resistivity of a conducting layer of comparable thickness (≥ 25 km) is 25 ohm-meters (Model 43), i.e. 2-3 times as high as the values derived for Penticton and Grand Forks.

A second group of model curves is shown in the lower set of Figure II-8c. These indicate that lower resistivities (15-20 ohm-meters) can be obtained for the conducting layer if we thin it down to about 8-10 km, (Models 45 and 46), or if we accept its depth at 25 km (Model 47). Such "structural" disagreement between Osoyoos and the Penticton/Grand Forks models is even more unacceptable than the previous set of models, which at least agreed in structure if not in the exact value of resistivities.

We conclude that no satisfactory agreement can be reached between the Osoyoos data and the combined Penticton/Grand Forks models, although the factor of 2-3 discrepancy in resistivities would perhaps not be considered prohibitive by the standards commonly applied to the consistency of MT data obtained at different locations. The Osoyoos data has therefore not been included in the final combined conductivity structure models. The justification for this omission is simply the lack of internal consistency, i.e. lack of agreement with all other stations. The omission can however also be rationalized on the more objective grounds that the site was far from ideal. In particular, it is likely that vertical earth-currents contributed towards the observed telluric amplitudes. Although theoretically irrelevant for horizontally stratified structures, such coherent vertical currents have been observed in practice (for example Jones and Geldart, 1967), with amplitudes comparable to those of the horizontal components. They could cause a significant increase in the observed

telluric amplitudes at a site such as Osoyoos where a) the electrodes were not at the same level or over level intervening ground, and b) there are significant changes in topography (few thousand feet) at short distances from the electrodes. It should be pointed out that the shape of the apparent resistivity curves at Osoyoos is the same as that obtained at the other two stations; a vertical frequency-independent shift by a factor of 4 in apparent resistivity (factor of 2 change in telluric amplitude) would bring the curve into almost perfect overlap with the Penticton data. Such a frequency-independent factor may be caused by either surface-anisotropic effects or vector addition of a vertical component.

It is very tempting to omit the Osoyoos data entirely from this paper, as without it the results could have been presented much more elegantly in a perfectly consistent pattern. They have nevertheless been included, even though not considered for the final models, in order to emphasize one of the weaknesses of MT models: the difficulty in obtaining consistent results from several stations.

II-F) Summary - Conductivity Structure

The combined data can be summarized in Figure II-9, with the addition of the following remarks:

- 1) A resistive upper crust is inferred at the eastern cluster. The exact value of the resistivity is indefinite; any value from about 250 ohm-meters up could fit the data, without upper limit.

- 2) At the eastern cluster the thickness of this resistive upper crust is 20-35 km; it is underlain by moderately conducting material, resistivity 30-50 ohm-meters.

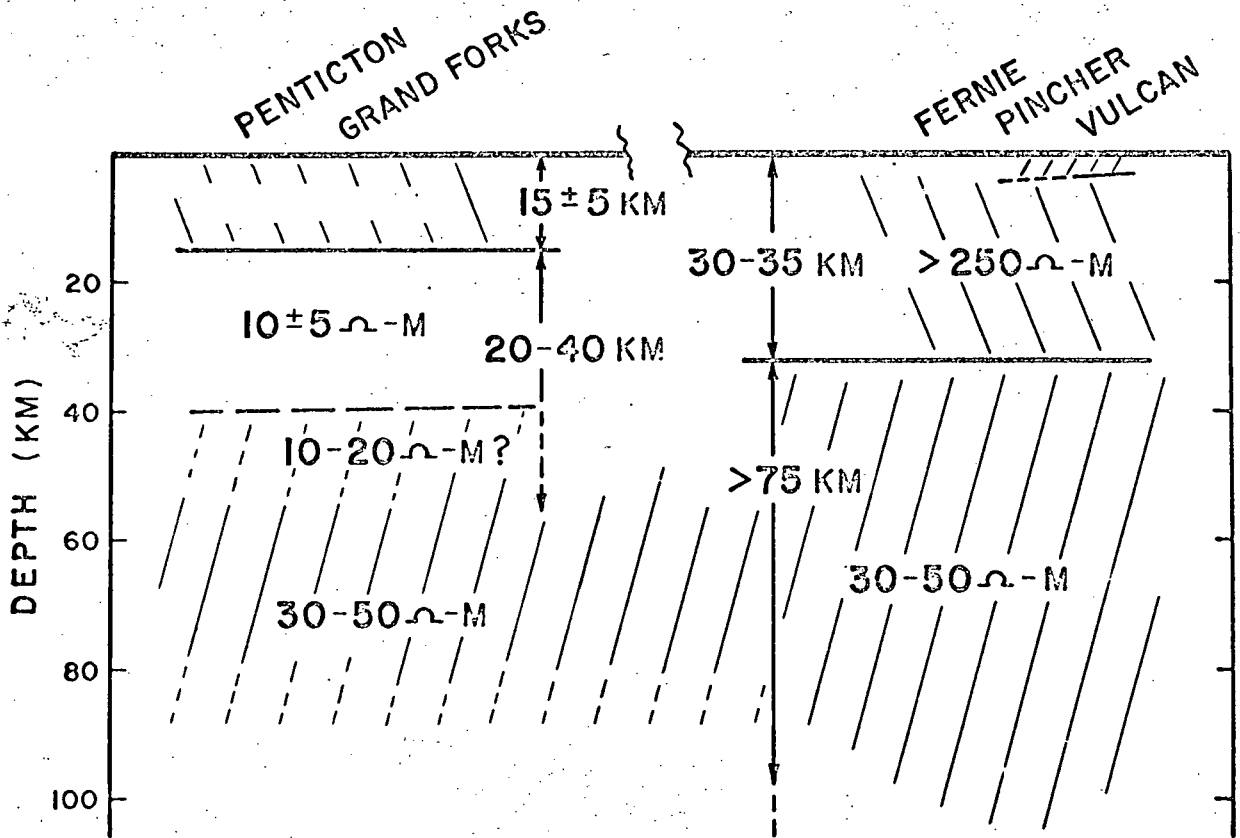


Figure II-9. Summary, combined conductivity structure models for the two regions.

3) No detail can be distinguished within this moderately conducting material, but there are no drastic changes in resistivity (to 1 ohm-meter or 1000 ohm-meters) down to a depth of at least 125 km, and not even moderate changes (to about 10 ohm-meters) to at least 100 km.

4) At the western cluster the upper crustal layer is only 15 ± 5 km thick, and its resistivity cannot be resolved. It is underlain by a conductive layer of resistivity 10 ± 5 ohm-meters and thickness at least 20 km.

5) Below this layer the resistivity increases again, apparently to the same "base" value as at the eastern cluster (30-50 ohm-meters).

6) No detail can be distinguished below the conductive layer. The layer could be uniform, extending to a depth of 35-55 km (thickness 20-40 km) and overlying directly the base material. Alternatively, the resistivity could shade gradually from 10 ohm-meters at depth 35 km towards the base-value (30-50 ohm-meters) at some undefined depth of the order of 75 km.

III. GEOMAGNETIC DEPTH-SOUNDING

III-A) Introduction

The GDS results are presented in two separate parts - "mapping" (section III-C) and "quantitative interpretation" (section III-D). The former is the main purpose of the GDS work; since GDS models are ambiguous, quantitative information is best obtained from the representative MT clusters. Nevertheless, the MT models should at least fit as one of the possible solutions to the GDS data, to confirm the validity of using the MT models as "calibration" for the GDS surveys. It should however be clearly understood that the GDS models derived in section III-D are not independently derived solutions which can be used to reinforce the MT interpretation. It is simply a demonstration that the MT derived conductivity structure model is one of the possible solutions to the GDS data.

III-B) Instrumentation

The basic instruments used for almost all the GDS work described in this report are Askania type GV-3 three-component portable variographs. On occasion these have been supplemented by Fluxgate magnetometers - Serson's (1957) IGY station magnetometer, or a later transistorized version developed at the Dominion Observatory in Ottawa. The Askania GV-3 variograph is a self-contained unit comprising the three variometers (suspended-fibre type), light-source and optical transmission system, calibration coils, recording magazine (motor driven film spool), and internal thermostat controlled heaters. Their main advantage is their stability. After a 24-hour "settling-in" period, the recorded traces are usually stable to within 1-2 gamma; temperature effects are minimized by temperature-

compensated suspension systems (dual fibres) and internal thermostats.

Quantitative work can therefore be carried out to very long periods, such as the diurnal 24-hour variation.

The frequency response of the variographs is linear from DC to about 2 sec period, but in practice is limited to about 200 sec period by the time-scale resolution and sensitivity of the recordings. This is adequate for GDS work, but for MT work the magnetic data at shorter periods must be obtained from another set of instruments. Recording is on continuous rolls (10 meters long) of photographic paper (12 cm. wide), permitting up to 3 weeks of unattended operation when recording at 2 cm/hour.

The original drive system for the recording reels was found to be highly unsatisfactory; designed by the manufacturer for 50 cps operation, the motors were found to be erratic and unreliable when operated on 60 cps line power. In earlier years up to 25% loss in record was encountered, requiring in effect continuous supervision of the stations. A new set of drive units was therefore designed and built at Victoria, using 60 cps motors with appropriate gear trains. Record loss with the new units is negligible; they were also designed to provide variable chart speeds by changes in an externally accessible gear set. In particular, non-metric chart speeds (1 or 2 inches/hour) are now available in addition to metric speeds (20 or 40 mm/hour). This permits better time-scale resolution and also facilitates direct visual comparison with telluric strip-chart recordings obtained on non-metric chart drives.

The accuracy of the instruments is of the order of 2-3%, and even including reading errors an overall accuracy of better than 5% in amplitude

can readily be maintained for moderate and large disturbances (say 25-50 gamma). No attempt has usually been made to use marginal-quality data, i.e. small amplitude fluctuations where reading errors become significant. Operation at each station was usually continued for as long as necessary to obtain the required amount of "good" data, i.e. 2 or 3 reasonably large disturbances. Even during the "quiet-sun" years this did not usually exceed 3-6 weeks.

The main limitation on the more extensive use of Askania variographs is their high cost - over \$12,000 each. With the advent of reasonably stable transistorized fluxgate instruments and of simplified, and considerably cheaper variographs (Gough and Reitzel, 1967), it would appear that the use of Askania variographs for large-scale surveys will be limited in the future. They are more likely to be used for either smaller-scale surveys of discontinuities and local anomalies, or as "anchor" stations in large-scale surveys in combination with larger numbers of lower-quality instruments.

III-C) Mapping

The results of earlier work in North America have already been outlined in section I-B. Figure III-1 shows samples of record obtained on the 3 profiles operated on this project before 1966: the same type of attenuation in the vertical component (Z) is observed at the western station of each pair. Spectral analysis of these data indicated that the frequency dependence of the attenuation was within the same range for all three profiles (Caner et al, 1967). The derived attenuation curve has been used in subsequent mapping profiles as the "characteristic signature" of the conductivity structure contrast.

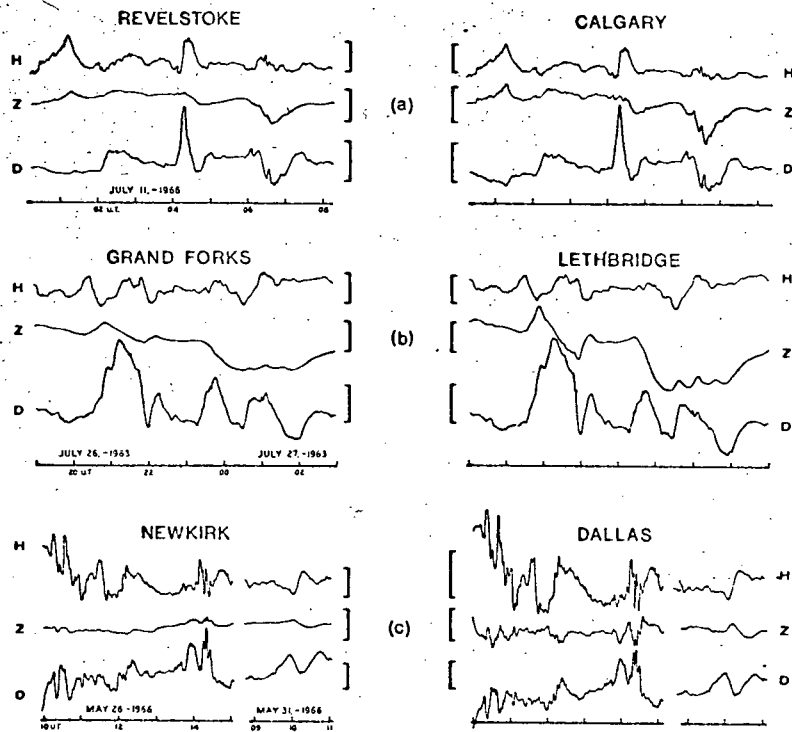


Fig. III-1. Magnetogram copies from pairs of stations at:
 (a) latitude 51°N (profile D of Fig. I-1)
 (b) latitude 49.5°N (profile C)
 (c) latitude 33°-35°N (profile B)
 Scale bars are 50 gammas, time marks are 1 hour.

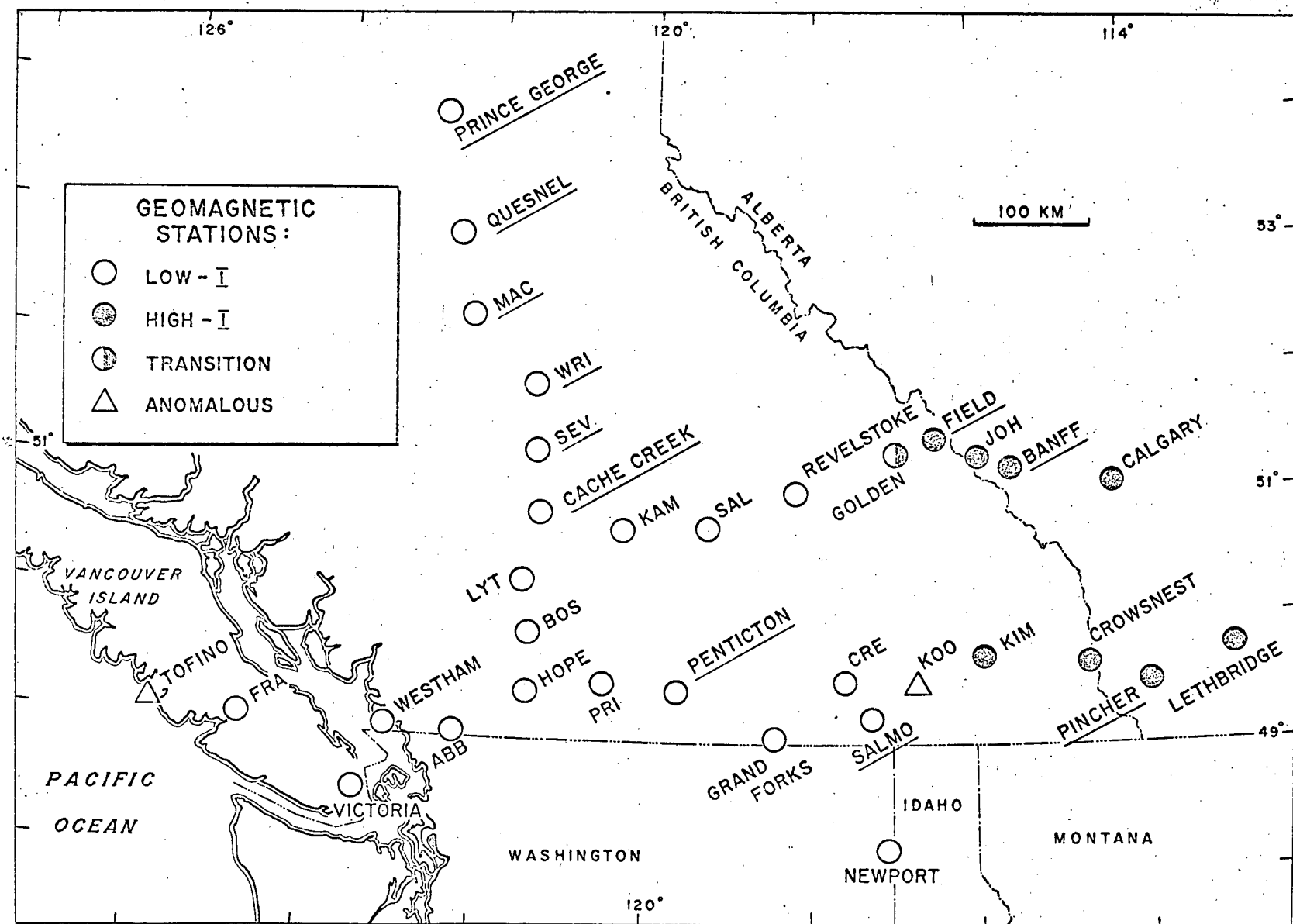


Fig. III-2. Location of GDS stations in western Canada, and of the permanent magnetic observatories at Victoria and Newport. New (post-1966) stations are underlined.

Figure III-2 shows in more detail the location of the GDS stations in southwestern Canada, both for the earlier surveys reported previously and for the subsequent work outlined in the following report. The two profiles at latitudes 49.5°N and 51°N have been improved by the addition of a few stations in the vicinity of the discontinuity. On the northern profile, stations at Banff and Field were found to be of the same "eastern" type as Johnston Canyon (JOH on Fig. III-2) and Calgary. The station at Golden is transitional in Z/H ratio between this "eastern" type and the "western" type recorded at Revelstoke, Salmon Arm (SAL), and further west. The discontinuity is therefore placed at or slightly (10-20km) to the west of the Rocky Mountain Trench. For the southern profile, no transition station could be identified. The station at Kimberley airport (KIM), in the Kootenay River Valley, is of eastern type, same as Crowsnest to Lethbridge; the stations at Crescent Valley (CRE) and Salmo are western-type. Detailed mapping of the discontinuity in this region is complicated by the existence of a local anomaly (i.e. anisotropy in Z/H ratio) near Kootenay Lake (KOO), as reported by Hyndman, 1963, and Caner et al, 1967. This anomaly is presently being studied in detail by J. Lajoie of this Department; it is not yet clear if it is caused by an independent shallow conductivity structure, or by a convolution in the main discontinuity. However, below Kootenay Lake the discontinuity can be placed with reasonable confidence within 20-30 km to the west of the Kootenay River Valley, the presumed southern continuation of the Rocky Mountain Trench (Robinson, 1968).

The stations in the vicinity of the discontinuity are shown in more detail in Figure V-1 (page 99) of the summary. It is tempting to

interpolate between the two points defined by the above profiles, using geological or tectonic boundary trends as a guide; for example, we could specify the discontinuity as "running 10-30 km to the west of the Rocky Mountain Trench from 49° to 51° latitude". However, experience in other areas (particularly in Texas-Oklahoma, profile B on Figure I-1) has shown that surface features are not a reliable indicator for the course of the discontinuity. Until very closely spaced profiles are available, the above interpolation over about 200 km must be considered as tentative, particularly in view of the existence of anisotropic features which may indicate convolutions in the discontinuity.

During 1967 a new profile was operated running north from Cache Creek towards Prince George, in an attempt to define a northern boundary for the "western-type" conductivity structure region. The six stations (Figure III-2) were occupied simultaneously, using four Askania variographs and two transistorized Fluxgate magnetometers. The profile ties in at Cache Creek with the earlier east-west profile (Cache Creek to Calgary), and with a short north-south profile between Cache Creek and Hope. All these earlier data, although not simultaneous, can therefore be reduced to a common reference station used as the "western-type" standard - either Cache Creek, or Victoria which was operating continuously throughout all these surveys.

Figure III-3 shows sections of record obtained simultaneously at the six stations, as well as at the Victoria Observatory. Unlike the earlier profiles which were operated in east-west directions, the inducing field is not even roughly constant over the length of the profile, and location of discontinuities can no longer be carried out by simple visual

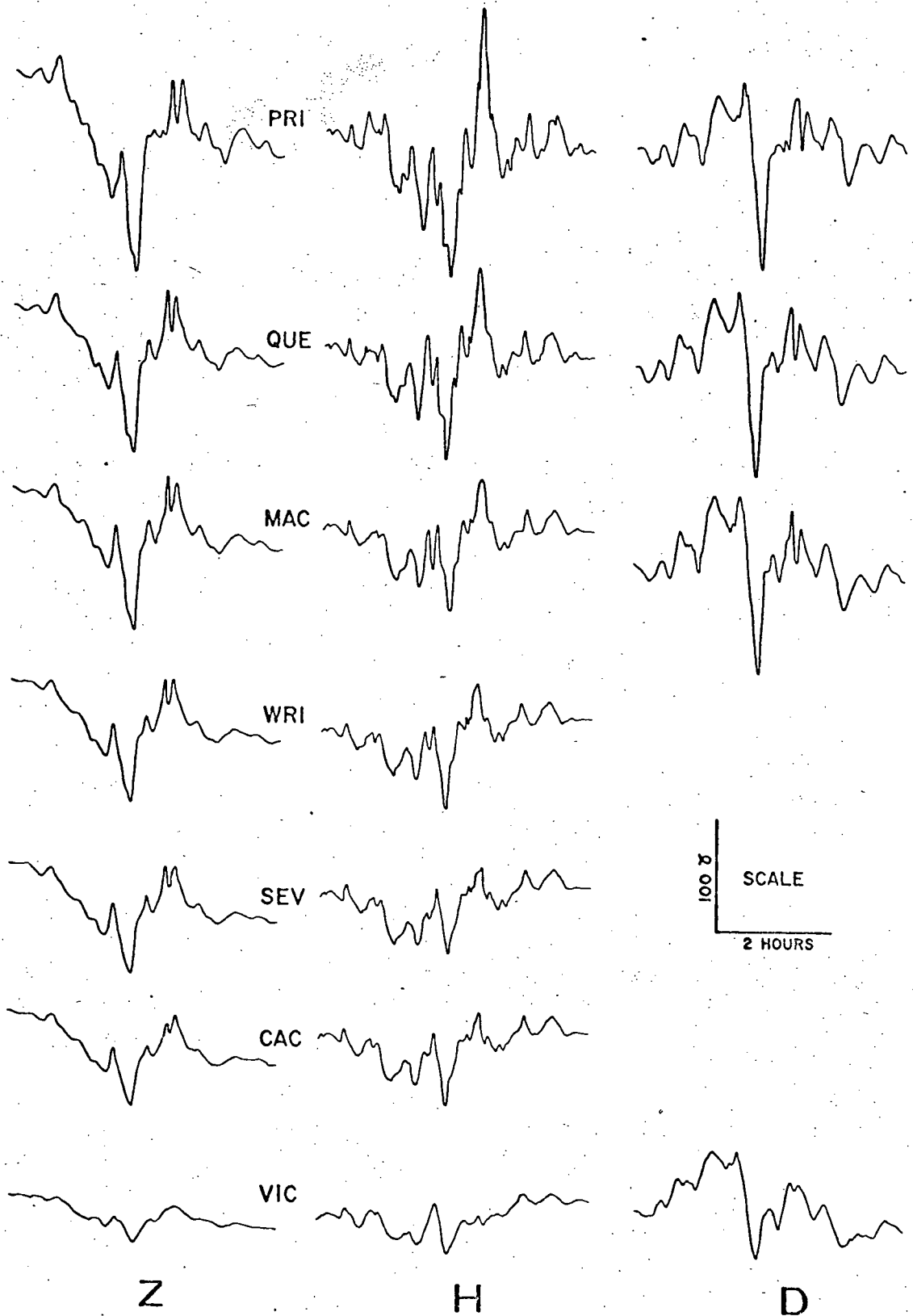


Fig. III-3. Recordings from Cache Creek - Prince George profile, and from the magnetic observatory at Victoria.

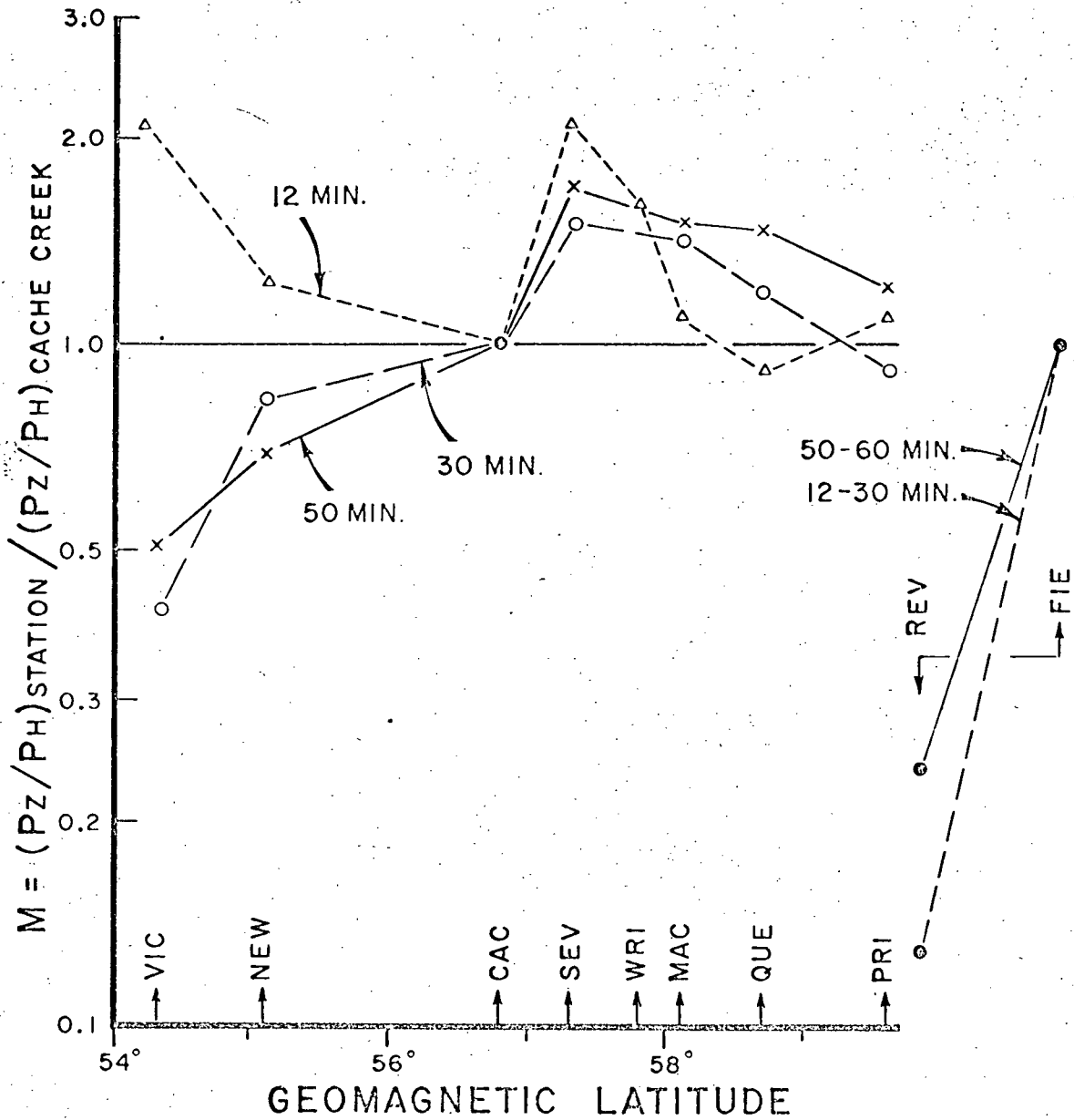


Fig. III-4. M-ratios as a function of geomagnetic latitude for Cache Creek - Prince George profile.

inspection. In particular, as the profile reaches higher geomagnetic latitudes (i.e. as the source currents are approached), the uniformity is lost even over relatively short distances. Prince George lies at geomagnetic latitude 59.6°N ; it is doubtful if much useful profile work can be carried out further north than this latitude, unless the profiles can be laid out in arcs along geomagnetic parallels of latitude, i.e. parallel to the source currents. An attempt was made to include data from Meanook Magnetic Observatory (geomagnetic latitude 61.8°N) in this survey, but the fluctuations were barely recognizable as coherent with those recorded simultaneously at Prince George.

The vertical component (Z) amplitudes recorded along the profile (Fig. III-3) are seen to increase towards the north; at the start, from Cache Creek to Seventy-Mile House (SEV) or Wright (WRI), the increase is gradual, but it becomes quite steep towards the higher latitudes - particularly if the relatively close spacing ($< 75\text{-}100\text{ km}$) between the stations is considered. However, it can be seen that the horizontal component amplitude (H) increases at roughly the same rate, indicating that the increase is a source effect rather than a change in subsurface conductivity structure towards the "eastern" high-Z type.

Figure III-4 shows a plot of some Z/H power spectral ratios, normalized with respect to Cache Creek and plotted against the geomagnetic latitudes of the stations. The ratios from the permanent observatories at Victoria and Newport have also been included. The data is generally of poor quality. The primary objective of this profile was mapping, since no quantitative interpretation was to be attempted on a north-south profile at high latitude; consequently the stations were checked and serviced intermittently only during the 8-week period of operation. As a result only two short (5 hour) sections of record with an adequate

disturbance level were obtained for all stations simultaneously. These were digitized and spectral amplitudes obtained. Figure III-5 shows the results for three spectral bands which contained measurable energy: periods 12, 30 and 50 minutes. The scatter is rather high, but it should be kept in mind that these points represent the ratios of four powers: relatively minor inaccuracies in each component can result in large errors in these ratios. For example, 10% errors in each of two amplitudes can expand a Z/H power ratio into the range 0.67 to 1.48. A normalized ratio of two such power ratios can readily account for factor-of-two scatter, particularly in view of the poor quality of the samples used (short length of time series available for spectral analysis).

It is clear from Figure III-4 that there is no drastic discontinuity in Z/H ratio between Cache Creek and Prince George. Previous work on the Cache Creek-Hope section indicated that there is no discontinuity between Cache Creek and Victoria (Cannon, 1967; Caner et al, 1967), apart from the slight latitude dependence of the Z/H ratio. To indicate the magnitude of the discontinuity between the "eastern" and "western" regions, the change in power ratio observed between Field and Revelstoke (distance 125 km) is plotted on the same figure, to the same horizontal and vertical scale. Clearly no such discontinuity occurs along the Cache Creek/Prince George profile. This means that the northern extent of the discontinuity remains undefined, except that it lies east of Prince George at latitude 54°N. It will be shown in a subsequent chapter (section IV-D) that it can be located more closely using other geophysical information, and that its most likely course follows roughly the boundary between the Rocky Mountains to the east and the Cariboo Mountains to the west, as delineated by the

Rocky Mountain Trench. The above is not proposed as evidence for any deep geophysical significance of the location of the Rocky Mountain Trench; the Trench is here used simply as a convenient geographical landmark for expressing the course of the discontinuity. However, this apparent coincidence between the Trench and a discontinuity in at least two geophysical parameters (see section IV-D) justifies a closer examination of its possible tectonic significance.

III-D) Quantitative Interpretation

Earlier quantitative work was carried out on the combined data from several profiles, to obtain some "average" or "typical" structure model, and was based on fairly poor quality data (Caner et al, 1967). In order to obtain reliable data for a specific location, two GDS stations were operated for 7 weeks at Pincher and Penticton; these are the two "primary" MT stations described in Section II, for which MT-derived conductivity structure models are available. Figure III-5 shows examples of record obtained at these two stations, as well as at an intermediate western-type station at Salmo. The attenuation in Z at the western stations is clearly visible.

Spectral analysis of three data samples (duration 24 hours, sampling interval 72 secs) was carried out, and the computed normalized M-ratios are shown in Figure III-6. These have been plotted as a function of log period rather than on the frequency-linear scale previously used for GDS work. Only data points for which the coherence $Z(\text{Penticton}) - Z(\text{Pincher})$ exceeded 0.75 have been included, and those for which it exceeded 0.95 are identified by solid symbols. Using this criterion, no "valid" data were obtained for periods less than 1200 seconds, indicating that for these short periods: a) the inherently lower amplitudes combined

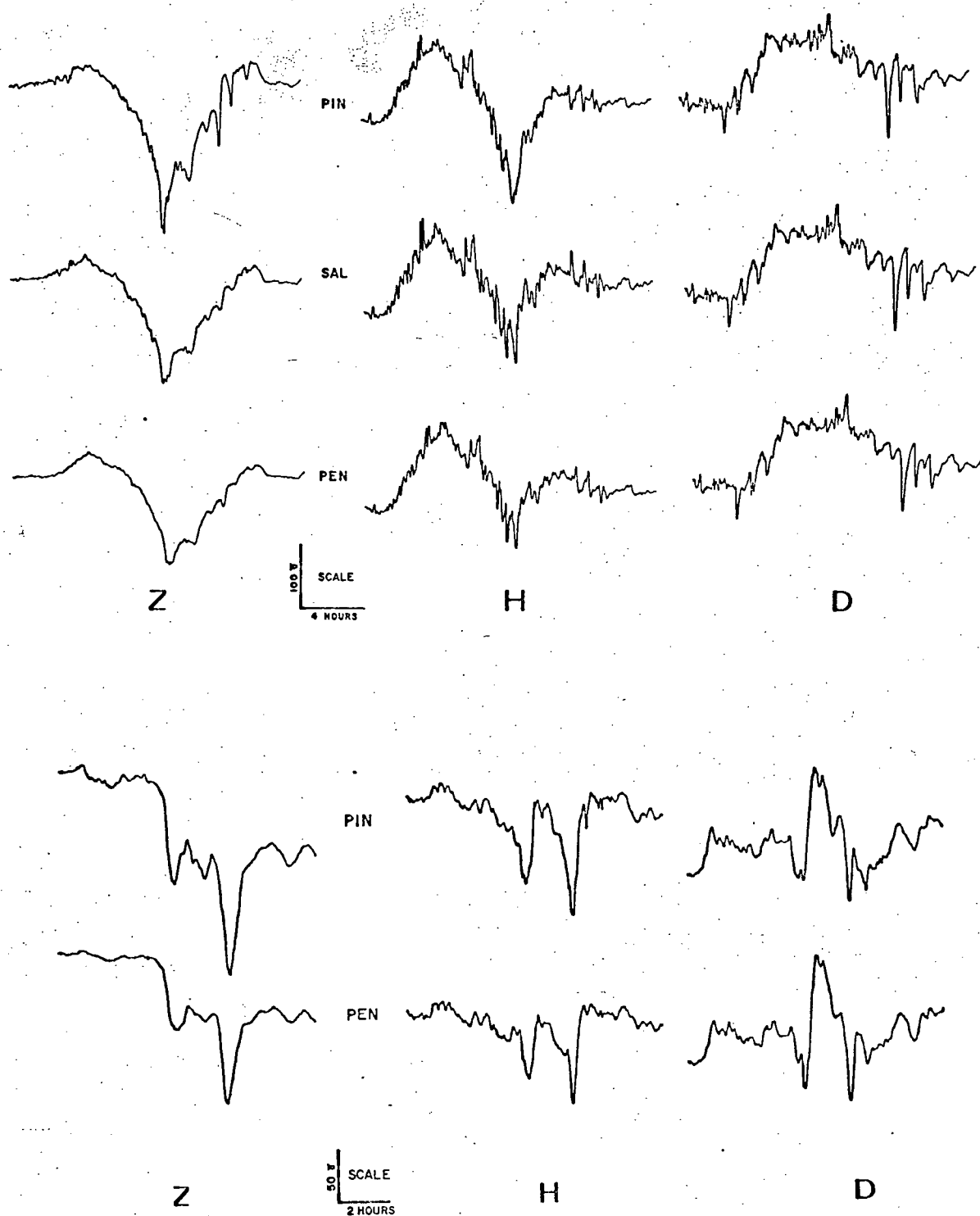


Fig. III-5. Sections of GDS recordings from Pincher (PIN), Salmo (SAL), and Penticton (PEN).

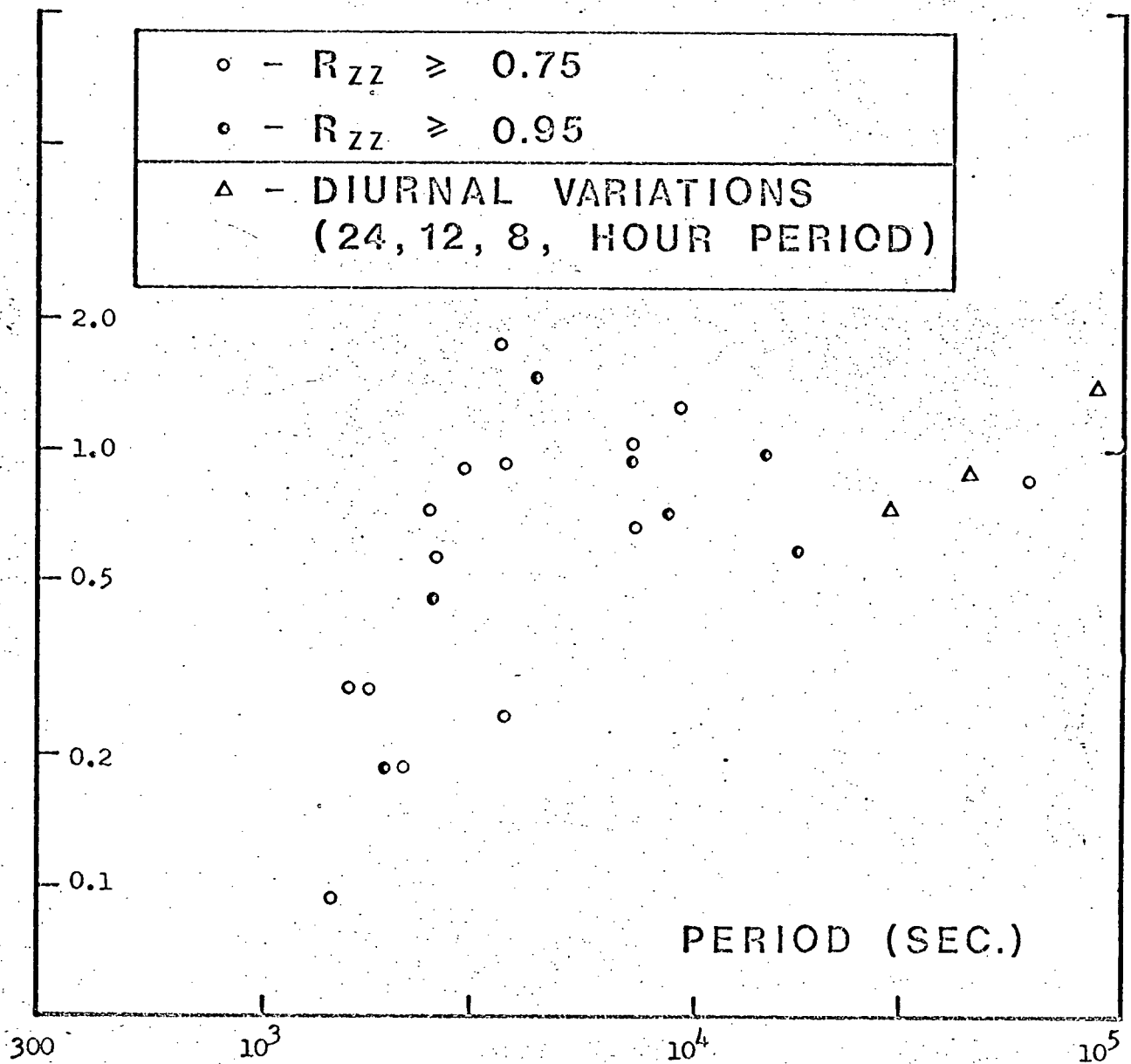


Fig. III-6. M-ratios, $(P_z/P_H)_{\text{Penticton}} / (P_z/P_H)_{\text{Pincher}}$, plotted as a function of period (Penticton normalized with respect to Pincher).

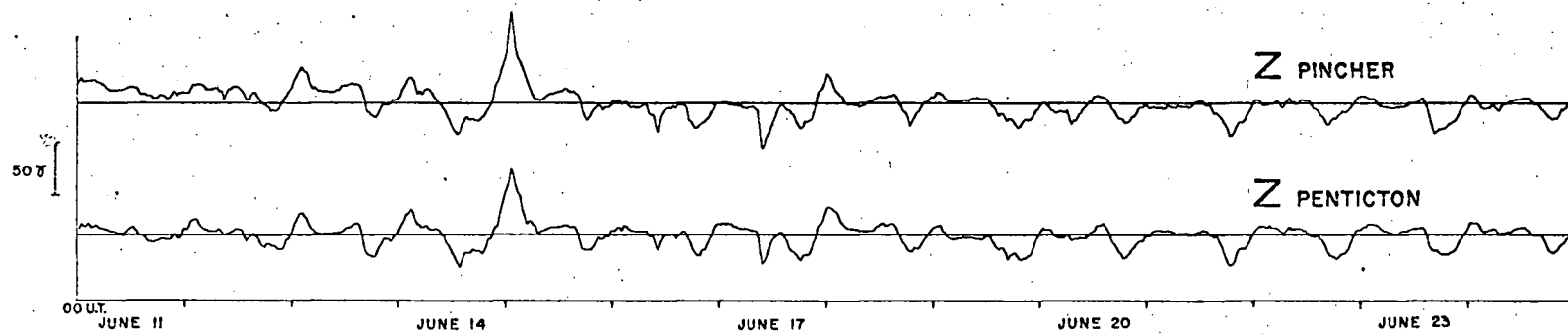


Figure III-7. 14 day recordings of the vertical component, Pincher and Penticton.

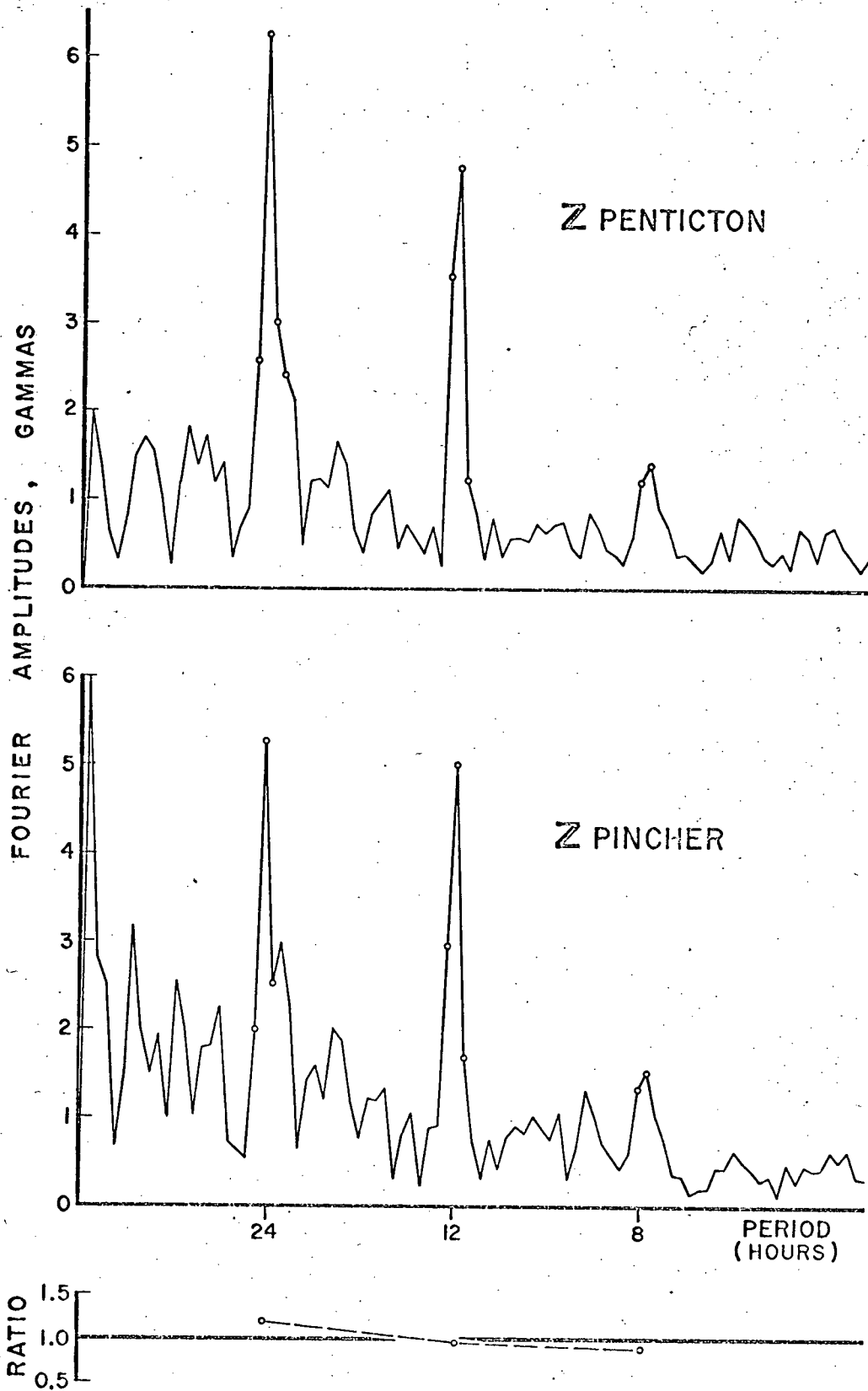


Fig. III-8. Fourier amplitudes and ratio (Penticton/Pincher) for the diurnal variations.

with the heavy attenuation in the western region to produce low signal/noise ratios, and/or b) the spatial coherence over the 400 km distance between the two stations is too low for short periods.

The scatter of the data points is very high, but as mentioned in section III-C this is not unreasonable for a ratio of four powers, each with its own errors in calibration, measurement, and spectral analysis. In addition it will be shown that in the range $10^3 - 10^4$ secs, the M-ratios are very sensitive to variations in spatial source wavelength, justifying some additional scatter for combined data from several disturbances.

The analysis has been extended to very long periods with a 14-day section digitized at half hour intervals, in order to derive the amplitudes of the diurnal fluctuation and its harmonics. These data are shown in Figure III-7. Spectral analysis was carried out, and the diurnal peaks are clearly resolved (Fig. III-8). The computed energy ratios for periods 24, 12, 8 hours have been included on Figure III-6. The amplitude ratios are within 15% of unity, which is about the accuracy which can be expected from such a short sample containing some irregular activity as well (see Fig. III-7). No significance has therefore been ascribed to the departure from unity of the ratio at 24 hours period.

Theoretical models of conductivity structure have been fitted to the data of Figure III-6, using the MT-derived structures as a guide to choice of models. The following table specifies the parameters of the various models shown in Figures III-9, 10, 12. Unless otherwise indicated on the drawings, the models are normalized with respect to the structure designated as "I" at Pincher.

PENTICTON								PINCHER		
MODEL	101	102	103	104	105	106	107	I	II	III
H_1	15	15	10	10	10	10	10	H_2	-	- 4.8
ρ_1	1000	1000	1000	100	1000	1000	1000	ρ_2	-	- 11
H_2	20	40	20	20	10	40	10	H_1	35	35 35
ρ_2	10	10	5	5	5	5	2	ρ_1	1000	9900 1000
ρ_3	40	40	40	50	40	40	40	ρ_3	40	50 40

SUFFIX	NONE	A	B	C	D
$V(KM^{-1})$	0.000157	0.001250	0.002100	0.006280	0.010000
$\lambda(KM)$	40,000	5,000	3,000	1,000	628

Model 101 on Figure III-9 shows the M-ratios for a structure with the median values derived from the MT data, i.e. a conducting layer of thickness 20 km and resistivity 10 ohm-meters starting at depth 15 km. It is clear that not enough attenuation at short periods can be obtained with this model, even if we increase the thickness of the conducting layer to 40 km (Model 102). If we change the western parameters to the limit of the acceptable MT-derived range, we obtain Model 103 ($H_1 = 10$ km, $\rho_2 = 5$ ohm-m); this provides enough attenuation at the short periods, but too much attenuation at the long periods. If we push all the parameters (east and west) to the limit, including base resistivities and maximum contrast in upper layer resistivities (100 vs. 10,000 ohm-m), a slight improvement is obtained (Model 104/II); however, the change is not significant enough to warrant such complications. Nor do more complex models (such as the 4-layers structure suggested in Section II-E, Fig. II-8b) provide any better fit. The only really effective way of modifying the curves are either a) changes in the spatial source field

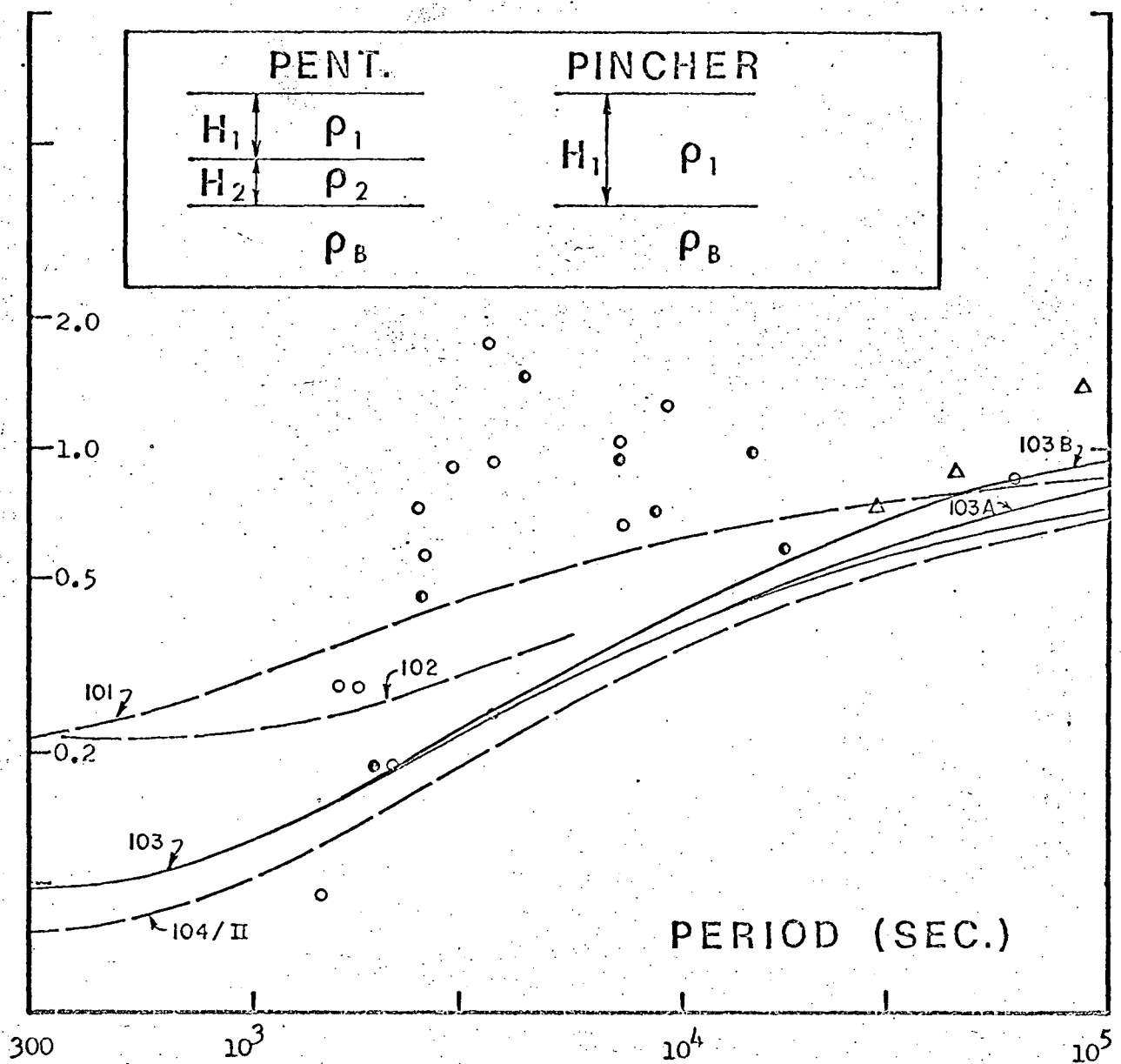


Fig. III-9. GDS conductivity structure models for long spatial wavelengths (≥ 3000 km), compared to M-ratios Penticton/Pincher. See page 67 for parameters.

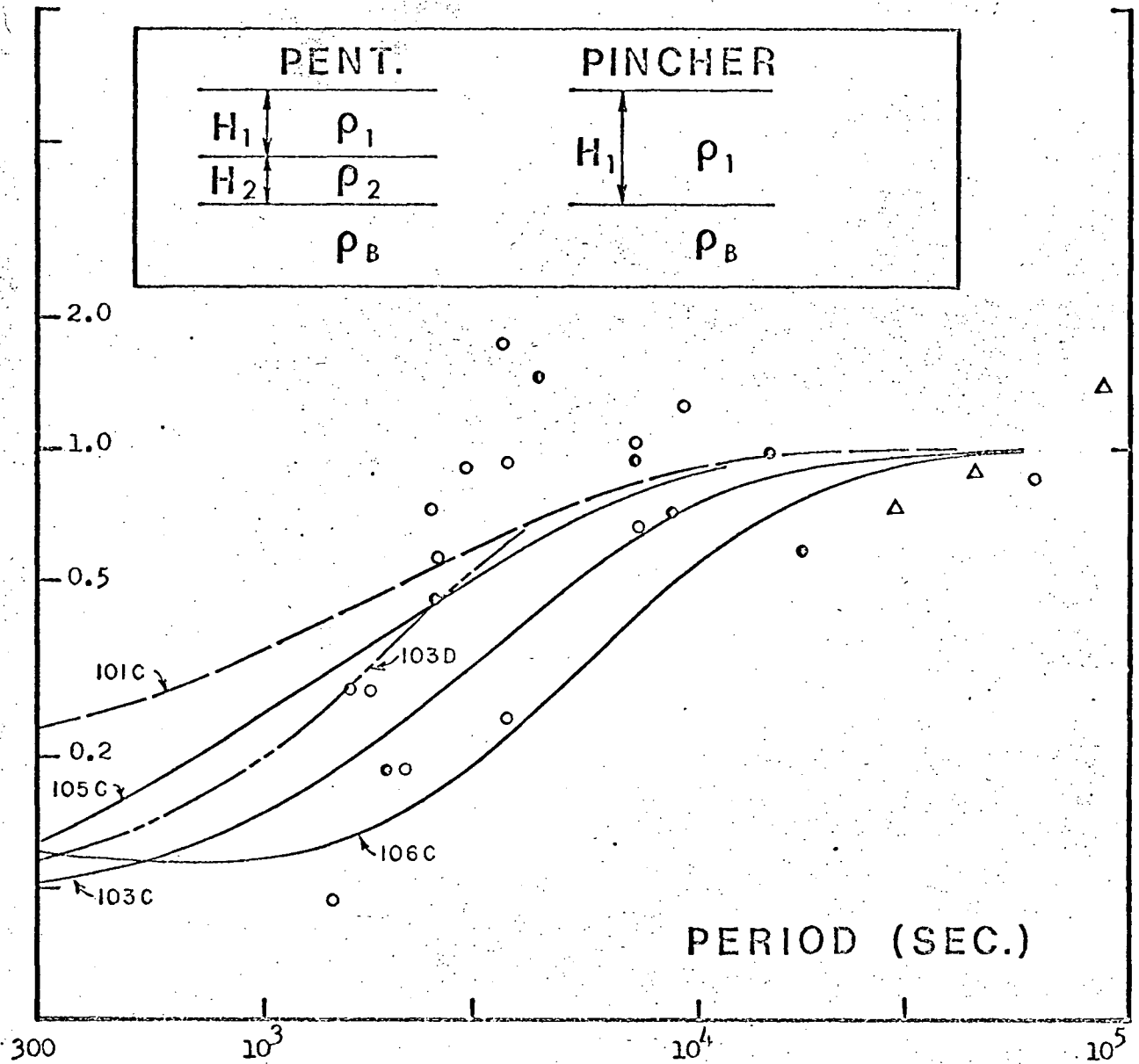



Fig. III-10. GDS conductivity structure models for short spatial wavelengths (≤ 1000 km), compared to M-ratios Pentiction/Pincher. See page 67 for parameters.

parameter V (discussed in the next paragraph), or b) changes in conducting layer parameters (depth and/or resistivity) which are outside the limits imposed by the MT models.

Models 101-103 were derived with an assumed spatial wave-number $V = 0.000157 \text{ km}^{-1}$, corresponding to a wavelength of 40,000 km, the limiting value suggested by Price (1962). The models for longer wavelengths ($V = 0, \lambda = \infty$), and those for shorter ones down to about 15,000 km, are indistinguishable from the above within the frequency range under consideration, and for this particular assumed conductivity structure model (this needs to be emphasized - dependence of the models on V is strongly affected by the assumed structures). Even for $\lambda = 10,000 \text{ km}$, the change in M is less than 3% at period 10^5 sec .

Models 103A and 103B on Figure III-9 show the effects of decreasing the wavelength even further: 5,000 and 3,000 km respectively, compared to Model 103 with $\lambda = 15,000 \text{ km}$. This does provide some improvement in the long-period response, but not enough, and we have to move to even shorter wave-lengths to obtain the characteristic  shape of the curves - i.e. no attenuation at long periods and heavy attenuation ($\geq 10 \text{ db}$) at short periods.

Several model curves for shorter spatial wavelengths are shown in Figure III-10. For $V = 0.00628$ ($\lambda = 1,000 \text{ km}$), Models 101C and 103C show significant improvement over the equivalent long-wavelength models (101 and 103). The effect of altering the thickness of the conducting layer from 20 km to either 10 km (Model 105C) or 40 km (Model 106C) is apparently significant, and the models would indicate that the thinner layers (i.e. 10-20 km) provide better fit to the data. In practice

however, the GDS data is not useful to help define this parameter, since at this stage the models become very sensitive to even small changes in spatial wavelength; it is virtually impossible to distinguish reasonable changes in conductivity structure parameters from slight variations in spatial wavelength. For example, Model 103D ($\lambda = 628$ km) with $H_2 = 20$ km falls right between the $H_2 = 10$ km and $H_2 = 20$ km curves for $\lambda = 1,000$ km. Similarly, the curve for $H_2 = 40$ km with $\lambda = 628$ km (not shown) is virtually indistinguishable from Model 103C ($H_2 = 20$ km with $\lambda = 1,000$ km).

Since there is no GDS mapping coverage east of Lethbridge, it is not clear if the Pincher structure outlined above is representative of the entire eastern region, or just of some local structure in the southwest corner of Alberta. The latter appears to be indicated, since all published MT data further east or north indicate greater depths (70 - 150 km) to the conducting layer (Niblett and Sayn-Wittgenstein, 1960; Srivastava and Jacobs, 1964). Even at Brooks (only about 100 km to the east of Vulcan), the conducting layer was estimated to start near depth 100 km (Vozoff and Ellis, 1966). This would mean that the Pincher/Vulcan region already lies above the "western" uplifted geotherm zone, or above a transitional structure; the distinction between this region and the western "low-I" region which is so sharply delineated west of the Rocky Mountain Trench, is mainly the absence of the conducting lower crustal layer, not a significant difference in upper mantle conductivities.

The question will probably be resolved once GDS mapping coverage is extended towards the east. It should however be pointed out that this may not be as straightforward as detection of the main western discontinuity:

GDS data is not particularly sensitive to changes in the depth of a moderately conducting ($\rho = 30\text{--}50\text{ ohm-m}$) zone. Figure III-11 shows M-ratios computed for a comparison between the Pincher/Vulcan structure and a hypothetical "normal eastern" structure (depth of 70 km to the moderately conducting zone). In the period range 2000 to 5000 secs in which most of the GDS data is concentrated, the amplitude attenuation for this structural difference ranges between 0.81 and 0.87 for "infinite" (i.e. $> 20,000\text{ km}$) spatial wavelength; it is barely significant (> 0.90) for the shorter spatial wavelengths ($\sim 1,000\text{ km}$) indicated by the Penticton/Pincher models. If the "normal eastern" depth is greater than 70 km, then the difference may be resolvable; for example if $H_{(\text{east})} = 100\text{ km}$, the ratio could be as low as 0.75 in amplitude for this period range (Fig. III-11). It is clear that the GDS data cannot resolve changes in depth in the range 35-80 km to a moderately conducting zone. Consequently, the mapping of this structure towards the east would not be expected to show an easily recognizable first-order discontinuity such as that observed west of the Trench, particularly if the change is gradual and/or partly masked by differences in conducting surface layers.

The preceding models were all based on a simple 2-layer structure at Pincher. If we include a thick conducting surface layer at Pincher, as estimated from the MT data and well-logs, the Penticton/Pincher GDS model curves are drastically altered - particularly at the shorter periods. Figure III-12 shows two such models (103/III and 103C/III), with the equivalent no-surface-layer models shown in dashed lines. If such a massive surface layer is to be used at Pincher but not at Penticton, the

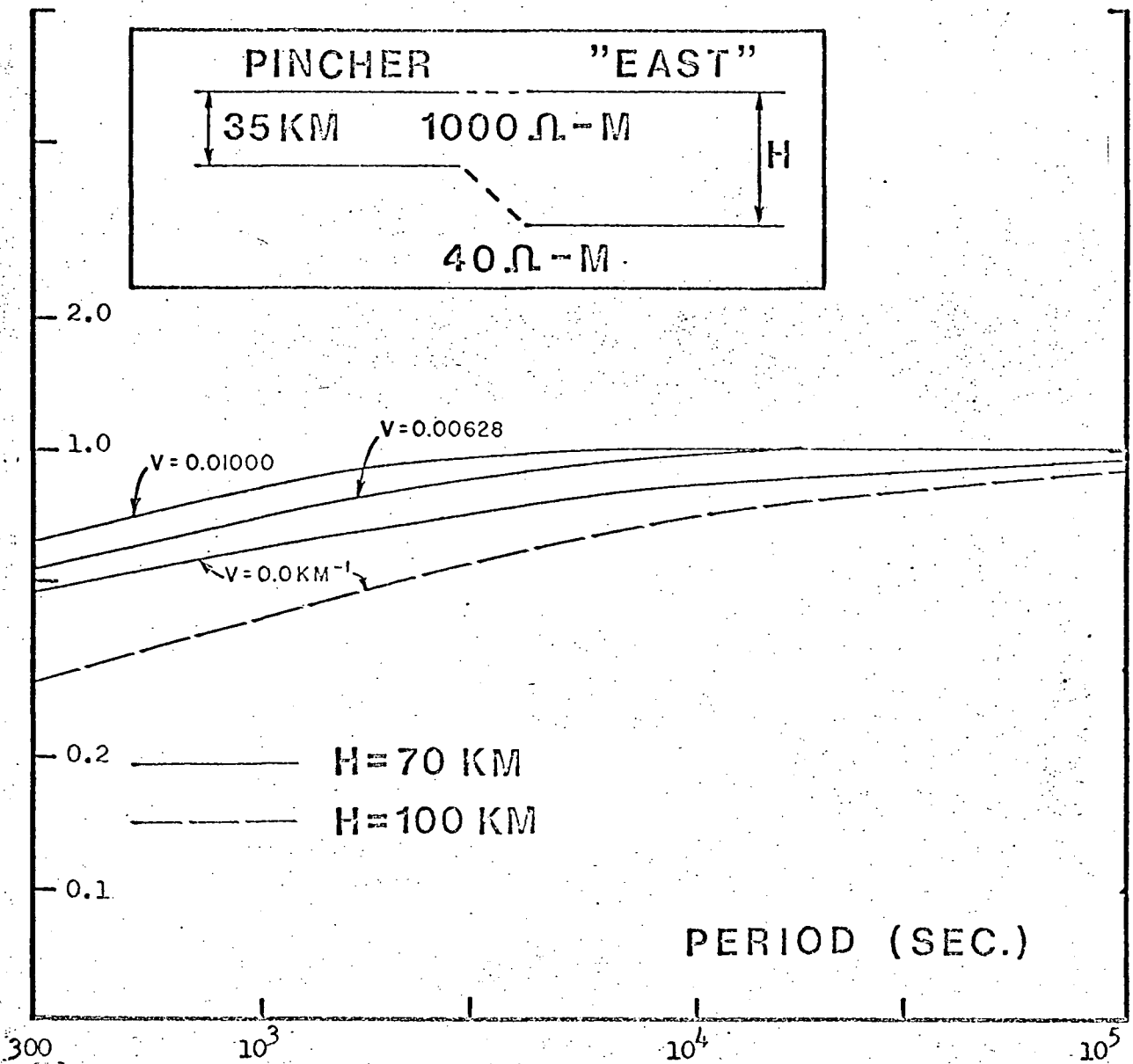


Fig. III-11. GDS conductivity structure models: M-ratio as a function of period, Pincher normalized with respect to hypothetical "eastern" structure.

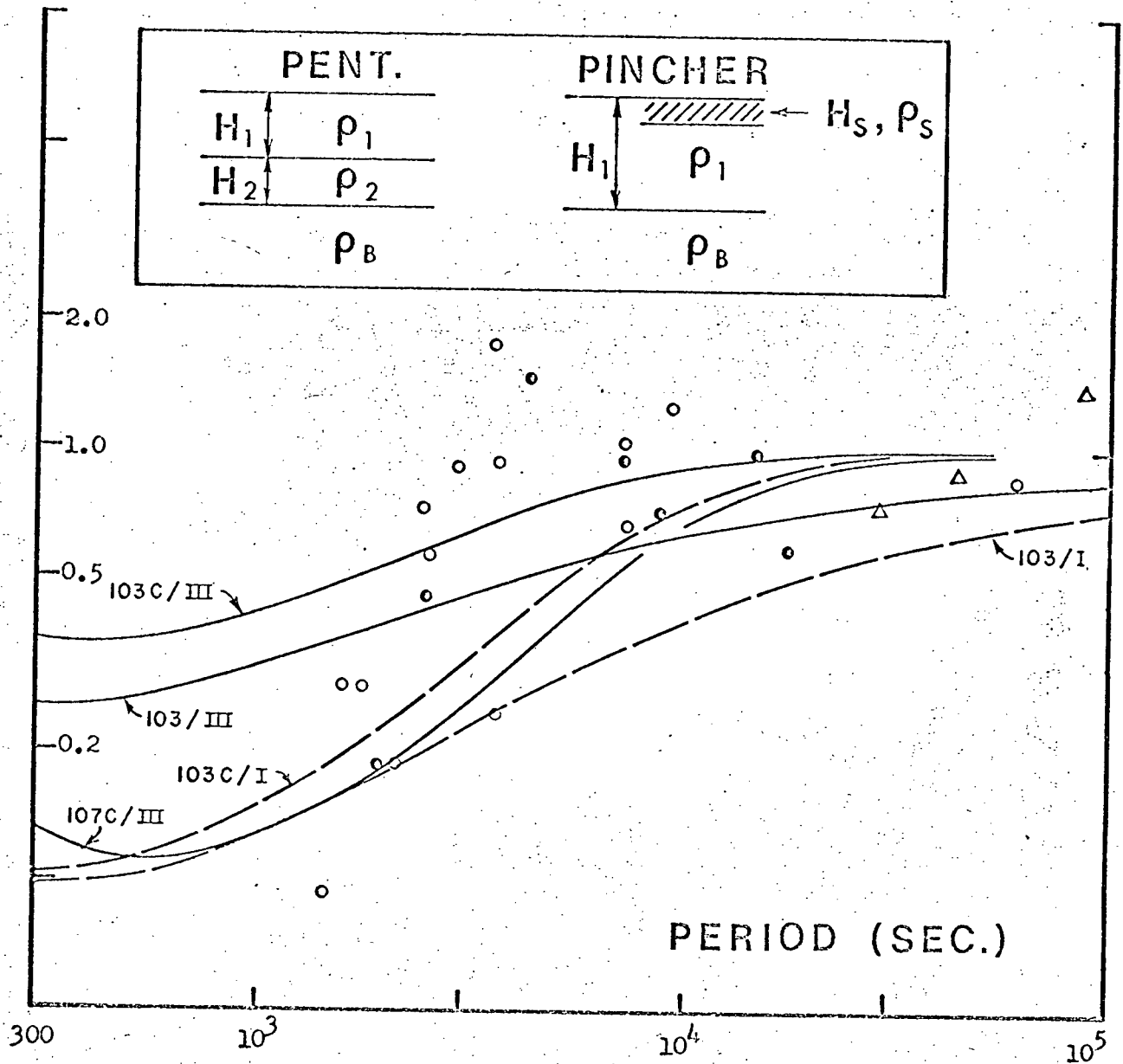


Figure III-12. GDS conductivity structure models with surface layer at Pincher compared to M-ratio Penticton/Pincher. See page 67 for parameters.

parameters of the western structure would have to be altered beyond the limits imposed by the MT data. For example, reducing the resistivity of the lower crustal layer from 5 ohm-m to 2 ohm-m (Model 107C/III) compensates for the addition of the surface layer. However, there is no real need for such changes, as a fairly significant upper crustal conductivity is indicated by the MT data at Penticton as well. Since no short-period MT data or well-logs were available near Penticton, the parameters of the upper crust could not be resolved. However, the integrated upper crustal conductivity appears to be of the same order as at Pincher - see for example the MT models on Figure II-8 (0.45 km of 2 ohm-m + 15 km of 1000 ohm-m, or 19 km of 35 ohm-m, or other equivalent combinations). This would compensate for the surface layer effects at Pincher, leaving GDS models which are compatible with those derived from MT.

This sensitivity of the M-ratio to surface layers (for this particular pair of structural models) raises some questions about the validity of the GDS models previously derived for the southwest USA - profile B on Fig. I-1. The region of high attenuation in Z was found to continue well east of the Rocky Mountains, into an area of very thick sedimentary layers (Caner et al, 1967; Livingstone, 1967). Quantitative work was based on different assumed conductivity structures, since no MT "calibration" was available; for these models the effects of surface layers were found to be negligible, and it was concluded that the main discontinuity does indeed swing that far east - even though this caused some difficulties in interpretation: a) poorer agreement with the area of high heat flow; b) very sharp swings in the discontinuity would be required, since it was recovered much nearer to the Rockies both to the south and to the north (Schmucker, 1964; Gough and Anderson, 1968).

More detailed work has since been carried out in this area (Gough and Anderson, 1968; Porath, 1969), and has confirmed the extension of the low-Z type of recording towards the east. However, their interpretation indicated that this could be caused by the effects of massive conducting surface layers in this area (Porath, 1969). In view of the results obtained on the present models (using MT "calibration" rather than assumed structures), this interpretation is now considered possible. This would remove one of the obstacles to better agreement with heat flow and other geophysical data.

It is clear that the GDS data by itself is incapable of independent solution, even if it were less scattered. By varying one or several parameters at either one or both of two stations, as well as the spatial wavelength, any number of possible solutions can be "confirmed", particularly for data sets with high scatter. Some useful conclusions can however be drawn:

- a) The MT-derived conductivity structures can fit the GDS data, provided we use the more conductive end of the acceptable MT-derived limits: 10 km depth rather than 15 ± 5 km, and resistivity 5 ohm-m rather than 10 ± 5 ohm-m. With these values the thickness of the layer would also be at the lower end of the MT-derived range - about 20 km rather than 20-40 km.
- b) The three-layer nature of the western structure is confirmed, although the base (upper mantle) resistivity remains uncertain. The fact that the M-ratio at 24-hour period trends above unity might indicate slightly higher base resistivities in the west than in the east - for example 75 vs 40 ohm-m, which is within the MT-derived range.

- c) The spatial wavelengths for which GDS models can be fitted vary between about 600 km and 1,500 km, which is compatible with the MT results. Within this range, the models are very sensitive to even slight variations in this parameter; this probably accounts for the large scatter observed when combining data from several events (quite apart from the already high scatter which can be expected for the ratio of four powers). The sensitivity to changes in spatial wavelength is particularly evident in the crucial period range $10^3 - 10^4$ secs in which most of the GDS data is concentrated.
- d) No coherent short-period ($< 1,000$ sec) data could be obtained over the 400 km distance between the two stations. This is partly due to the sensitivity limitations of the instruments (particularly in Z at the western stations). However, it probably also indicates that the spatial wavelengths for these periods are smaller than those derived above for the long-period range. This would not affect the validity of the MT models, since in MT only the longest periods are affected by short spatial wavelengths.

IV. OTHER GEOPHYSICAL INFORMATION

IV-A) Introduction

For purposes of interpretation of the lower crustal and upper mantle structure delineated by the geomagnetic induction work, data from three disciplines is of particular relevance and is discussed in the following sections: heat-flow, seismology, and aeromagnetic surveys. It should be stated that the relations between the results derived from these disciplines and those derived from geomagnetic induction are not at all clear-cut. The "western region" delineated by GDS is also a distinct geological region, and it is hardly surprising to find various geophysical parameters differing between this region and the rest of North America. Although it is tempting to find a common interpretation, some of these differences may be entirely unconnected with the electrical conductivity structure, having neither cause/effect connection nor even a common cause. Although the following sections are all compatible with a common causative agent (higher temperatures in the upper mantle under the western region), it will be shown that alternative explanations are possible.

IV-B) Heat-flow

Heat-flow data in western Canada is as yet too sparse for regional analysis. The few available observations indicate higher heat-flow values in southern Alberta than in the Canadian Shield - of the order of 1.5 HFU as compared to 0.8 - 1.0 HFU over the Shield (Garland and Lennox, 1962; Anglin and Beck, 1965). The HFU (Heat-flow unit) is defined as 1 microcal /cm² sec. In Canada, there is no evidence for (or against) any further

increase in heat-flow in the western region delineated by GDS; the value observed at Penticton is 1.5 HFU (A.M. Jessop, personal communication). However, in the U.S.A. the average heat-flow west of the Rockies is considerably higher than the average from other North American areas. Regions of high heat-flow have been delineated in the Basin and Range Province and west of the southern Rocky Mountains in Colorado (Roy et al, 1968a; Decker, 1969), as well as in the northwest U.S.A. (Blackwell, 1969). Two high heat-flow observations (2.0 and 2.3 HFU) have been reported on the border just south of the GDS station at Salmo (see Fig.III-2). Blackwell (1969) concluded that the Northern Cordillera, Columbia Plateaus, and the Basin and Range Province form a continuous physiographic region, the "Cordilleran thermal anomaly zone". Roy et al (1968b) combined heat-flow measurements at a number of selected sites, and derived "representative" crustal geotherms for several regions. They concluded that the contribution from the mantle towards the observed heat-flow is considerably higher in the Basin and Range Province than in the eastern U.S.A. The temperatures at depth 35 km. derived from these models are 460°C (eastern U.S.A.) and 860°C (Basin and Range Province). Similar values of temperature at depth 37 km have been derived in Australia (Howard and Sass, 1964): 460°C for the shield area, 650°C - 780°C for the off-shield areas.

The geotherms derived by Roy et al (1968b) have been used in all subsequent work in this thesis. This choice is based primarily on subjective judgement: it is felt that geotherms based on selected high-quality observations grouped in dense clusters are more reliable than those derived from regional "average" values. However, it is clear that any assumed

geotherms for the lower crust and upper mantle must be considered as speculative. It is simply impossible to extrapolate reliably to great depths from data obtained over the topmost few km. This thread of uncertainty runs throughout all the following discussions, and a qualifying phrase must be implicitly understood ahead of any mention of a specific temperature: "if the geotherms derived by Roy et al (1968b) are valid...".

We can summarize the heat-flow results as following:

- a) average heat-flow in the western U.S.A. is about twice as high as in the eastern U.S.A.; no reliable conclusions about lower crustal and upper mantle temperatures can be drawn from such average values, because of the overriding control of heat-flow by upper crustal composition.
- b) the region of high heat-flow is in fairly good spatial agreement with the high-conductivity region delineated by GDS. Only in one area (south-west U.S.A.) is the density of heat-flow observations sufficient to confirm exact (± 25 km) coincidence between the transition zones.
- c) detailed studies in the Basin and Range Province indicate a significant contribution of upward heat-flow from the mantle. In view of the continuity of the high heat flow region to the Northwest U.S.A., these results can be applied with some confidence throughout the entire western region.
- d) in this region, temperatures at depth 35 km are estimated at 860°C - about 400° higher than in the eastern U.S.A.
- e) similarly high temperatures ($650^{\circ} - 780^{\circ}$) have been derived in eastern Australia; there is some evidence that higher electrical conductivities are associated with this area as well (Everett and Hyndman, 1967).

IV-C) Seismology

The western region delineated by GDS is characterized by low Pn velocities (compressional seismic wave refracted along the top of the mantle), both in Canada (White and Savage, 1965; White et al, 1968) and in the United States (Herrin and Taggart, 1962; Pakiser and Zietz, 1965). East of the Rocky Mountains the Pn velocities are everywhere greater than 8.0 km/sec, typically 8.1 - 8.2 km/sec. West of the Rockies (except for the California coastal region) the Pn velocities are generally less than 8.0 km/sec, typically 7.8 - 7.9 km/sec. Exact coincidence between the regions of high electrical conductivity and of low Pn velocity has not been established, mainly because of the poor horizontal resolution of seismic refraction data. It is unlikely that such exact agreement can be achieved economically to the degree of accuracy with which the GDS boundary can be established (about $\pm 10 - 20$ km), since observed Pn velocities are average values obtained from long profiles. However, it would seem worthwhile to attempt such spatial correlation by long refraction profiles shot parallel to the GDS discontinuity, one on each side of it: for example, in Canada a profile between Prince George and Creston in the west, and between the Hart Mountain Range and Calgary in the east. Such confirmation of the relation between the two discontinuities could be of considerable practical interest; it could provide seismologists with a practical method to:

- a) plan the optimum location of refraction profiles, and b) interpret data from profiles which were shot across the discontinuity.

The low Pn velocities have generally been interpreted on the basis of composition changes rather than temperature effects (Thompson and Talwani, 1964; Dehlinger et al, 1964); in this case they would be unconnected with

the observed changes in electrical conductivity, since geomagnetic induction data are insensitive to composition contrasts (see Chapter V), However, there is ample evidence for the alternative (temperature effect) explanation. Laboratory data for the temperature-dependence of compressional wave velocities are very sparse, particularly for temperatures above about 400°C. Even at the lower temperatures, the coefficients for rock samples vary over a fairly wide range: from about -2.5×10^{-4} km/sec/°C for some basalt samples to as high as -38×10^{-4} for one dunite sample (Hughes and Maurette, 1957). Even for two different dunites, the coefficients varied between -10×10^{-4} for a 90% olivene sample (Hughes and Cross, 1951) and -38×10^{-4} for a 99% olivene sample (Hughes and Maurette, 1957); both were measured at the same pressure (5 Kbar). However, the latter value was obtained over a very narrow temperature range (25°C - 225°C); Hughes and Maurette (1957) state that the data "should be suspected of being in error".

For pure minerals of relevance to upper mantle compositions, the thermal coefficients are better defined, and average about -4×10^{-4} km/sec/°C for Forsterite (the magnesium end-member of the olivene suite) and Garnet, and -5×10^{-4} for Periclase (Anderson et al, 1968). Soga et al (1966) have derived relations for extrapolating the lower-temperature (<800°C) laboratory data for these minerals to temperatures as high as 2200°C. For example, for Forsterite the relation is:

$$V_p(\text{km/sec}) = 7.75 - 3.62 \times 10^{-4}T - 7.46 \times 10^{-8}T^2 + 3.66 \times 10^{-11}T^3,$$

where T is the absolute temperature (°K). For low temperatures (<500°C) only the first term is important, but as the temperature increases towards 1000°C the second term has to be included. For example, at T = 1000°K (727°C), the effective mean coefficient is 4.4×10^{-4} km/sec/°C.

Although the mineral data show well-behaved relations towards higher temperature, justifying some extrapolation, the whole-rock data show significant scatter, and steepening of the gradients in some cases (Hughes and Maurette, 1957). This raises doubts about the validity of linear extrapolation from the laboratory range (400°C) to the range of interest ($\sim 800^\circ\text{C}$) for the western upper mantle - particularly if we consider the second-order coefficients derived for the minerals. Nevertheless, the extrapolated low-temperature data can probably be accepted as the lower limit for the coefficients at these temperatures.

Using the coefficient for Forsterite ($-4.0 \times 10^{-4} \text{ km/sec/}^\circ\text{C}$) as the extreme lower limit, the inferred temperature difference of 400°C between the western and eastern regions results in a V_p differential of only 0.16 km/sec, not enough to account for all the observed difference in P_n velocity. However, this coefficient is almost certainly too low for realistic upper mantle materials. Toksoz et al (1967) considered the velocity distribution patterns under oceanic and continental regions, and concluded that $(\partial V_p / \partial T)_p$ of $-5 \times 10^{-4} \text{ km/sec/}^\circ\text{C}$ was much too low for upper mantle materials.

Using the lowest laboratory-derived coefficient for dunite ($10 \times 10^{-4} \text{ km/sec/}^\circ\text{C}$), a velocity difference of 0.40 km/sec is derived for a temperature difference of 400°C - more than enough to account for the observed decrease in P_n velocity. It is clear that no definite conclusions can be drawn until better laboratory data become available for whole-rock samples, but the observed reduction in P_n velocity can apparently be accounted for by increases in temperature of the order indicated by heat-flow data. The above argument is of course inconclusive,

since changes in composition (particularly towards a less mafic upper mantle) provide a much more direct way to change the velocities.

To summarize the seismic data: if the geotherms derived by Roy et al (1968b) are valid, the observed decrease in Pn velocity in the western region can be accounted for by temperature effects. However, laboratory data on ultramafic rocks at high temperatures and pressures is required for any valid quantitative work in this field.

IV-D) Aeromagnetic Surveys

Statistical studies have been carried out on several long aeromagnetic profiles (Serson and Hannaford, 1957; Alldredge and Van Voorhis, 1961; Alldredge et al, 1963). If short-wavelength fluctuations are filtered out, the remaining fluctuations in field strength cover a wide range of wavelengths. Spectral analysis of one very long profile (37,000 km) indicated that the "energy" (amplitude squared in a fixed wavelength-width filter) is relatively uniformly distributed between about 20 km and 250 km, with a significant drop-off for longer wavelengths (Alldredge et al, 1963); these were attributed to crustal sources. A second block of spectral "energy" at much longer wavelengths ($> 3,700$ km) was attributed to sources within the core.

It is intuitively tempting to equate longer wavelengths with sources at greater depth, but it should be kept in mind that no unique determinations can ever be derived from such surface measurements of the static magnetic field strength; long-wavelength anomalies can be explained equally well by shallower sources of larger areal extent. It can only be argued that certain source configurations are more attractive than others on the basis of other geophysical and geological considerations.

There is generally no correlation between "static magnetic" anomalies and "geomagnetic induction" anomalies, since they are sensitive to entirely different parameters. However, a study of the U.S. Trans-continental Profile has shown that the filtered aeromagnetic profiles are generally much flatter and more featureless in the west than in the east (Pakiser and Zietz, 1965). The profile runs roughly along a great circle from Norfolk, Virginia, to near San Francisco, crossing the Rocky Mountains near Denver, Colorado. The transition to the smooth "western-type" profile occurs about 160 km west of Denver, i.e. in good agreement with the position of the GDS discontinuity at this latitude (Gough and Anderson, 1968). Pakiser and Zietz (1965) and Zietz et al (1966) suggested that this "smoothing" of long wavelength features could be caused by an upwelling of the Curie isotherm to shallower depth in the western region, i.e. absence of sources in the lower crust. They did however emphasize the ambiguity of aeromagnetic data, and the possibility of alternative explanations such as a more silicic crust or more abrupt lateral variations.

In this section, some aeromagnetic data from western Canada have been examined for similar effects. Figure IV-1 shows the location of the four profiles used in this analysis. Profiles A and B were derived from Map 749G of the Geological Survey of Canada (Morley, 1959), which covered a 12 mile wide strip north of latitude 49°N; these are total-field (F) surveys obtained at flight altitudes ranging from 1,000 to 11,000 feet, depending on topography. Profiles C and D are based on data from the Dominion Observatory's three-component survey (Serson et al, 1957 ; Dawson and Dalgetty, 1966), flown at an altitude of 11,000 feet. For

profiles C and D the vertical component Z was used, as more complete coverage was available for this component. At these latitudes the anomalies in F and Z are very similar; in particular the same considerations of source depth vs. anomaly wavelength can be made for either one of these components.

On profiles A and B, the magnetic data were digitized at one-mile intervals, and replot traces of these data are shown on Figures IV-2 and IV-3. Also shown on these figures are topography and average flight altitudes (dashed line). The unfiltered plot shows large fluctuations (up to 1000 gamma amplitude) over a wide range of wavelengths. Low-pass filtering was then applied to these data, using computational operations in the wave-number domain (i.e. Fourier transform, linear filtering, and inverse Fourier transform to reconstitute the traces). The numbers shown to the right of the filtered traces are the cut-off wavelengths. As the cut-off wavelength is increased, the large-amplitude features in the western section are progressively smoothed out, and for cut-off wavelengths between about 100 and 150 km the western section becomes smooth and featureless. The long-wavelength feature east of the Purcell Mountains remains unattenuated at nearly 1000 gamma amplitude. The location of the "discontinuity" is in good agreement with the location of the GDS discontinuity, i.e. about 50 km west of the Rocky Mountain Trench and its southern continuation through the Kootenay River Valley.

Some of the properties of the computational filter should be noted at this stage. It is rectangular and provides sharp cut-off in terms of wave-number. However, there is some spectral leakage into adjacent bands and at the longer wavelengths the cut-off is less sharply defined when expressed in terms of wavelength rather than wave-number,

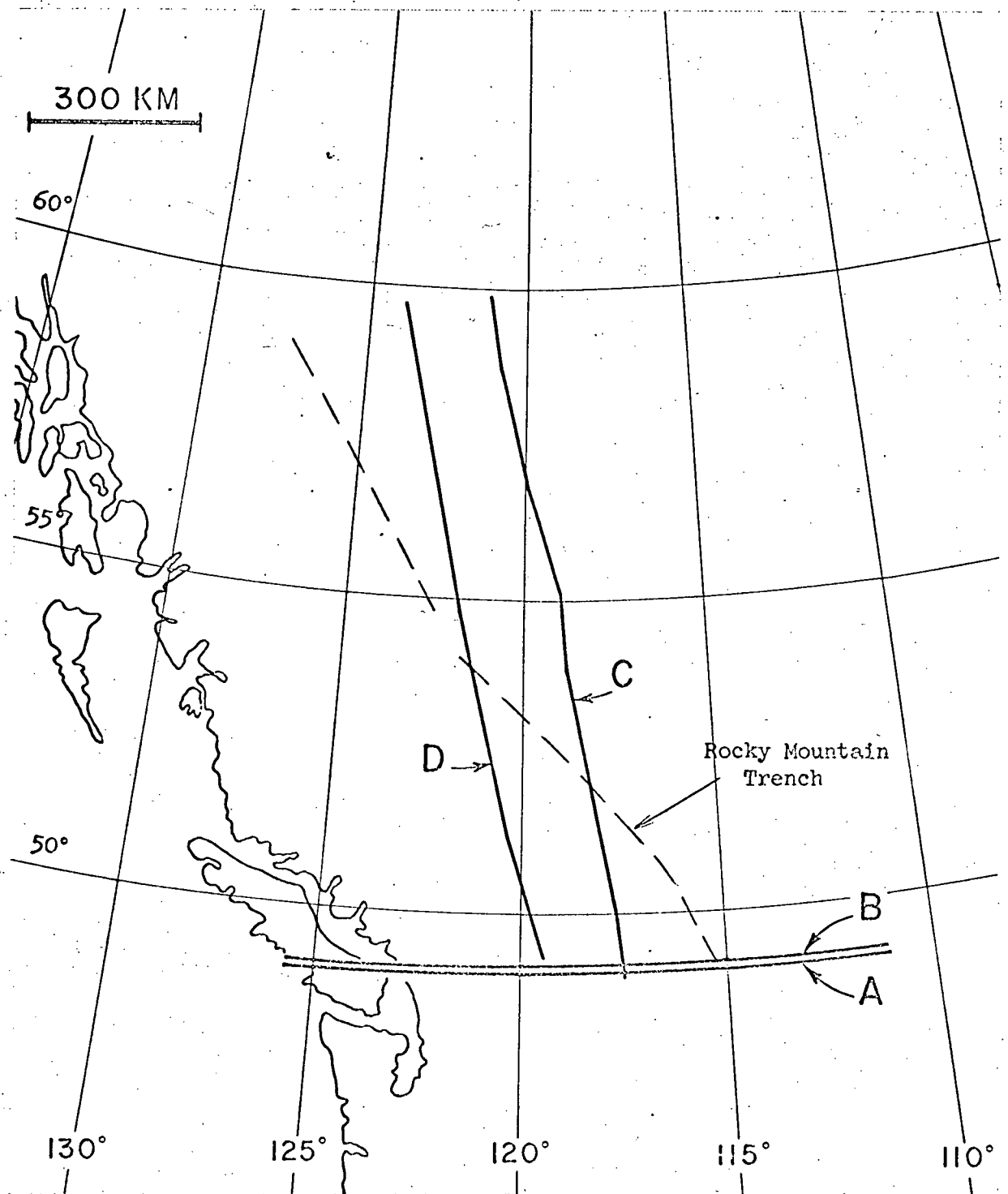


Fig. IV-1. Location of aeromagnetic profiles; A and B from Geological Survey of Canada, C and D from Dominion Observatory.

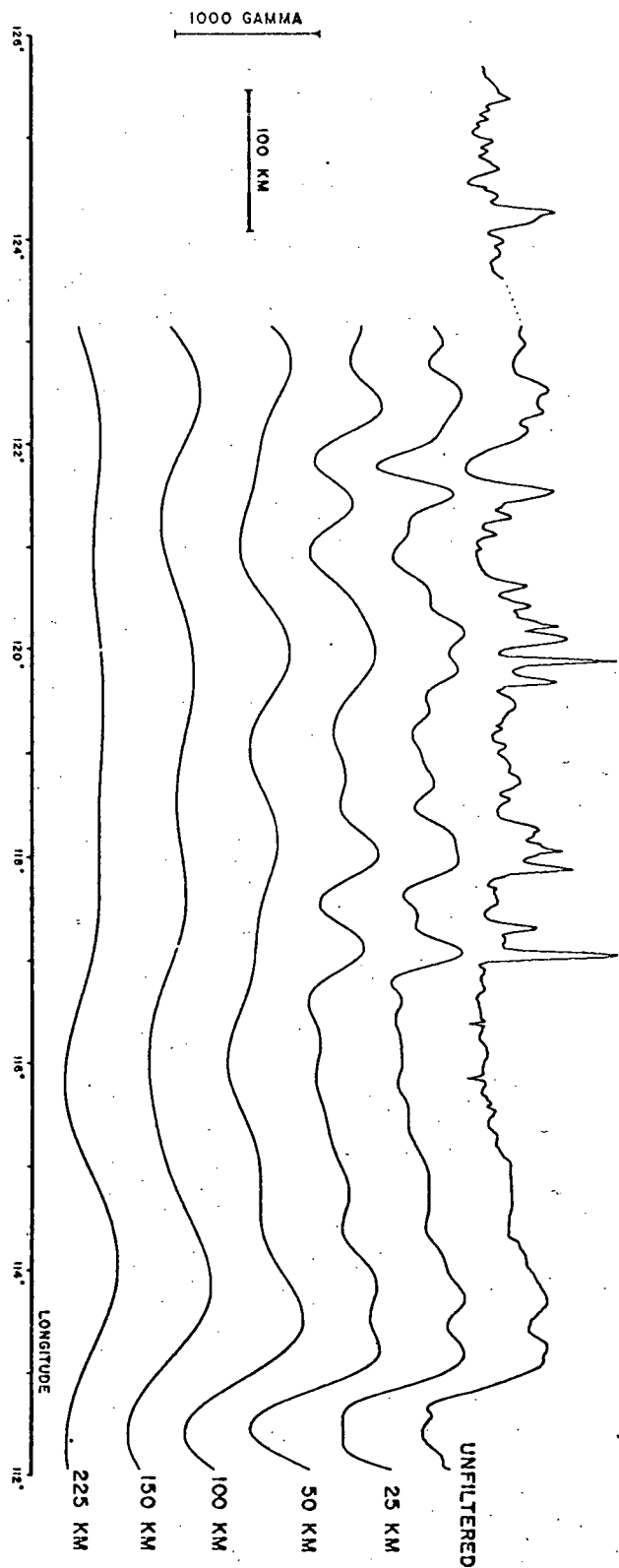
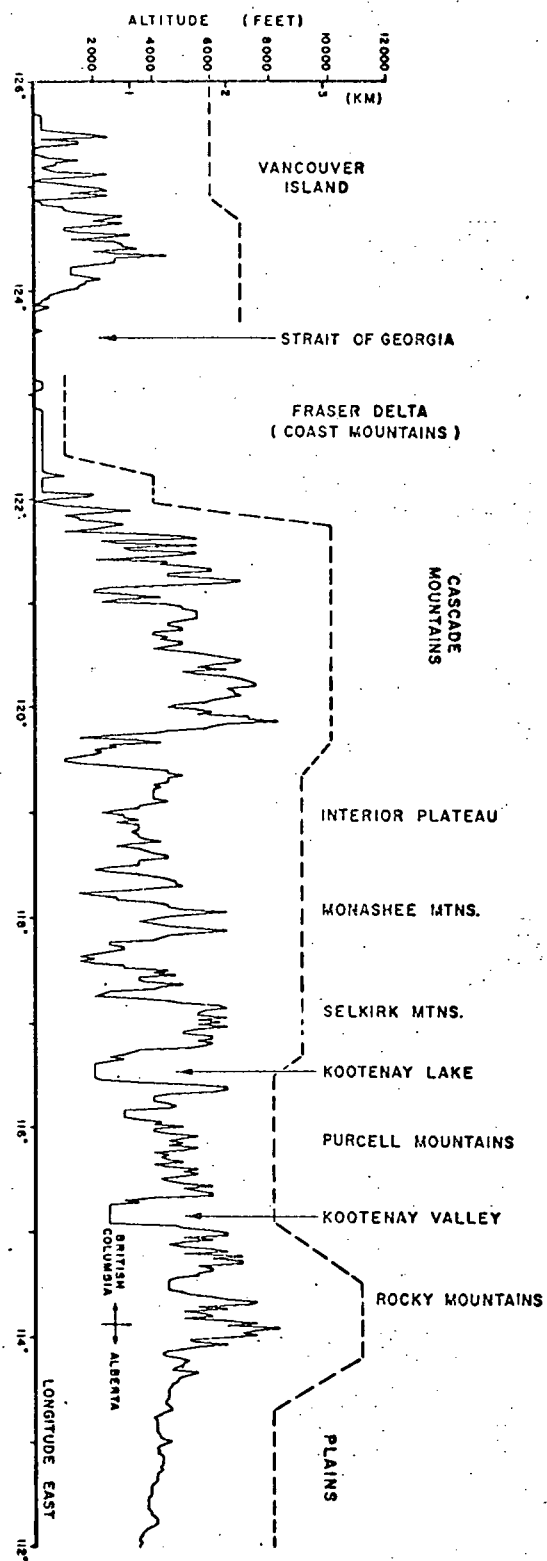
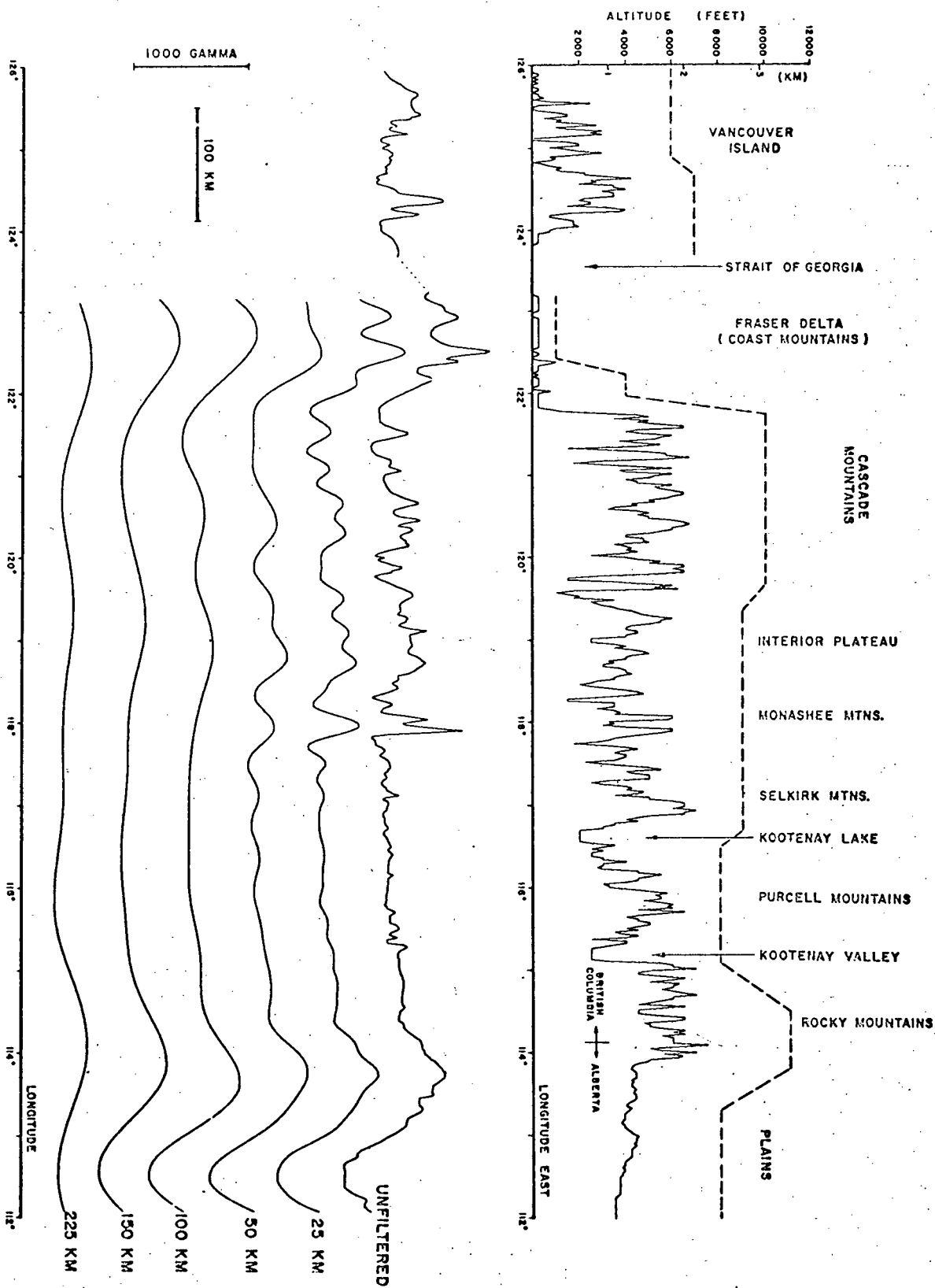


Fig. IV-2. Profile A: magnetic profiles, topography and average flight altitude (dashed line).

Fig. IV-3. Profile B: magnetic profiles, topography, and average flight altitude (dashed line).



particularly for pass-band characteristics. For example, if $L_c = 100$ km, the rejection is still total for $L < 82$ km, but there is now significant attenuation of wavelengths as high as 120 km. This explains the apparent progressive attenuation of the eastern feature (actual wavelength about 150 km) on the filtered traces of Fig. IV-2 and IV-3. It does not mean that this anomaly contains shorter-wavelength components which are progressively removed with stronger filtering; it simply emphasizes the fact that for this particular profile length (~ 800 km) the filter is not sharp enough to discriminate between wavelengths of about 120 to 250 km.

The results are in good agreement with those obtained in the U.S.A., where the long-wavelength anomalies which characterized the eastern region were absent in the western zone. Some longer-wavelength features remain in the western section of the filtered traces shown in Figures IV-2 and IV-3, although of lesser amplitude than the eastern feature. In order to estimate their significance, the filtered traces from both profiles are shown superimposed on each other in Figure IV-4. It is clear that for two profiles spaced only 11 km apart, the effects of either deep-seated or of areally-extended sources should be coherent between the two profiles. Figure IV-4 shows that this is the case only for the eastern feature; the others are not coherent and can presumably be accounted for by either flight altitude effects and diurnal contamination, or by genuine sources which are linearly extended only in the direction of flight. The longer wavelength feature in the Fraser Delta could be "genuine"; its amplitude is higher than could be accounted for by the change in flight altitude. Unfortunately the profiles are discontinuous at this point (no data across the Strait of Georgia), and analysis of this feature could not be carried out.

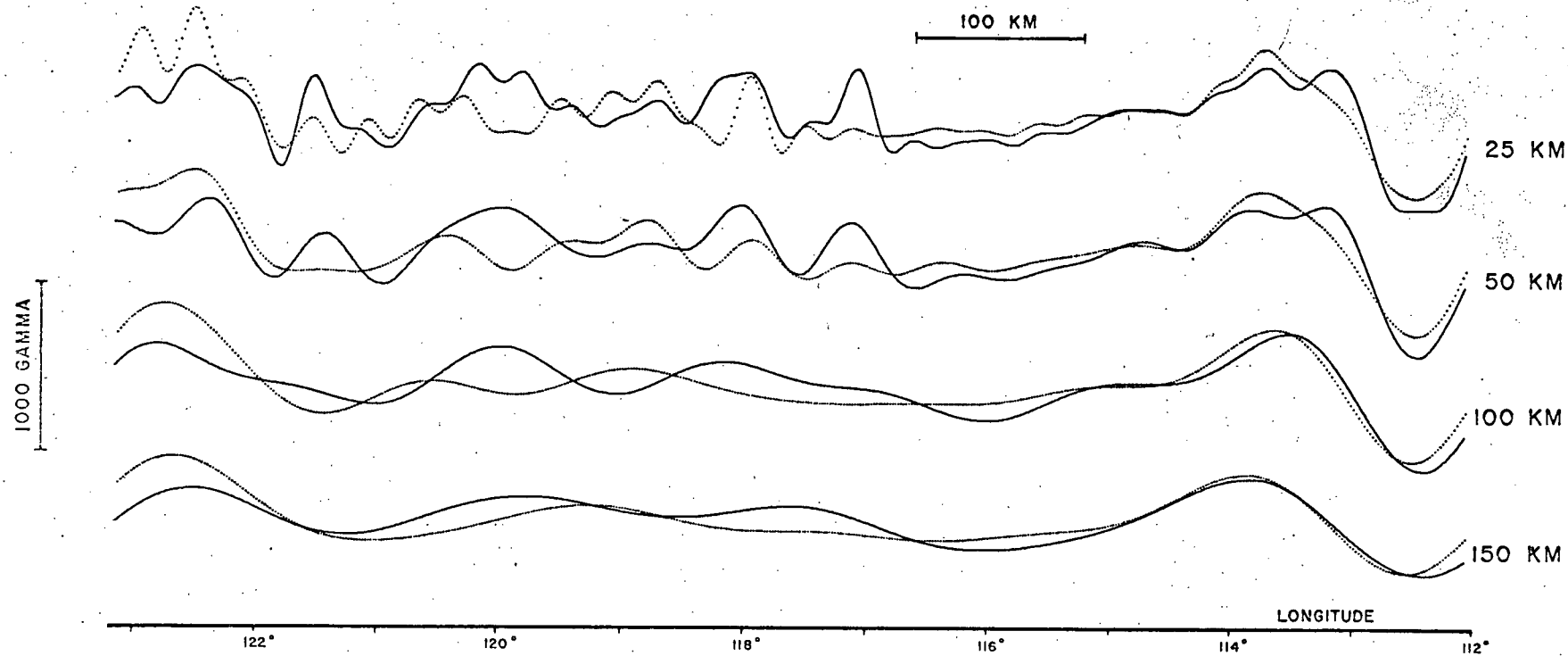


Fig. IV-4. Superimposed filtered traces for profiles A (solid curves) and B (dotted curves).

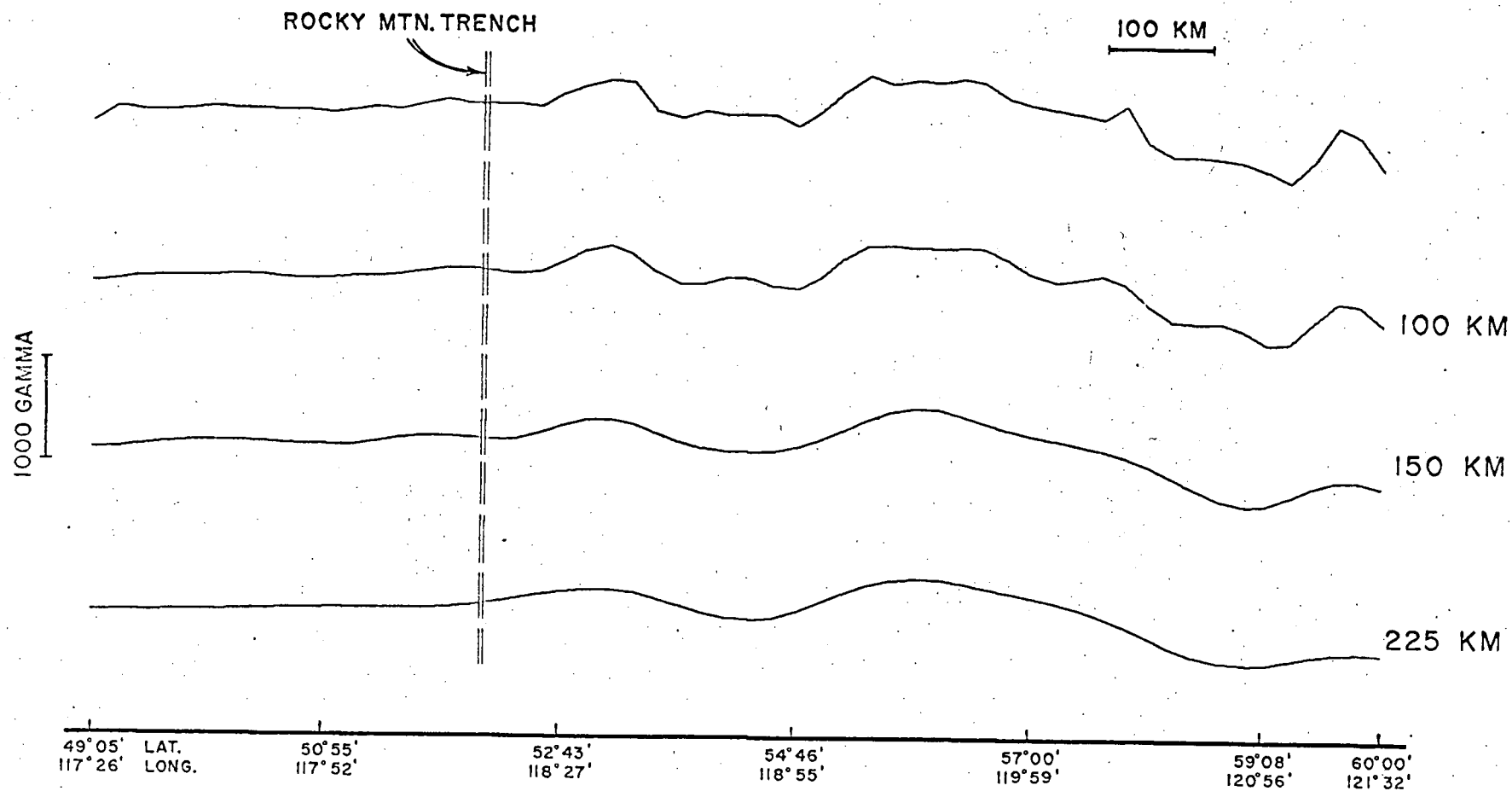


Fig. IV-5. Filtered magnetic data, Profile C.

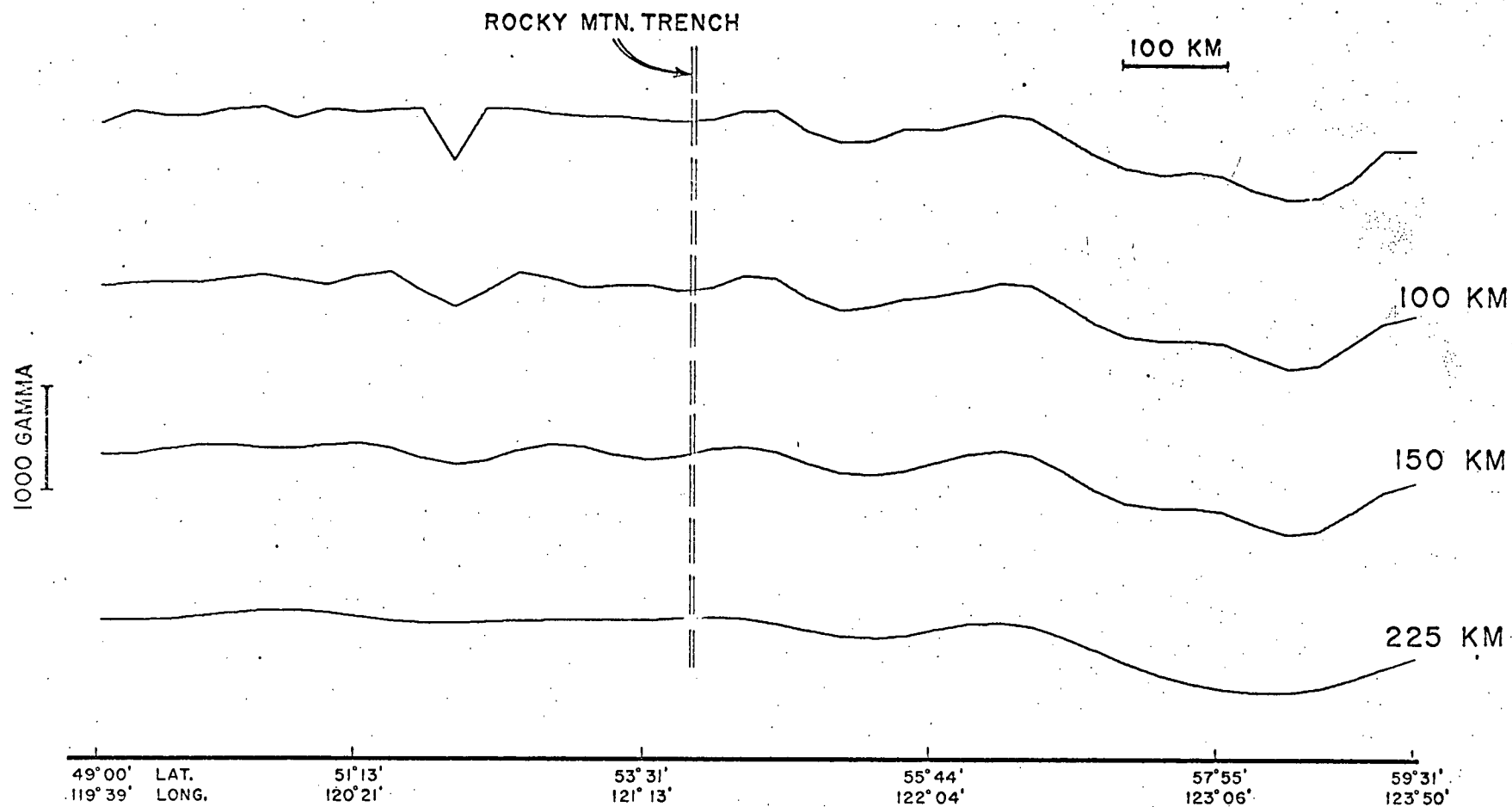


Fig. IV-6. Filtered magnetic data, Profile D.

Similar analysis was carried out on the data from profiles C and D (Figures IV-5 and IV-6). These data were in the form of average values over 5 minutes of flight (about 30 km), i.e. already pre-smoothed to remove the short wavelengths which appeared so prominently in the unfiltered data from profiles A and B. Since the number of data points was considerably lower than for the previous profiles, some care had to be taken in the Fourier transform operations. In particular, exact coincidence of the end points had to be enforced by subtraction of an arbitrary linear gradient, in order to avoid end-range distortions of the reconstituted traces due to Gibbs oscillations.

The pattern evident on the filtered traces of Figure IV-5 and IV-6 is of the same type as that observed on profiles A and B. East of the Rocky Mountain Trench, long wavelength fluctuations of significant amplitude (± 500 gamma) are observed, as reported by Serson and Hannaford (1957), and by Pakiser and Zietz (1965) in the U.S.A. West of the Trench, the filtered profiles are smooth to a remarkable degree: on profile C within ± 15 gamma up to the Trench, and within ± 5 gamma to a point 25 km west of the Trench. On profile D a one-point discontinuity (possibly of instrumental origin) introduced some distortion, but even there the profile is smooth to within ± 65 gamma from the U.S. border up to the Trench. The flight lines intersect the Trench at an angle of about 50° ; if the strike of the discontinuity does follow the Trench direction, we can therefore not expect sharp definition for the location of the discontinuity. However, judging from the most heavily filtered trace, we can place it within ± 40 km of the Trench, with somewhat higher likelihood towards the western limit of this range.

Quantitative interpretation of the smoothed profiles is virtually impossible; it is difficult enough to interpret the long-wavelength anomalies in the eastern section in view of the inherent ambiguity of magnetic data. Serson and Hannaford (1957) estimated that most of the sources lie in the upper crust (down to depth 11 km under the continents). Vacquier and Affleck (1941) estimated that the bottom of magnetic inhomogeneities lies at depths between 17.7 km and 24.1 km. However, all these estimates are obviously dependent upon some assumption of structure - no unique solution is possible. Interpretation of some specific long-wavelength anomalies in eastern Canada was carried out by Bhattacharya and Morley (1965); by imposing restraints on the shape and orientation of the structures, they derived depths to the bottom between 17.7 km and 24 km, with a mean of 20 km - same as the value derived by Vacquier and Affleck (1941). These depths were assumed to define the Curie point isotherm for crustal materials.

Although a figure of 475°C is sometimes quoted in the literature as the Curie point for basaltic materials, the Curie point for magnetite (578°C) is a more relevant limiting temperature; magnetite is the most common ferromagnetic component of igneous and metamorphic rocks, and variations in magnetic intensity are primarily produced by variations in magnetite content (Nagata, 1961; Zietz et al, 1966). Using the geotherm derived by Roy et al (1968b) for the eastern U.S.A., magnetization could therefore persist well into the uppermost 10 km of the mantle; the depths derived by Vacquier and Affleck (1961) and Bhattacharya and Morley (1965) are therefore well within the acceptable range for the existence of magnetic sources. The fact that magnetic structures can exist down to upper mantle depths does of course not imply that sources do actually

exist down to this depth. In the western region, this Curie point temperature would be reached at a much shallower depth (20-25 km according to the geotherm derived by Roy et al, 1968b).

It is clear that no interpretation can be attempted on the absence of features which cannot themselves be interpreted uniquely. If the long-wavelength anomalies observed east of the Trench are caused by deep-seated (lower crustal) inhomogeneities, then their absence in the western region can best be explained by an upwelling of the Curie point isotherm. However, if the eastern anomalies are caused by shallower structures of large areal extent and uniform magnetisation, then the most likely interpretation for their absence would be more violent "jumbling-up" of these structures in the west. Such an interpretation is in full agreement with the geological evidence; in the east geologic lineaments can be followed over long distances, but west of the Rocky Mountain Trench the structures are very complex, having been broken up by several ages of deformation, numerous intrusions, and widespread regional and contact metamorphism (White, 1959; Armstrong, 1959; Henderson, 1959). This explanation for the absence of long-wavelength anomalies in the west would be valid for whatever interpretation is accepted for the eastern anomalies. A third, even more "trivial" explanation can also not be ruled out: a more silicic crust in the west. This is also in agreement with the geological evidence; there are numerous and vast acidic intrusions west of the Trench, but none in the Rocky Mountains or to the east.

The results derived from the aeromagnetic data can be summarized as following:

a) Long aeromagnetic profiles can apparently be used to delineate a region which appears to coincide with the region of high electrical conductivity delineated by GDS. This would provide a method for expanding GDS mapping

coverage to areas beyond the reach of surface transportation.

b) The observed smoothing of long-wavelength magnetic anomalies in the western region cannot be interpreted in any unique way. Possible explanations are: upwelling of the Curie point isotherm, break-up of large structures by tectonic and metamorphic mechanisms, and/or a more silicic crust.

V. PETROLOGICAL INTERPRETATION

V-A) Summary of Data

The following two figures (V-1 and V-2) summarize virtually all the information that can be extracted from the previous sections:

(a) From GDS and aeromagnetic surveys we define the eastern boundary of a region with some distinct magnetic and electrical characteristics. The position of the boundary is defined in four places between latitudes 49°N and 54°N; since only its location (not its strike) is defined, no "border" lines have been shown on Fig. V-1.

(b) From MT and GDS, self-consistent conductivity structure models are obtained. The western structure can be applied to the entire western region defined above; the eastern structure is probably applicable only to the southwest corner of Alberta.

V-B) Electrical Conductivity of the Lower Crust and Upper Mantle

Figure V-3a shows the resistivities of some relevant materials as a function of temperature. All dry crystalline rocks are classed as "solid electrolytes" or insulators", i.e. the dominant conduction mechanisms are ionic rather than electronic. The conductivity can be expressed as a summation of several terms of form $S = S_0 e^{-U/kT}$, one term for each conduction mechanism. For any particular temperature range one of these mechanisms usually predominates, so that plots of log conductivity against inverse absolute temperatures are formed by a succession of linear segments. On Figure V-3a the right-hand segments represent ionic impurity conduction, merging into the steeper segments representing intrinsic ionic conduction for temperatures above about 500 - 700°C. Throughout this temperature range, electronic conduction is negligible.

GEOMAGNETIC STATIONS :

- ☐ LOW-I
☒ HIGH-I
☐ TRANSITION

$$I = \frac{|\Delta Z|}{[(\Delta D)^2 + (\Delta H)^2]^{1/2}}$$

AT PERIODS FROM
10 TO 120 MINUTES

AEROMAGNETIC PROFILES :

- EASTERN-TYPE
 SMOOTHED

200 km

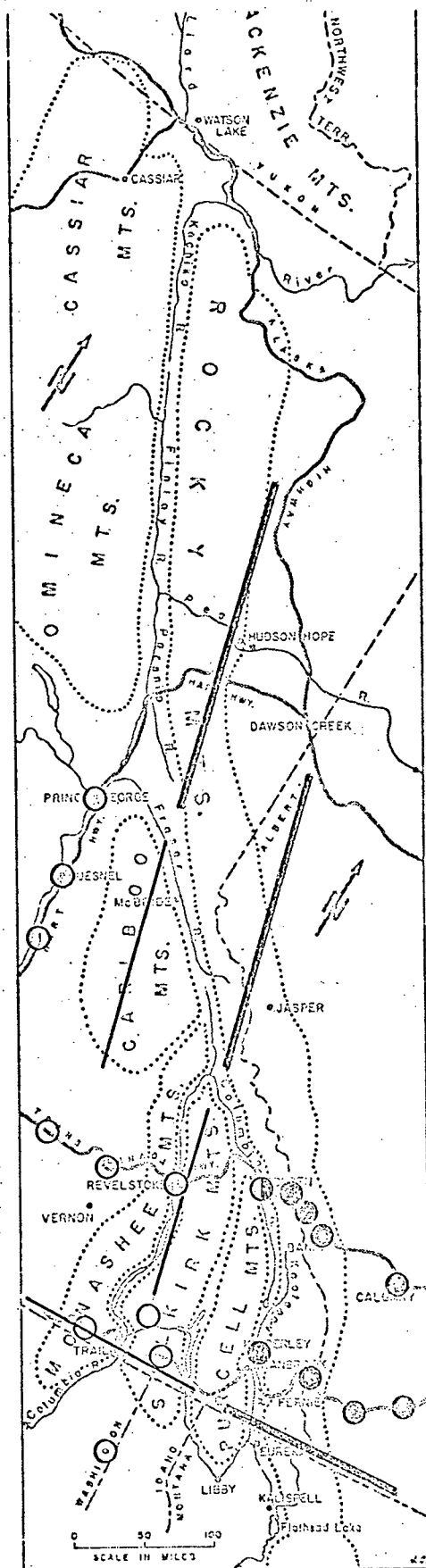


Fig. V-1. Outline of discontinuity defined by GDS and aeromagnetic data; base map after Robinson (1968).

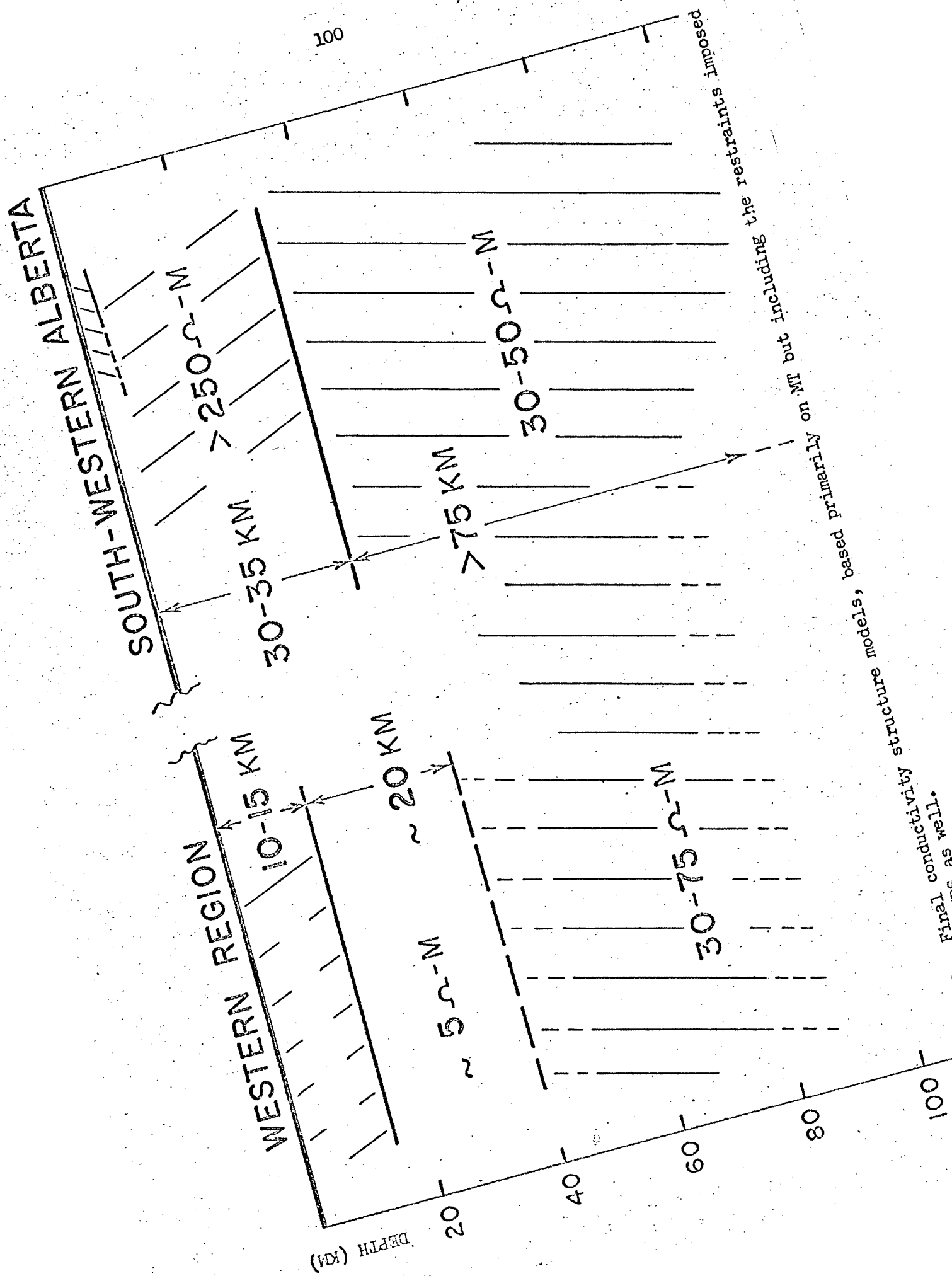
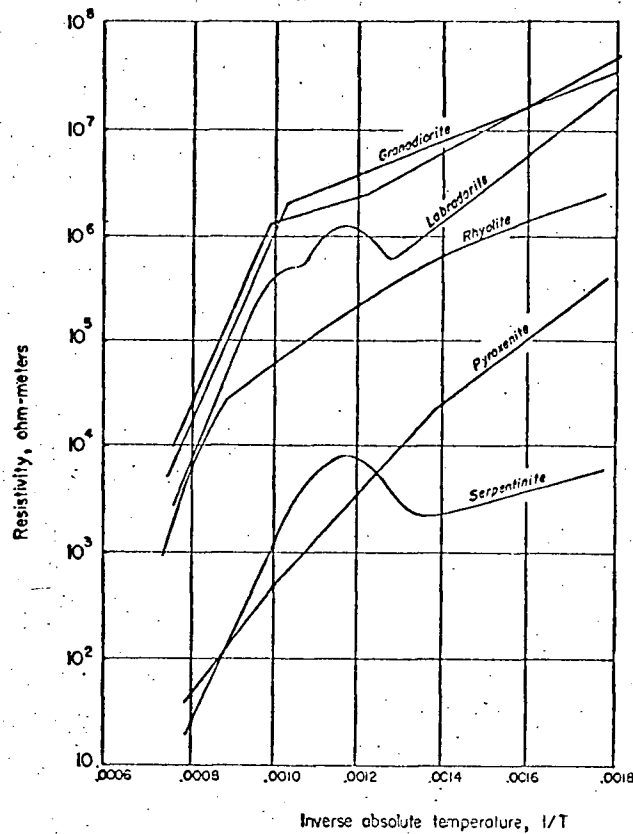


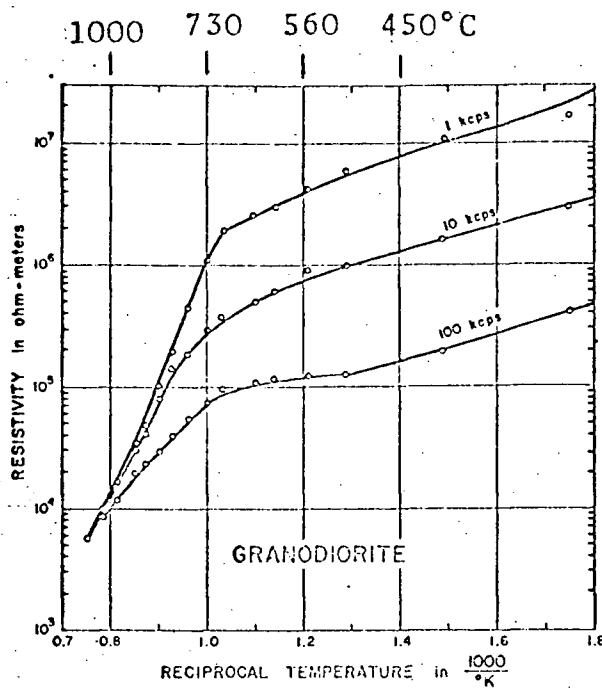
Fig. V-2.

Final conductivity structure models, based primarily on MT but including the restraints imposed by GDS as well.



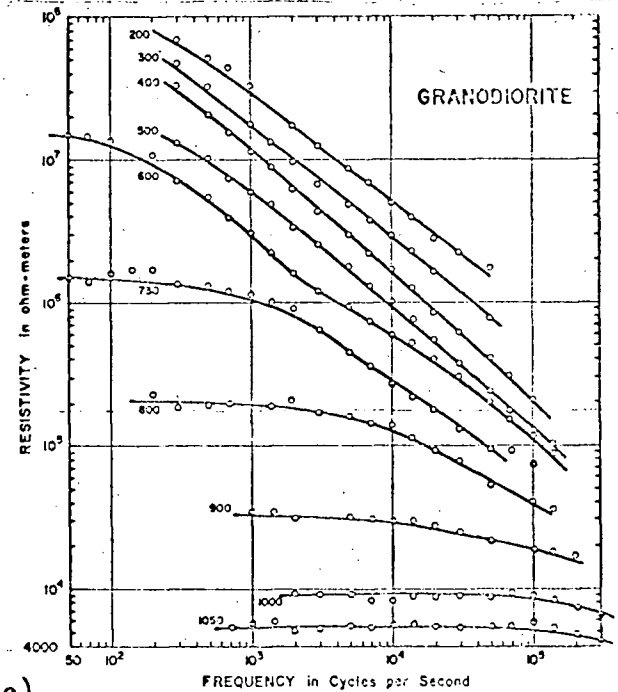
a) Resistivity as a function of $1/T$ for several rocks. The right-hand segments of the curves represent extrinsic conduction by impurities and crystal defects, the left-hand, or high-temperature portions, represent intrinsic conduction.

(after Keller and Frischknecht, 1966)



b)

(after Keller, 1963)



c)

(after Keller, 1963)

Fig. V-3. Electrical resistivity of some rocks and minerals, and frequency-dependence of such data.

Derivation of the coefficients for the exponential terms is based entirely on laboratory data, since analytic techniques cannot be applied to the ionic conduction, particularly the lower temperature impurity mechanism, for complex rock assemblages. The "typical" coefficients often quoted in the literature should be used with caution, for two reasons: a) the great variability in results obtained for the same type of rock, and b) the fact that much of the laboratory data is obtained with A.C. techniques (usually in the audio range). Figures V-3b and 3c (Keller, 1963) demonstrate the effects of frequency on conductivity measurements. For higher temperatures the effect is not too serious. However, at temperatures below 700°C, order-of-magnitude errors may be introduced when essentially "D.C." geomagnetic induction data is compared with A.C. laboratory measurements. This frequency dependence is often overlooked; for example, the 1 Kcps curve for granodiorite (Fig. 3b) has migrated into the textbook literature (Fig. 3a) without mention of its A.C. derivation, i.e. order-of-magnitude uncertainty at lower temperatures.

Several conductivity/temperature plots for ultrabasic materials are shown in Figure V-4. The olivine data have been restricted to those obtained at the pressures relevant to the lower crust and uppermost mantle; the peridotite and basalt data were obtained at atmospheric pressure. Generally, pressure effects up to 10 - 15 Kb are negligible (< 50%) compared to the effects of temperature (Keller and Frischknecht, 1966). A number of other determinations are available for basalts (for example, Noritomi, 1961); these span several orders of magnitude, presumably depending on exact composition. All the basalts described by Noritomi (1961) have resistivities above 1000 ohm-meters for temperatures up to 700°C. The

curve on Fig. V-4 has therefore been considered as the lower limit for basaltic materials.

It is clear from Figure V-4 that where "eastern-type" ($< 10^{\circ}\text{C}/\text{km}$) geothermal gradients exist, peridotite and basalt are resistive ($> 500\text{ ohm-m}$) to depths of 50 km. As seen in the previous sections, geomagnetic induction methods cannot resolve resistivity differences in regions where the resistivity exceeds 250 ohm-meters. Consequently, geomagnetic induction methods cannot be expected to "see" any discontinuities in composition within this range, such as the Conrad or Mohorovičić discontinuities. At greater depths this is not necessarily true; for example the olivine/spinel phase transformation appears to be associated with an increase in conductivity (Akimoto and Fujisawa, 1965) which may well be detectable by geomagnetic induction methods.

Exceptions to the above statement are of course possible, since the available laboratory data does not cover all relevant materials. However, the only exception which is well defined by experimental data is iron-rich olivine. The olivine suite, $(\text{Fe}_2\text{Mg}_2)\text{SiO}_4$, ranges continuously from Fayalite (Fe_2SiO_4) to Forsterite (Mg_2SiO_4), and the composition is indicated by the mole percent content of one of these end-members. For Fayalite mole percentages of 50 and over, the resistivities are well below 100 ohm-meters, even for moderate temperatures (Fig. V-4); for the higher-pressure spinel phase of Fayalite the resistivity is even lower (under 1 ohm-meter; Akimoto and Fujisawa, 1965). The assumption that upper mantle olivines are magnesium-rich is based on the evidence of surface samples, and to a lesser extent on the composition of chondritic meteorites. For example, the composition of nine olivine nodules associated with basalt lavas ranges only between Fo 89.7 and Fo 91.0, even though they come from widely separated locations (Wager, 1958); similar ranges

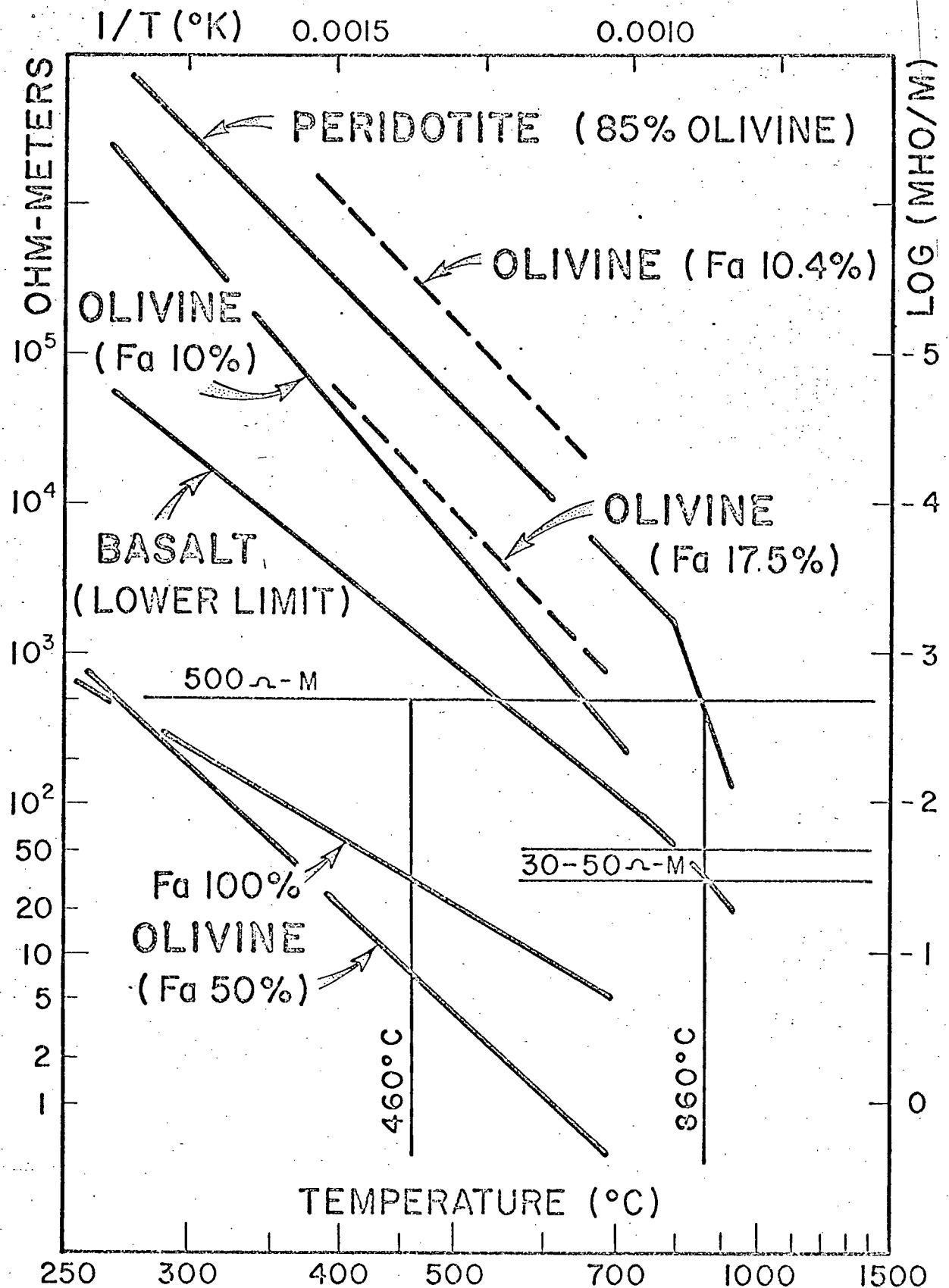


Fig. V-4. Electrical conductivity as a function of temperature, using data from Coster (1949), Bradley et al (1964), and Hamilton (1965). Dashed lines are AC-derived data.

are obtained for alpine-type dunites. Although the olivines of peridotites associated with gabbros are somewhat less Mg-rich than those from alpine-type dunites, they are still above Fo 85.

The evidence of surface samples is of course not a fully reliable indicator of upper mantle composition. However, the fractionation processes of ultramafic materials are such that magma-derived surface samples would normally be Fe-enriched with respect to the parent stock (Wager, 1958). Consequently the upper mantle olivines can be expected to be even more Mg-rich than the surface samples, and Wager (1958) estimated the upper mantle olivine composition at Fo 90. The possibility of iron-rich olivines as an explanation for low resistivities has therefore been rejected; other, as yet undefined, geochemical factors can of course not be ruled out in view of the limited amount of laboratory data.

V-C) Petrological Models

1) Eastern Region

The conductivity structure in the Pincher/Vulcan area (and probably as far west as the Rocky Mountain Trench) is characterized by a moderately conducting zone (resistivity 30-50 ohm-meters) starting at depth 30-35 km. Using the "eastern-type" geotherm of Roy et al (1968b), the temperature at depth 35 km would be 460°C and is shown as a vertical line on Fig. V-4. None of the usually accepted mafic or ultramafic materials for which laboratory data are available reach such low resistivities at this temperature; it is therefore concluded (as had already been proposed earlier on other evidence) that this southwestern corner of Alberta is not representative of the normal eastern structure. For example, if the temperature at depth 35 km is 360°C (see vertical line

on Fig. V-4), the extrapolated olivine (Fa 10%) curve gives a resistivity of about 50 ohm-meters. If we assume a steepening of the ρ/T curves for the higher temperatures, as observed for other samples, the observed resistivity (30-50 ohm-meters) can be interpreted for even lower temperatures (about 750°C).

It is concluded that under the Pincher/Vulcan area the temperature at depth 35 km must be at least 750°C, provided that this region is composed of ordinary basaltic materials. No GDS mapping is available towards the east to verify the relation of this area to the rest of North America. It is however likely that this is an anomalously high temperature, i.e. already within (or transitional towards) the high-temperature western region. The suggested structure is outlined in Figure V-7.

2) Western Region

Similar considerations indicate that the mantle below 35 km is also moderately conductive, and consistent with a temperature greater than 750°C. The lower crust is however different, being relatively highly conductive. The explanation can hardly involve temperature alone, for two reasons: a) improbably high temperatures would be required - well over 900°C at depth 20 km; and b) a temperature inversion would be required. This leaves two alternative explanations: a) partial melting in the lower crust, as suggested by Caner et al (1967), or b) hydrated lower crustal materials, as suggested by Hyndman and Hyndman (1968).

a) Partial melting: Complete melting of basalt increases the electrical conductivity by about a factor of 10. Melting data for a basalt (after Barus and Iddings, 1892) is shown on Figure V-5; point "b" denotes the start of melting, point "C" the temperature at which a homogeneous melt is reached. Similar results have been reported by Khitarov and Slutskiy (1965). For granites the increase in conductivity is much

more pronounced - up to about 3 orders of magnitude. Data from Lebedev and Khitarov (1964) and from Noritomi (1961) are shown on Fig. V-5. The main objection to partial melting of dry rocks is the required high temperature; start of melting for these materials is at 1000°C or higher, which is unlikely to be reached at the required depths of 10-15 km.

b) Hydration: Hyndman and Hyndman (1968) proposed a tectonic model which would account for a hydrated lower crust under tectonically young areas. This lower crust is subsequently dehydrated by the upwards migration of granite-water melts, leaving the stable (dehydrated and granite-depleted) lower crust of shield areas. The electrical resistivity of granite is markedly lowered by any water content; for example, the resistivity of granite at 600°C is decreased by at least three orders of magnitude for $P_{H_2O} = P_{total} = 1 \text{ Kbar}$ (Lebedev and Khitarov, 1964) - see Fig. V-5. This corresponds to a water concentration of about 4% by weight. Even lower resistivities (under 1 ohm-meter for $T = 600^\circ\text{C}$) are obtained for higher partial water pressures (Lebedev and Khitarov, 1964). Unfortunately, hydrous data is available only for $P_{H_2O} = P_{total}$, i.e. rocks fully saturated at the particular temperature. Since the saturating water content varies markedly with temperature, such hydrous experiments are not a reliable measure of real conditions; the changing water content as well as the changing temperature affect the conductivity. No experimental data is available for fixed water concentrations less than saturation.

No experimental data is available for hydrated mafic and ultramafic rocks at high temperatures and pressures. However, it is likely that a similar increase in conductivity exists; the melting point of mafic materials is significantly lowered by water content, so that we could also expect lower activation energies for ionic conduction (Hyndman and Hyndman, 1968).

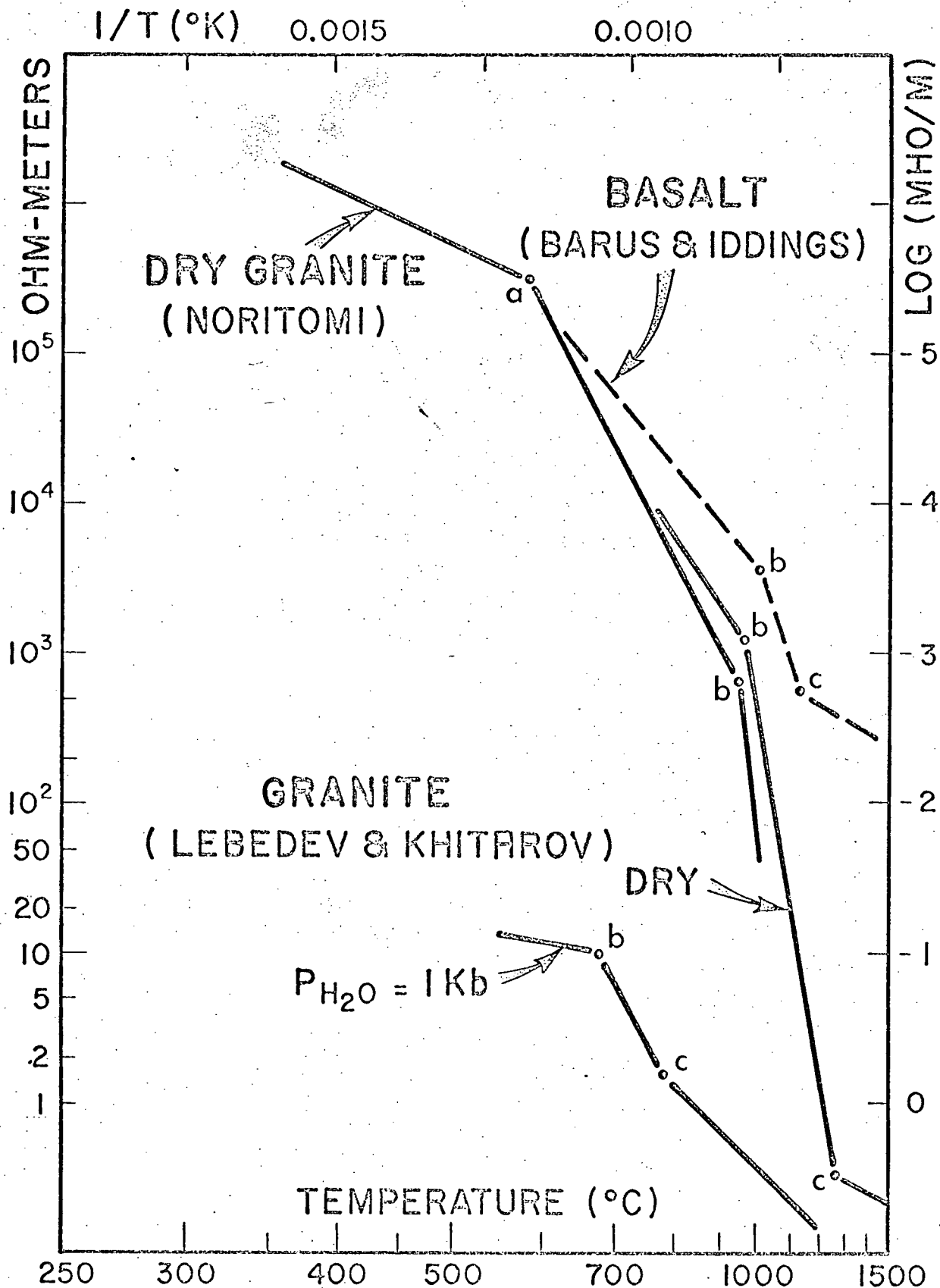


Fig. V-5. Effects of hydration and melting on electrical conductivity of rocks. Basalt data is DC-derived, granite data is AC-derived. Sections b - c of the curves are the partial melting zones.

It is clear from Fig. V-5 that a reasonable water concentration can readily account for the conductivities observed for the lower crust in the western region, either with or without any assumptions of higher temperatures. However, it should be noted that the melting point of granitic and mafic materials is also markedly lowered by hydration (Tuttle and Bowen, 1958; Yoder and Tilley, 1962); at depth 20 km the melting temperature can be lowered by as much as 250°C for full hydration. Consequently, if the lower crust is hydrated, and if we accept the higher temperatures indicated by the moderate conductivities in the upper mantle, then partial melting should occur in this lower crustal layer.

Figure V-6 shows some of the relevant data for melting and hydration depths. The "western" geotherm (after Roy et al, 1968b) clearly does not intersect the melting zone for dry basalt within the crust; it does however intersect the solidus for "wet" granite well within the crust. The width of the melting zone (i.e. between start and completion of melting) depends on the water content. The curves shown in Fig. V-6 are for 2% H₂O; for higher concentrations, the melting zone would be narrower, and at the limit of full saturation (about 9-10% H₂O) it would coincide with the start of melting curve. By postulating specific water content percentages, the width of this melting zone can therefore be adjusted to any desired value, but the starting point remains fixed at 24 km for this particular assumed geotherm.

V-D) Conclusions

Figure V-7 provides a summary of the petrological models; there are two distinct results:

- 1) In southwestern Canada (boundaries not clearly defined, but at least

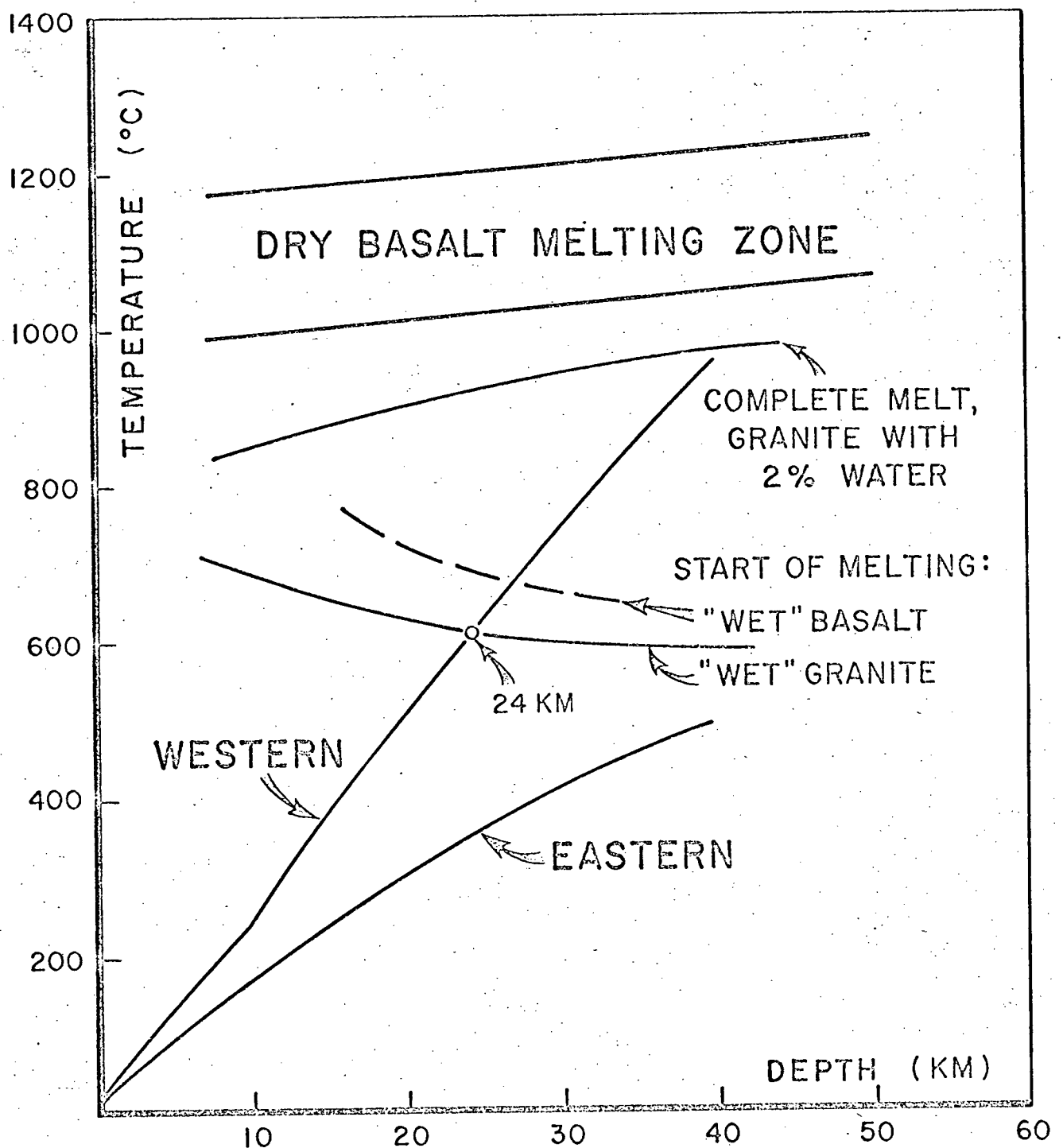


Fig. V-6. Geotherms (after Roy et al, 1968b) and melting zones, using data from Tuttle and Bowen, 1958; Yoder and Tilley, 1962; Lambert and Wyllie, 1968.

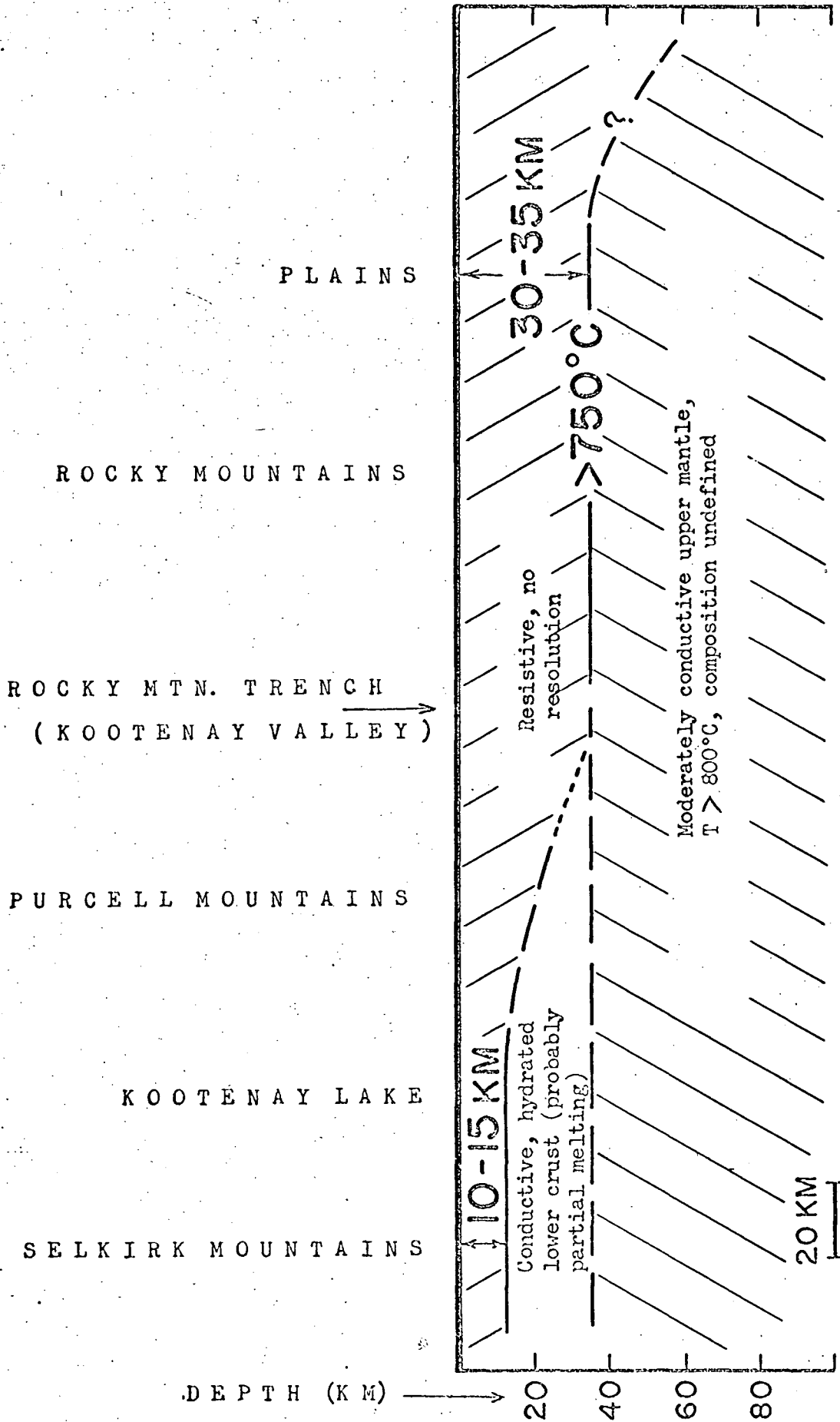


Fig. V-7. Combined petrological model, latitude 49.3°N (horizontal scale = vertical scale)

as far east as Pincher), the uppermost mantle is moderately conducting down to a depth of at least 100 km. Excluding geochemically improbable explanations (such as a regionally iron-rich upper mantle), a temperature of at least 750°C at depth 35 km is indicated. This provides independent confirmation of heat-flow derived estimates; unlike interpretation of heat-flow data, the geomagnetic induction results are not dependent on any assumptions of crustal structure and composition.

2) In a sharply delineated region, starting from about 0-50 km west of the Rocky Mountain Trench, the lower crust is conductive. The most likely interpretation is a hydrated lower crust, as proposed by Hyndman and Hyndman, 1968. Hydration alone is sufficient to explain the observed data, i.e. higher temperatures are not necessarily required for this model. However, given the information from (1) above, some partial melting probably occurs in this zone since the melting temperature is lowered by hydration.

REFERENCES

- ADAM, A., 1964. Über die Berechnung der magnetotellurischen (MT) Anisotropie. Freiburger Forschungshefte, C168, 1-48.
- AKIMOTO, S., and FUJISAWA, H., 1965. Demonstration of the electrical conductivity jump produced by the Olivine-spinel transition. J. Geophys. Res., 70, 443-449.
- ALLDREDGE, L.R. and VAN VOORHIS, G.D., 1961. Depth to sources of magnetic anomalies. J. Geophys. Res., 66, 3793-3800.
- ALLDREDGE, L.R., VAN VOORHIS, G.D., and DAVIS, T.M., 1963. A magnetic profile around the world. J. Geophys. Res., 68, 3679-3692.
- ANDERSON, O.L., SCHREIBER, E., and LIEBERMANN, R.C., SOGA, N., 1968. Some elastic constant data on minerals relevant to Geophysics. Rev. Geophys., 6, 491-524.
- ANGLIN, F.M. and BECK, A.E., 1965. Regional heat flow pattern in western Canada. Can. J. Earth Sc., 2, 176-182.
- ARMSTRONG, J.E., 1959. Physiography of the Rocky Mountain Trench. Bull. Can. Inst. Min. & Metallurgy, 52, 318-321.
- BARTELS, T., HECK, N.H., and JOHNSTON, H.F., 1939. The three-hour-range index measuring geomagnetic activity. Terr. Magn., 44, 411-454.
- BARUS, C. and IDDINGS, J.P., 1892. Note on the change of electric conductivity observed in rock magmas of different composition on passing from liquid to solid. Am. J. of Science, 3rd Series 44, 242-249.
- BHATTACHARYYA, B.K. and MORLEY, L.W., 1965. The delineation of deep crustal magnetic bodies from total field aeromagnetic surveys. J. Geomagn. Geoelectr. Japan, 17, 237-252.
- BLACKMAN, R.B. and TUKEY, J.W., 1959. The Measurement of Power Spectra. Dover Publication, New York.
- BLACKWELL, D.D., 1969. Heat-flow determinations in the northwestern United States. J. Geophys. Res., 74, 992-1007.
- BOSTICK, F.X. and SMITH, H.W., 1962. Investigation of large-scale inhomogeneities in the earth by the magneto-telluric method. Proc. Inst. Radio Eng., 50 (No. 11), 2339-2346.

- BRADLEY, R.S., JAMIL, A.K., and MUNRO, D.C., 1964. The electrical conductivity of olivines at high temperatures and pressures. *Geochem. Cosmochim. Acta*, 28, 1669-1678.
- CAGNIARD, L., 1953. Basic theory of the magneto-telluric method of geophysical prospecting. *Geophysics*, 18, 605-635.
- CAGNIARD, L., 1956. "Electricite tellurique", in *Encyclopedia of Physics*, Vol. XLVII (Geophysics I), Springer-Verlag (Berlin), 407-469.
- CANER, B. and WHITHAM, K., 1962. A semi-automatic magnetogram reader. *J. Geophys. Res.* 67, 5362-5364.
- CANER, B. and CANNON, W.H. 1965. Geomagnetic depth-sounding and correlation with other geophysical data in western North America. *Nature*, 207, 927-928.
- CANER, B., CANNON, W.H., and LIVINGSTONE, C.E., 1967. Geomagnetic depth-sounding and upper mantle structure in the Cordillera region of western North America. *J. Geophys. Res.* 72, 6335-6351.
- CANER, B. and AULD, D.R., 1968. Magneto-telluric determination of upper mantle conductivity structure at Victoria, British Columbia. *Can. J. Earth Sc.*, 5, 1209-1220.
- CANNON, W.H., 1967. Geomagnetic depth-sounding in southern British Columbia and Alberta. Unpublished thesis, University of British Columbia, Vancouver.
- CANTWELL, T. and MADDEN, T.R., 1960. Preliminary report on crustal magneto-telluric measurements. *J. Geophys. Res.* 65, 4202-4205.
- CANTWELL, T., NELSON, P., WEBB, J., and ORANGE, A., 1965. Deep resistivity measurements in the Pacific Northwest. *J. Geophys. Res.*, 70, 1931-1937.
- CANTWELL, T. and ORANGE, A., 1965. Further deep resistivity measurements in the Pacific Northwest. *J. Geophys. Res.*, 70, 4068-4072.
- COSTER, H.P., 1949. The electrical conductivity of rocks at high temperatures. *Geophys. Suppl., M.N. Royal Astr. Soc.*, 5, 193-199.
- DAWSON, E. and DALGETTY, L.C., 1966. Magnetic charts of Canada for Epoch 1965. *Dom. Obs. Pub.*, 31 (No. 9), 379-405.
- DECKER, E.R., 1969. Heat flow in Colorado and New Mexico. *J. Geophys. Res.*, 74, 550-559.
- DEHLINGER, P., CHIBURIS, E.F., and COLLIVER, M.M., 1964. Pacific northwest states local travel-time curves and their geologic implications. Paper presented at Western American Geophys. Union meeting, Seattle, Dec. 1964.

- EVERETT, J.J. and HYNDMAN, R.D., 1967. Geomagnetic variations and electrical conductivity structure in southwestern Australia. *Phys. Earth & Planet. Interiors*, 1, 24-34.
- FOURNIER, H.G., 1965. Abaque des solutions du système magnéto-tellurique en suivant la méthode L. Cagniard. Note No. 9, Institut de Physique du Globe, Université de Paris.
- FOURNIER, H.G., 1966. Essai d'un historique des connaissances magnéto-telluriques. Institut de Physique du Globe, Paris, Note No. 17.
- FOURNIER, H.G., WARD, S.H., and MORRISON, H.F., 1963. Magnetotelluric evidence for the low velocity layer. *Space Sc. Lab Report, Series 4, No. 76*, Univ. of California, Berkeley.
- GARLAND, G.D. and LENNOX, D.H., 1962. Heat flow in western Canada. *Geophys. J.*, 6, 245-262.
- GOUGH, D.I. and REITZEL, J.S., 1967. A portable three-component magnetic variometer. *J. Geomag. Geoelectr. Japan*, 19, (No. 3), 203-215.
- GOUGH, D.I. and ANDERSON, C.W., 1968. Magnetic deep sounding in the Rocky Mountains. Paper presented at CAP meetings, Calgary, June 5-8, 1968.
- HAMILTON, R.M., 1965. Temperature variation at constant pressures of the electrical conductivity of periclase and olivine. *J. Geophys. Res.*, 70, 5679-5692.
- HENDERSON, G.G.L., 1959. Summary of the regional structure and stratigraphy of the Rocky Mountain Trench. *Bull. Can. Inst. Min. & Metallurgy*, 52, 322-333.
- HERRIN, E. and TAGGART, J., 1962. Regional variations in Pn velocity and their effect on the location of epicenters. *Bull. Seism. Soc. Am.*, 52, 1037-1046.
- HOWARD, L.E. AND SASS, J.H., 1964. Terrestrial heat flow in Australia. *J. Geophys. Res.*, 69, 1617-1626.
- HUGHES, D.S. and CROSS, J.H., 1951. Elastic wave velocities at high pressures and temperature. *Geophysics*, 16, 577-593.
- HUGHES, D.S. and MAURETTE, C., 1957. Variation of elastic wave velocities in basic igneous rocks with pressure and temperature. *Geophysics*, 22, 23-31.

- HYNDMAN, D.H., 1963. Electrical conductivity inhomogeneities in the earth's upper mantle. Unpublished thesis, University of British Columbia, Vancouver.
- HYNDMAN, R.D. and HYNDMAN, D.W., 1968. Water saturation and high electrical conductivity in the lower continental crust. *Earth & Planet. Sc. Letters*, 4, 427-432.
- JACKSON, D.B., 1966. Deep resistivity probes in the southwestern United States. *Geophysics*, 31, 1123-1144.
- JONES, F.W. and GEIDART, L.P., 1967. Vertical telluric currents. *Earth Planet. Sc. Letters*, 2, 69-74.
- KELLER, G.V., 1963. Electrical properties in the deep crust. *IEEE Trans. on Ant. and Propag.*, Vol. Ap-11, 344-357.
- KELLER, G.V. and FRISCHKNECHT, F.C., 1966. *Electrical Methods in Geophysical Prospecting*. Pergamon Press, Oxford.
- KELLER, G.V., ANDERSON, L.A., and PRITCHARD, J.I., 1966. Geological Survey investigations of the electrical properties of the crust and upper mantle. *Geophysics*, 31, 1078-1087.
- KHITAROV, N.I. and SLUTSKIY, A.B., 1965. The effect of pressure on the melting temperatures of albite and basalt (based on electroconductivity measurements). *Geochemistry International*, 2, 1034-1041.
- LAMBERT, A. and CANER, B., 1965. Geomagnetic depth-sounding and the coast effect in western Canada. *Can. J. Earth Sc.*, 2, 485-509.
- LAMBERT, I.B. and WYLLIE, P.J., 1968. Stability of Hornblende and a model for the low-velocity zone. *Nature*, 219, 1240-1241.
- LEBEDEV, E.B. and KHITAROV, N.I., 1964. Dependence of the beginning of melting of granite and the electrical conductivity of its melt on high vapor pressure. *Geochemistry International*, 1, 193-197.
- LEE, W.H.K. and UYEDA, S., 1965. Review of heat flow data. *Terrestrial Heat Flow*, Geophys. Monograph No. 8, American Geophysical Union, 87-190.
- LIVINGSTONE, C.E., 1967. Geomagnetic depth-sounding in the southwest U.S.A. and in southern British Columbia. Unpublished thesis, University of British Columbia, Vancouver.
- MADDEN, T. and NELSON, P., 1964. A defense of Cagniard's magnetotelluric method. *Geophysics Lab Report*, Mass. Inst. of Techn., Cambridge, Mass.
- MATSUSHITA, S., 1960. Studies on sudden commencements of geomagnetic storms using IGY data from the United States stations. *J. Geophys. Res.*, 65, 1423-1435.
- MORLEY, L.W., 1959. Aeromagnetic survey across the Cordillera. Map No. 749G, Geological Survey of Canada, Ottawa.

- NAGATA, T., 1961. Rock Magnetism, Maruzen Publ. Co., Tokyo.
- NIBLETT, E.R. and SAYN-WITTGENSTEIN, C., 1960. Variation of electrical conductivity with depth by the magneto-telluric method. *Geophysics*, 25, 998-1008.
- NORITOMI, K., 1961. The electrical conductivity of rock and the determination of the electrical conductivity of the earth's interior. *J. of Mining College, Akita University*, 1, 27-59.
- O'BRIEN, D.P. and MORRISON, H.F., 1967. Electromagnetic fields in an N-layer anisotropic half-space. *Geophysics*, 32, 668-677.
- PAKISER, L.C. and ZIETZ, I., 1965. Transcontinental crustal and upper-mantle structure. *Rev. Geophys.*, 3, 505-520.
- PARKINSON, W.D., 1962. The influence of continents and oceans on geomagnetic variations. *Geophys. J.*, 6, 441-449.
- PLOUFF, D., 1966. Magnetotelluric soundings in the southwestern United States. *Geophysics* 31, 1145-1152.
- PORATH, H., 1969. Electrical conductivity anomalies in New Mexico and West Texas (Abstract), *Trans. AGU*, 50, 136.
- PRICE, A.T., 1962. The theory of magnetotelluric methods when the source field is considered. *J. Geophys. Res.* 67, 1907-1918.
- RIKITAKE, T., 1959. Anomaly of geomagnetic variations in Japan. *Geophys. J.*, 2, 276-287.
- RIKITAKE, T., 1962. Possibility of detecting the mantle low-velocity layer by geomagnetic deep sounding. *Bull. Earthq. Res. Inst., Tokyo Univ.*, 40, 495-509.
- RIKITAKE, T., 1966. *Electromagnetism and the Earth's Interior*, Elsevier Publ. Co., Amsterdam.
- RIKITAKE, T. and WHITHAM, K., 1964. Interpretation of the Alert anomaly in geomagnetic variations. *Can. J. Earth Sc.*, 1, 35-62.
- ROBINSON, J.L., 1968. The Rocky Mountain Trench in Eastern British Columbia. *Can. Geograph. J.*, 77, 132-140.
- ROY, R.F., DECKER, E.R., BLACKWELL, D.D., and BIRCH, F., 1968a. Heat flow in the United States. *J. Geophys. Res.*, 73, 5207-5221.
- ROY, R.F., BLACKWELL, D.D., and BIRCH, F., 1968b. Heat generation of plutonic rocks and continental heat flow provinces. *Earth & Planet. Sc. Letters*, 5, 1-12.
- SCHMUCKER, U., 1964. Anomalies of geomagnetic variations in the southwestern United States. *J. Geomag. Geoelectr. Japan*, 15, 193-221.
- SERSON, P.H., 1957. An electrical recording magnetometer. *Can. J. Phys.*, 35, 1387-1394.

- SERSON, P.H. and HANNAFORD, W.L.W., 1957. A statistical analysis of magnetic profiles. *J. Geophys. Res.*, 62, 1-18.
- SERSON, P.H., MACK, S.Z., and WHITHAM, K., 1957. A three-component airborne magnetometer. *Pub. Dom. Obs. Ottawa*, 19, No. 2.
- SOGA, N., SCHREIBER, E., and ANDERSON, O.L., 1966. Estimation of bulk modulus and sound velocities of oxides at very high temperatures. *J. Geophys. Res.*, 71, 5315-5320.
- SRIVASTAVA, S.P., 1965. Method of interpretation of magnetotelluric data when source field is considered. *J. Geophys. Res.* 70, 945-954.
- SRIVASTAVA, S.P., 1967. Magneto-telluric two and three-layer master curves. *Publ. Dom. Obs. Ottawa*, 35, No. 7, 309-316.
- SRIVASTAVA, S.P., DOUGLASS, J.L., and WARD, S.H., 1963. The application of the magnetotelluric and telluric methods in central Alberta. *Geophysics*, 28, 426-446.
- SRIVASTAVA, S.P., and JACOBS, J.A., 1964. Determination of the resistivity distribution at Meanook, Alberta, Canada, by the magnetotelluric method. *J. Geomagn. Geoelectr. Japan*, 15, 280-288.
- SWIFT, C.M., 1967. A magnetotelluric investigation of an electrical conductivity anomaly in the southwestern United States. Ph.D. thesis, Dept. of Geology and Geophysics, M.I.T., Cambridge, Mass.
- THOMPSON, G.A. and TALWANI, M., 1964. Geology of the crust and upper mantle, western United States. *Science*, 146, 1539-1549.
- TOKSÖZ, M.N., CHINNERY, M.A., and ANDERSON, D.L., 1967. Inhomogeneities in the earth's mantle. *Geophys. J.*, 13, 31-59.
- TUTTLE, O.F. and BOWEN, N.L., 1958. Origin of granite in the light of experimental studies. *Geol. Soc. Am. Memoir* No. 74.
- VACQUIER, V. and AFFLECK, J., 1941. A computation of the average depth to the bottom of the earth's magnetic crust, based on a statistical study of local magnetic anomalies. *Trans. Am. Geophys. Union*, 22, 446-450.
- VOZOFF, K. and ELLIS, R.M., 1966. Magnetotelluric measurements in southern Alberta. *Geophysics*, 31, 1153-1157.
- WAGER, L.R., 1958. *Beneath the Earth's Crust*. Adv. of Science (London), 15, 31-45.
- WAIT, J.R., 1962. Theory of magnetotelluric fields, *J. Res. NBS*, Vol. 66D, 509-541.

- WATANABE, T., 1964. A "self-consistent solution" method for determining the electrical conductivity in the subsurface regions of the earth. *Can. J. Earth Sc.*, 2, 206-210.
- WHITE, WM. H., 1959. Cordilleran tectonics in British Columbia. *Bull. Am. Ass'n., Petroleum Geol.*, 43, 60-100.
- WHITE, W.R.H. and SAVAGE, J.C., 1965. A seismic refraction and gravity study of the earth's crust in British Columbia. *Bull. Seism. Soc. Am.* 55, 463-486.
- WHITE, W.R.H., BONE, M.N., and MILNE, W.G., 1968. Seismic refraction surveys in British Columbia 1964-1966: a preliminary interpretation. *The Crust and Upper Mantle of the Pacific Area, Geophys. Monograph No. 12, Amer. Geophys. Union*, 81-93.
- WHITHAM, K., 1963. An anomaly in geomagnetic variations at Mould Bay in the Arctic Archipelago of Canada. *Geophys. J.*, 8, 26-43.
- WHITHAM, K., 1965. Geomagnetic variation anomalies in Canada. *J. Geomagn. Geoelectr. Japan*, 17, 481-498.
- WHITHAM, K. and ANDERSEN, F., 1962. The anomaly in geomagnetic variations at Alert in the Arctic Archipelago of Canada. *Geophys. J.*, 7, 220-243.
- WIESE, H., 1965. Geomagnetische Tiefentellurik. *Geomagn. Inst. Potsdam, Abh. No. 36*.
- YODER, H.S. and TILLEY, C.E., 1962. Origin of basalt magmas: an experimental study of natural and synthetic rock systems. *J. Petrology*, 3, 342-532.
- ZIETZ, I., KING, E.R., GEDDES, W., and LIDIAK, E.G., 1966. Crustal study of a continental strip from the Atlantic Ocean to the Rocky Mountains. *Geol. Soc. Am. Bull.*, 77, 1427-1448.